# A STUDY OF THE EFFECT OF COASTLINE CONTOURS ON ELECTROMAGNETIC INDUCTION

by

GEE HUNG CHAN

B.Sc., University of Victoria, 1976

A THESIS SUBMITTED IN PARTIAL FULFILLMENT

OF THE REQUIREMENTS FOR THE DEGREE OF

MASTER OF SCIENCE

in the Department

of

Physics



We accept this thesis as conforming

to the required standard

[redacted]

(H.W. Dosso)

[redacted]

(L.K. Law)

[redacted]

(T.W. Dingle)

[redacted]

(J.T. Weaver)

Supervisors: Dr. H.W. Dosso and Dr. L.K. Law



## ABSTRACT

In this thesis, the effect of coastline contours on electromagnetic induction is investigated with the aid of an analogue model study of various idealized non-rectilinear coastline models. The laboratory modelling system is essentially that first described by Dosso (1966b) and more recently by Nienaber et al. (1967). A laboratory analogue model study of an actual bay, the San Juan Bay on the southwestern coast of Vancouver Island is also carried out and the results are compared with field station measurements.

Two simple models of non-rectilinear coastlines consisting of a semi-circular bay and a cape are first considered. The perturbation in the induced electromagnetic fields due to these structures are obtained from the analogue model measurements of the magnetic and electric field components for the E and H polarizations of a uniform horizontal inducing field. The effect of these irregularities along an otherwise straight sea-land interface is found to be confined to small local regions. The vertical magnetic field changes by as much as a factor of two along the bay- or the cape-shaped coastline. The enhancements in the horizontal magnetic field component which is parallel to the straight coastline, as well as the spatial variations in the two horizontal electric field components, indicate the deflection of the induced currents by the contours of the bay and cape.

The simple cape and bay models are modified by including an elliptical island in the shallow ocean near the continental coastlines.

The perturbation of the induced electromagnetic fields over the island due to the bay or cape coastlines are then examined. A more complex model (called the bay-cape model) in which a bay is situated beside a cape is also treated. Results are compared with those of the simple bay-shaped and cape-shaped coastline models. The coast effect along traverses for the bay-cape model and for a simple straight coastline model are compared with Launay's (1970) model results. It is observed that the coast effect is largest for the case of a cape, intermediate for the straight coastline and least for the bay.

In the San Juan Bay model study, the results in both the E and H polarizations of the source field indicate the deflection of induced current for the two frequencies studied. The induction arrows at locations near the bay are found to point towards a direction parallel to the coastline of the bay for a very high frequency. Values of the vertical magnetic field component obtained from measurements at field stations are found to be in good agreement with the laboratory analogue model results.

[redacted]

H.W. Dosso

[redacted]

L.K. Law

[redacted]

T.W. Dingle

[redacted]

J.T. Weaver

TABLE OF CONTENTS

Page

# LIST OF FIGURES

# ACKNOWLEDGEMENTS

I would like to thank my supervisors, Dr. H. W. Dosso of the Department of Physics and Dr. L. K. Law of the Pacific Geoscience Center, for suggesting this research problem and providing support and guidance throughout the work.

I would also like to thank Mr. G. Heard, Mr. T. Miles and Dr. W. Nienaber of the University of Victoria for many useful and stimulating discussion.

I wish to acknowledge the financial support from my supervisor Dr. H. W. Dosso through research funds and from the University of Victoria in the form of a Scholarship and a Fellowship.

# CHAPTER 1

# INTRODUCTION

## 1.1 Development in Solving Electromagnetic Induction Problems

Natural variations of the electromagnetic field at the surface of the earth have been studied for many years. One of the goals in such work is to probe the electrical conductivity distribution within the earth, which will lead to better understanding of the earth's interior structure.

Some of these variations originate from perturbations in the ionosphere due to solar activity. The periods of these disturbances vary from 0.1 sec to a few days. Of these, there are two variations with regular patterns, the $S_q$ and the $L_q$ variations, with periods of 24 hrs. and 24 hrs. and 50 mins., respectively; and the irregular but statistically predictable magnetic storms, designated as Dst, which produce a prolonged disturbance of large amplitude with a duration of the order of one day. The details of these variations are reviewed extensively by Chapman (1967) and Matsushita (1967). Another type of well known electromagnetic variations is of a random nature. The variations are short events, collectively called micropulsations, with duration ranging from minutes to 0.1 sec. Sub-classification with respect to frequenceis, characteristics and corresponding phenomena are discussed by Troitskaya (1964) and Campbell (1967).

These time varying magnetic fields induce electrical currents in the conducting earth. The induced currents, in turn, give rise to secondary electromagentic fields. The attenuation, and hence also the penetration, of the inducing fields depends upon the frequency and configuration of the source field, as well as on the magnetic and electrical properites of the medium. A superposition of the inducing and the induced fields is observed at the earth's surface. By comparing these observations with results for various induction models, many workers have attempted to map the conductivity structure of the earth.

In early studies concerning the earth as a whole, the conductivity was generally considered to vary only radially. An harmonic analysis was used to separate the contribution due to the external and due to the induced fields for comparatively long period variations (e.g. Lamb, 1883; Schuster, 1889; and Chapman and Whitehead, 1922). Rikitake's review (1973) includes the more recent approaches in this type of work. Over a small region of the earth, however, the local inhomogeneity of the electrical conductivity plays an important role in affecting the induced currents. This leads to local induction problems.

Price (1950) considered a model in which the region of interest was treated as a flat earth occupying a semi-infinite uniform conducting half space. A method to obtain the induced fields for an arbitrary source was outlined. Uniformly layered conductivity models were subsequently considered by Tikhonov (1950), Lipskaya (1953) and Cagniard (1953). Wait (1954) and Price (1962) improved Cagniard's (1953) model by imposing a restriction on the size of the uniform source fields. Dosso (1967) presented a comprehensive work for a multi-layered earth problem, assuming

a plane wave source field and a horizontally uniform earth. The response of the fields with respect to frequency and location of the source, and the conductivity contrast between successive layers were studied.

It is well known that there are many locations on the earth where the geomagnetic field at stations relatively close together consistently shows considerable differences in both amplitude and, or phase. Also, the pattern of this difference between stations varies with frequency of the natural disturbances. Such anomalous fields were observed along the coast of Australia (Parkinson, 1959, 1962); within a large sector in Northern Germany (Schmucker, 1959; Kertz, 1964 and Vozoff and Smith, 1968) and on the North American continent (Swift, 1967; Caner et al., 1969 and Schmucker, 1970). To cope with these diversified geological structures, various techniques are used to deal with the perturbation of the induced currents system by a lateral conductivity inhomogeneity.

D'Erceville and Kunetz (1962) studied the case of a vertical fault, simulated by a model with two media of different conductivities in contact along a vertical plane overlying a horizontal basement. Numerous other models have been studied yielding exact solutions to problems involving geological structures such as a dyke (Rankin, 1962), a vertical fault of infinite depth (Weaver, 1963; Mann, 1970; and Weaver and Thomson, 1972) and tilts (Yukutake, 1967; and Geyer, 1972). Weidelt (1971) studied induction in two adjacent half sheets with different uniform conductivities and Schmucker (1971) obtained a numerical solution for a model with a non-uniform surface layer above a layered substratum.

In general, only idealized structures of simple nature are considered in using the analytical approach. More realistic three

dimensional models which involve inhomogeneities of arbitrary shape have been studied using several numerical techniques. Dulaney and Madden (1962) applied the transmission line analogy method for the case of a vertical fault. Zienkiewicz (1971) described the finite element method, which used the principle that electromagnetic fields behave in such a way as to minimize the energy of the system. This technique was used by Reddy and Rankin (1975) on an anisotropically lateral inhomogeneous earth, and by many others. The finite difference method, which calculated the field values at grid points of a mesh, was used by Neves (1957), Latke (1966) Patrick and Bostick (1969). More recent use of this technique was made by Jones and Price (1970. 1971) and Jones and Pascoe (1971), and Brewitt-Taylor (1975).

Another method of studying an induction problem employs the use of a laboratory analogue model. This technique is particularly suitable for models too complex to yield to analytical mathematical analysis. The theory of electromagnetic scale modelling was developed by Sinclair (1948); and has been discussed by Strangway (1966), Ward (1967), and Frischknecht (1971) in further detail. Simulations employing metallic thin sheets, such as copper and aluminium, have been used by many authors (including Roden, 1964; Hermance, 1968; Launay, 1970. and Kulik, 1973). These studies dealt with the perturbations of the induced electromagnetic fields due to oceanic islands and land-sea interfaces.

Dosso (1966b) developed a modelling system in which a bath of saturated salt solution simulates the earth, while graphite and concrete structures of variable shape and size, model the conductivity anomalies. This modelling facility has been used to carry out model studies of

electromagnetic variations near vertical faults and dykes (Dosso, 1966b), over an anisotropic conductor (Dosso, 1969), over sphere embedded in a conducting earth (Ogunade, 1973; Ogunade et al., 1974, 1977), and over conducting cylinders (Dosso, 1966a; and Ramaswamy and Dosso, 1977). Various types of source fields have been used including a uniform field (Dosso, 1966a), an oscillating line current (Dosso and Jacobs, 1968; and Ramaswamy and Dosso, 1977), overhead magnetic dipoles (Dosso, 1969; Thomson et al., 1972; Ogunade et al., 1974; and Ramaswamy and Dosso, 1977), and buried dipole sources (Ramaswamy, 1973; and Ramaswamy and Dosso, 1978). The effect of various field sources on a single structure has been studied by Dosso (1969), Ramaswamy and Dosso (1977), and Hibbs et al., (1978). Dosso (1966) considered the model of a shelving ocean over an upwelling in the mantle. The results upheld Schmucker's (1964) prediction based on measurements of the fields at the California coast. A comparison of analogue model measurements and finite-difference numerical calculations for constant depth and shelving oceans was carried out by Dosso et al., (1974). Ogunade et al., (1974) have compared analogue model measurements with numerical calculations for the response of a buried conducting sphere to an overhead vertical magnetic dipole source. Both comparisons have shown very good agreement between the results for the analogue model and the theoretical calculations. Nienaber et al., (1976) studied the induced current system for the Vancouver Island, Canada, region. The analogue model measurements showed appreciable agreement with observed field station results for that region.

## 1.2 Induction Studies for Sea-land Interfaces

The well known coast effect is a type of anamalous field, characterized by the enhancement of the vertical magnetic field as the coast is approached from the landward side. Furthermore, the magnetic field vectors are confined to a plane which would be inclined upward towards the coastline. This phenomenon has been observed by many authors (e.g. Parkinson (1962) in Australia; Schmucker (1964) along the California coast; Cox et al., (1970) and Everett and Hyndman (1967) in Australia). Numerous induction studies for a sea-land boundary have been carried out using theoretical techniques (e.g. Weaver, 1963; Parker, 1968; Brewitt-Taylor, 1975; Jones and Price, 1970, 1971; Lines and Jones, 1973b and others, and by analogue modelling methods (e.g. Roden, 1963; Dosso, 1966c, 1973; Dosso and Jacobs, 1968; Thomson et al., 1972; and Nienaber et al., 1976, 1977).

Observations of geomagnetic field anomalies have been recorded at location on the Japanese Islands by Tikitake (1966); on the British Islaes by Edwards et al., (1971) and on the Vancouver Island in Canada by Nienaber et al., (1977). The effect of an island on the induced current in the waters surrounding it was considered by Mason (1963); Honkura (1971) and Klein (1976). Lines and Jones (1973a,b) calculated the deflection of electric currents around a three-dimensional island structure, and discussed its effect upon a nearby continental coastline. Nienaber et al., (1976) carried out a laboratory model study of square and circular islands near a continent, and found that the perturbation of the island on the coast effect over the continental shoreline becomes negligible when the channel width is larger than half the dimension of the island. There is

at present much interest in the study of the effect of the channel upon the induced electric currents in the surrounding ocean. Observational studies were carried out by Edwards et al., (1971) for the English Channel region; by Hyndman and Cochrane (1971) along the Canadian St. Lawrence River, and by Bailey and Edwards (1976) in the North Sea and Irish Sea region. The numerical model of Jones (1974b) showed that electric current may be channeled by ocean channels. Nienaber et al., (1978) obtained good agreement between analogue model measurements and field results obtained at stations at the coast on either side of the Strait of Georgia and Juan de Juca Strait in the Vancouver Island region.

Another interesting feature in the study of induction anomalies along a coastal region is the effect of the shape of the coastline. Rokityanskii (1963) studied the vertical magnetic field anomalies at Mirny, which is roughly a cape-shaped area on the northeastern coast of U.S.S.R.; and at points along the winding Crimean coastline. Launay (1970) showed the relative magnitudes of the $H_z/H_y$ ratios for traverses crossing a straight coastline, a bay, and a cape. Kulik (1973) used an aluminium and graphite model to study the effect of a cape and a rising sea floor on induced magnetic fields. Jones (1974b) and Jones and Lokken (1975) applied the finite difference method to obtain a solution for the field over a very irregular coastline and demonstrated that electric currents may be channelled by shallow bays.

## 1.3 Summary of the Work Covered in This Thesis

The analogue modelling method was used in this work to investigate the effect of the shape of the coastline for a uniform inducing

electromagnetic field. The four simple contours studied are: i) a straight coastline, ii) a semi-circular bay, iii) a semi-circular cape, and iv) a combination of a bay and a cape. Both constant depth ocean and sloping sea floor cases are considered. Further, the case of an elliptical island situated at a distance of roughly half its width from the continental shorelines was also included. Electric and magnetic fields measurements were carried out for two orientations of the inducing field (with the electric field of the source field (a) parallel to the rectilinear portion of the coastline, the E polarization case, and (b) perpendicular to the coast, the H polarization case), for traverses over the models.

A scaled model of an actual bay, San Juan Bay on the southwestern coast of Vancouver Island, was constructed and analogue model measurements for this model were compared with field station measurements carried out at two locations in the San Juan Bay area in October, 1977.

# CHAPTER 2

## THE LABORATORY ANALOGUE MODEL

Some of the electromagnetic modelling studies mentioned in Chapter 1 (e.g. Roden, 1964; Hermance, 1968; Launay, 1970; and Kulik, 1973) employed thin metal sheets, suspended in air, to simulate the oceans. Such modelling systems suffer several disadvantages. First, only the magnetic fields can be measured. Further, the geophysical case consisting of a highly conducting ocean in contact with a host earth of non-vanishing conductivity is not adequately simulated by a metal plate in air. In addition, the large conducitivity scaling factor, normally used in models using metal plates, does not readily permit the modelling of a shallow shelving ocean at a coastline. A brine solution, an electrolyte, instead of air, can be used to simulate the earth (e.g. Rankin, 1965; Dosso, 1966a; Frischknecht, 1971) and suitably shaped graphite structures placed in the salt solution then simulate conducting bodies, such as an ocean in contact with a poorly conducting host earth. The use of a salt solution also readily permits the measuring of the electric fields.

### 2.1 The Model Scaling Conditions and Scaling Factors

To determine the conditions required for an electromagnetic analogue modelling system, one can apply the principle of electromagnetic similitude (Stratton, 1941) to Maxwell's equations. Such analysis is well known but will be briefly discussed here for completeness. SI units will be used throughout.

Assuming only homogeneous media are present in both the geophysical and the analogue modelling problem, Maxwell's equations are

$$(1) \quad \vec{\nabla}' \times \vec{E}' + \mu' \frac{\partial \vec{H}'}{\partial t'} = 0 ,$$

$$(2) \quad \vec{\nabla}' \times \vec{H}' - \varepsilon' \frac{\partial \vec{E}'}{\partial t'} - \sigma' \vec{E}' = 0$$

for the geophysical system, and

$$(3) \quad \vec{\nabla} \times \vec{E} + \mu \frac{\partial \vec{H}}{\partial t} = 0 ,$$

$$(4) \quad \vec{\nabla} \times \vec{H} - \varepsilon \frac{\partial \vec{E}}{\partial t} - \sigma \vec{E} = 0$$

for the model system.

Since the electric and magnetic properties of the media are linear and isotropic, the field variables in the two systems are related by simple linear transformations:

$$(5) \quad \vec{E}' = \vec{E} / K_E \quad , \quad \vec{H}' = \vec{H} / K_H \quad ,$$

$$(6) \quad \varepsilon' = \varepsilon / K_e \quad , \quad \mu' = \mu / K_m \quad ,$$

$$(7) \quad L' = L / K_L \quad , \quad \sigma' = \sigma / K_s \quad , \quad t' = t / K_t \quad ,$$

where $K_E$, $K_H$, $K_e$, $K_m$, $K_L$, $K_s$ and $K_t$ are the respective scale factors for the electric field, magnetic field, permittivity, permeability, length, conductivity and time.

Using (5) and (6), equations (1) and (2) transform to:

$$(8) \qquad \vec{\nabla} \times \vec{E} + \alpha\mu \frac{\partial \vec{H}}{\partial t} = 0 \ ,$$

$$(9) \qquad \vec{\nabla} \times \vec{H} - \beta\varepsilon \frac{\partial \vec{E}}{\partial t} - \gamma\sigma \vec{E} = 0 \ .$$

In order that (8) and (9) be equivalent to (3) and (4), the dimensionless coefficients $\alpha$, $\beta$ and $\gamma$ must have unit magnitude, i.e.,

$$(10) \qquad \alpha = \frac{K_t}{K_m K_L} \left(\frac{K_E}{K_H}\right) = 1 \ ,$$

$$(11) \qquad \beta = \frac{K_t}{K_e K_L} \left(\frac{K_H}{K_E}\right) = 1 \ ,$$

$$(12) \qquad \gamma = \frac{1}{K_s K_L} \left(\frac{K_H}{K_E}\right) = 1 \ .$$

When displacement currents are unimportant (i.e. $\sigma |\vec{E}| >> \varepsilon \frac{\partial |\vec{E}|}{\partial t}$) the second term for equations (2), (4) and (9), and hence conditions (11) can be ignored. Further, if we chose $\mu = \mu'$ equations (10) and (12) become:

$$(13) \qquad K_t K / K_L = 1 \ ,$$

$$(14) \qquad K_L K_s K = 1 \ ,$$

where $K = K_E/K_H$ has been introduced as the scale factor relating impedances in the two systems. Using the transformations (5) and (7), conditions (13) and (14) may be written in the form:

$$(15) \qquad f L = f' L' K \ ,$$

$$(16) \qquad \sigma L = \sigma' L' K^{-1} \ ,$$

where f = $2\pi/T$ is the frequency of the time harmonic field and

(17) $$K = (E/H)/(E'/H') .$$

Equations (15) and (16) consist of four unknowns, $\sigma/\sigma'$, L/L', f/f' and K, which are the conductivity, linear dimension, frequency and impedance scaling factors respectively. For each modelling system, $\sigma/\sigma'$ is determined by the selection of the model materials while the size of the laboratory restricts the ratio L/L'. Then, by equations (15) and (16), the scaling factors for frequency and impedance are determined to be respectively:

(18) $$(f/f') = (\sigma'/\sigma)(L'/L)^2 ,$$

(19) $$\frac{E/H}{E'/H'} = K = \left(\frac{\sigma'}{\sigma}\right)\left(\frac{L'}{L}\right) .$$

If magnetic fields only are studied, and the impedance scaling factor K is not of interest, K can be eliminated from (15) and (16) and scaling conditions becomes:

(20) $$\sigma f L^2 = \sigma' f' L'^2 .$$

If concentrated salt solution ($\sigma$ = 21 $Sm^{-1}$) and graphite plate ($\sigma = 1.2 \times 10^5$ $Sm^{-1}$) are used to simulate land ($\sigma$ taken as 3.6 $Sm^{-1}$), respectively, the conductivity scaling factor $\sigma/\sigma'$ will be $1/3 \times 10^5$. Using a length scaling factor of L/L' = $1/(5 \times 10^5)$ (i.e. 1 cm in the model represents 5 km in the geophysical case), the frequency scaling factor f/f' becomes $75 \times 10^5$ (i.e. a model frequency of 30 kHz simulates a frequency of 0.004 Hz in the geophysical case).

## 2.2 Description of the Laboratory Analogue Model

The experimental arrangement is shown in Fig. 1. The model consists of a plywood tank 2.44 m x 1.68 m and .76 m deep, filled with concentrated salt solution to a depth of .63 m. The bottom of the tank is lined with a 5 cm thick graphite plate to minimize the effects of the concrete floor of the laboratory. For a certain frequency range, it may also serve to model a more conducting lower layer in the earth. The two walls of the salt water tank, perpendicular to the electric field of the inducing source, are lined with stainless steel sheets, which are electrically connected by a heavy copper wire outside the tank. This permits currents induced in the salt solution to flow parallel to the source current right to the edge of the tank, thus minimizing the edge effects produced by the tank walls. The salt solution simulates a poorly conducting earth while the graphite layer simulates a deep highly conducting substratum. If this facility is used to study coast effects as in this work, graphite plates, shaped to model oceans of various shapes and sizes, are suspended at the surface of the salt solution. The graphite plate - salt solution interface then simulates a sea-land boundary.

A uniform source field is provided by two parallel oscillating line currents suspended 1.2 m (h in Fig. 1) above the surface of the salt solution, and separated by a distance of 2.4 m. These two lines are connected in parallel so that identical current flows in both lines. The current is generated by a 1000- Watt Savage power amplifier (Series KM2ZE), for the frequency range 3 kHz - 20 kHz, and by a 150-Watt McIntosh power amplifier (Model MC275), for frequencies greater than 20 kHz. A

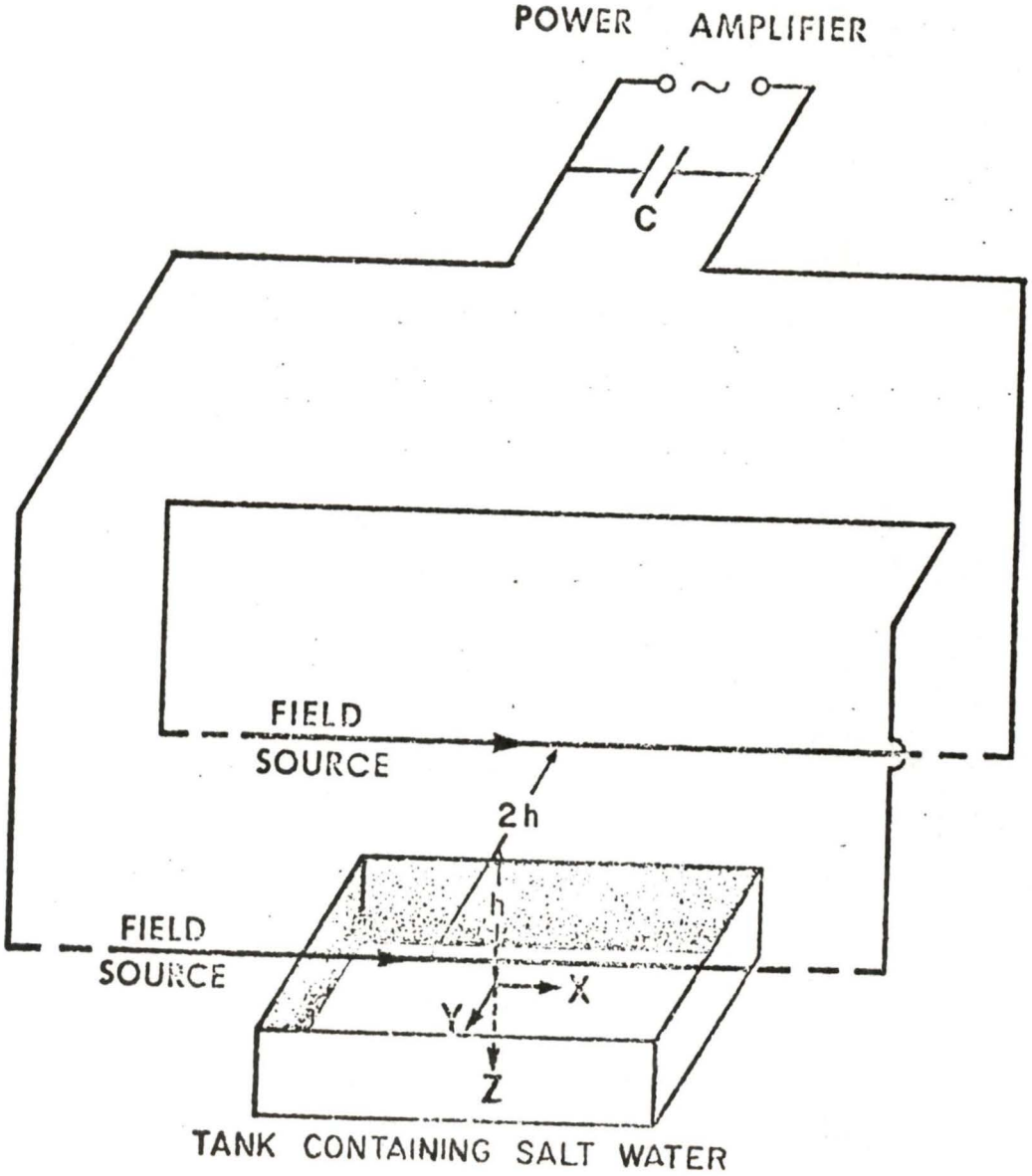


Fig. 1. The electromagnetic analogue model.

variable capacitor, connected in parallel to the power supply, is used to tune the source for resonance, thus, providing maximum current in the two line currents. This current is monitored by a small pick-up coil near the source leads. The voltage induced in the coil also provides a reference signal for measuring the phase angle of the field components.

The magnetic field detectors consist of two 1 mm long coils of 250 turns (#42 wire), with inside the outside diameters of 2.35 mm and 6.35 mm respectively. Each coil is mounted in a lucite tube in the appropriate orientation (i.e. the axis of the coil is parallel to the direction of the magnetic field component being measured). The horizontal electric field detector consists of three pins protruding through the sealed end of a lucite tube to make contact with the surface of the salt solution. This probe, designed to provide suitable input to a differential amplifier, measures the horizontal electric field between the two outer pins 1.48 cm apart.

For measurement of a particular field component, the appropriate detector is mounted on the motor driven carriage which moves horizontally over the tank. A block diagram of the detecting and recording equipment is shown in Fig. 2. The amplitude and the phase angle (obtained by comparing the detected signal with the reference signal in the AD-YU 524A2 digital phase computer) are recorded simultaneously on separate X-Y recorders (Model HP 7000 AM).

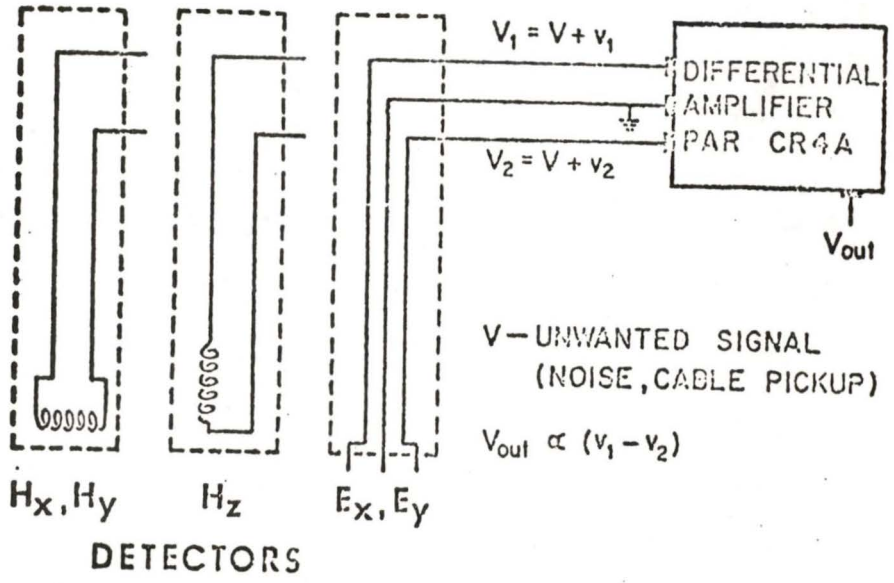


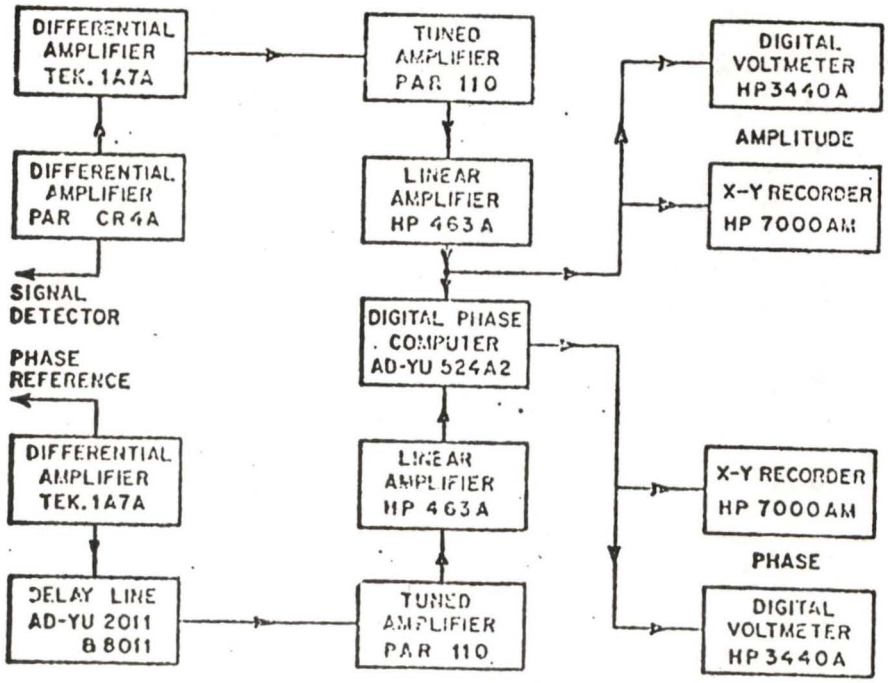


Fig. 2. The field detectors and measurement instrumentation.

# CHAPTER 3

## MODEL RESULTS

Several simple non-rectilinear coastline models were used to study the effect of the contour of a coastline on the induced electromagnetic field. The basic models were a cape and a bay, each situated along an otherwise straight coastline. Two different types of ocean models were considered: a) sloping-floor ocean and b) constant depth ocean. The spatial variations of the magnetic and electric fields (excluding the vertical electric field component) were studied for E and H polarizations for two source frequencies. The ratios of $H_z/H_y$ and $E_x/H_y$, the phase differences $\phi_z - \phi_y$, $\psi_x - \phi_y$, and the apparent resistivity $\rho_a$ were also examined.

A model which combined a cape and a bay was next considered for the E polarization for a frequency of 30 kHz. An attempt was made to compare the $H_z/H_y$ analogue model profiles with those of Launay's (1970). Another set of models studied consisted of an elliptical island situated near i) a bay, ii) a cape, and iii) a straight coast. The effect of these coastlines on the induced electromagnetic field over the island was examined.

To demonstrate the uniformity of the inducing source field, the sum of the induced and inducing fields was measured with only the concentrated salt solution and the lower graphite layer in the tank. These measurements are called the reference field measurements. A short description of the reference field at the surface of the salt solution is presented

in the next section.

## 3.1 The Reference Field Measurements

Figs. 3 and 4 show the amplitudes and phase angles of the magnetic and electric field components at the surface of the salt solution for a traverse along x = 0 (also, perpendicular to the electric field of the inducing source) at frequencies of 30 kHz and 3 kHz, respectively. Reference field measurements over other regions of the tank were also taken, but are not presented here since they do not show appreciable differences from the results of the x = 0 traverse. The calibration factors in brackets along the ordinates of the amplitude curves were associated with the detectors used to measure the fields. It can be seen that the reference fields are mainly horizontal for either frequency with the electric field parallel and the magnetic field perpendicular to the electric field of the inducing source. Since the $E_y$ component is very small, there is great difficulty in monitoring the corresponding phase angle $\psi_y$, and hence, it is not shown here. The uniformity of the reference field is readily verified by the fact that all the amplitudes and the phase angles remain fairly constant for the full length of the traverse. The current in the salt solution is seen to be mainly parallel to the electric field of the inducing source.

## 3.2 Analogue Model Study of the Cape and Bay Shaped Coastlines for a Sloping-Floor Ocean (E Polarization)

It was mentioned in Chapter 2 that concentrated salt solution ($\sigma$ = 21 $Sm^{-1}$) and graphite plate ($\sigma$ = 1.2 x $10^5$ $Sm^{-1}$) are used to simulate land ($\sigma$ taken as 6.3 x $10^{-4}$ $Sm^{-1}$) and ocean ($\sigma$ taken as 3.6 $Sm^{-1}$),

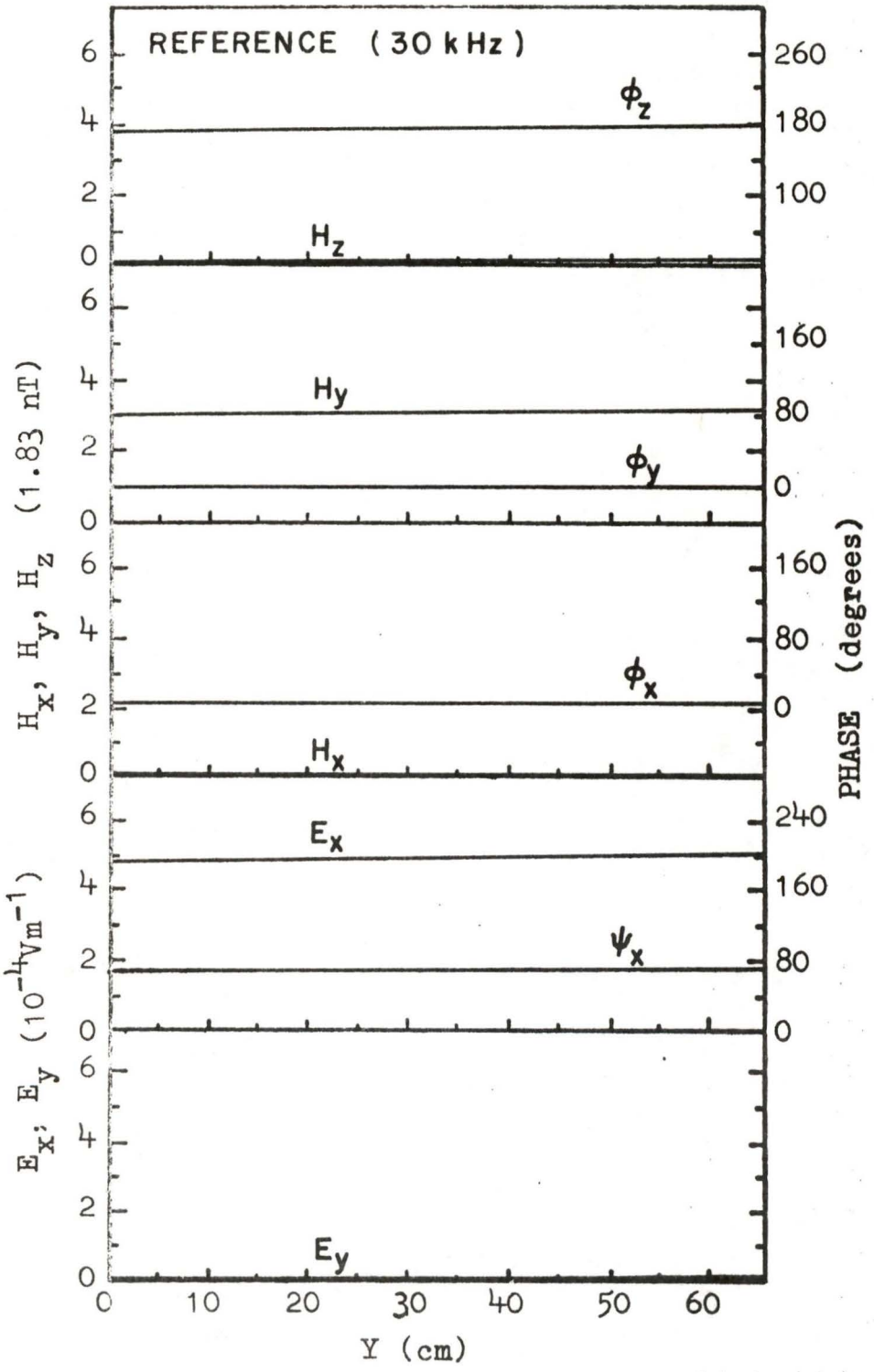


Fig. 3. Model measurements of the amplitudes and phase angles of the electric and magnetic reference field components for a traverse along x = 0 at the surface of the salt solution for a frequency of 30 kHz.

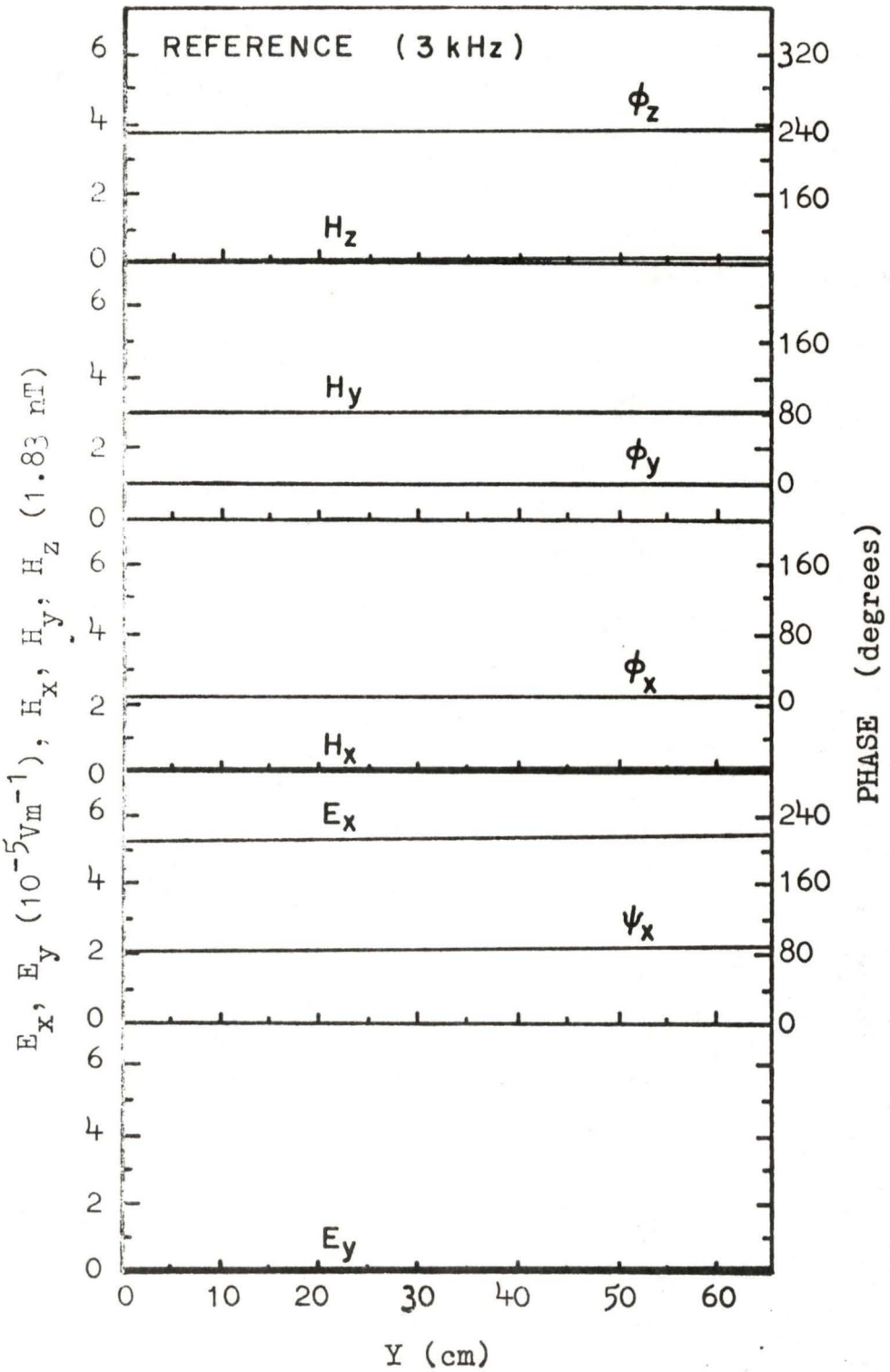


Fig. 4. Model measurements of the amplituses and phase angles of the electric and magnetic reference field components for a traverse along x = 0 at the surface of the salt solution for a frequency of 3 kHz.

respectively. The conductivity scaling factor $\sigma/\sigma'$ equals $1/3 \times 10^5$. The length and frequency scaling factors were chosen to be $L/L' = 1/(5 \times 10^5)$ and $f/f' = 75 \times 10^5$, respectively.

A graphite plate measuring 1 meter square and 3 mm thick was used to simulate a 1.5 km deep ocean. A semi-circular hole, radius 5 cm, was cut as shown in Fig. 5. This represents a semi-circular cape 25 km in radius. The graphite plate was then machined to have the cross section of a wedge as shown in Fig. 5, thus simulating an ocean with a sloping floor. Also shown in Fig. 5 is part of the graphite plate which simulated an ocean with a bay-shaped coastline. For the E polarization case, the model was positioned in the tank with the edge of the graphite plate, which simulates the non-rectilinear coastline, parallel to the electric field of the inducing source (i.e. parallel to the x-axis). The two ends parallel to the y-axis were electrically connected to the stainless stell sheets at the tank walls, to minimize the end effects of the graphite plate. Measurements of the amplitudes and phases of the electric and magnetic fields were carried out for traverses over the bay and cape models.

Laboratory model results for the bay model (with sloping-floor ocean) for the E polarization case at a frequency of 30 kHz (simulating a 0.004 Hz geophysical variation) for six traverses are presented in Fig. 6. In general, results for all field components for traverses for x greater than 11.0 cm for the bay model show little difference from that for traverse 6, and hence, it is concluded that the effect of the bay is confined to within a distance of one bay diameter (from the centre of the bay) along the coastline.

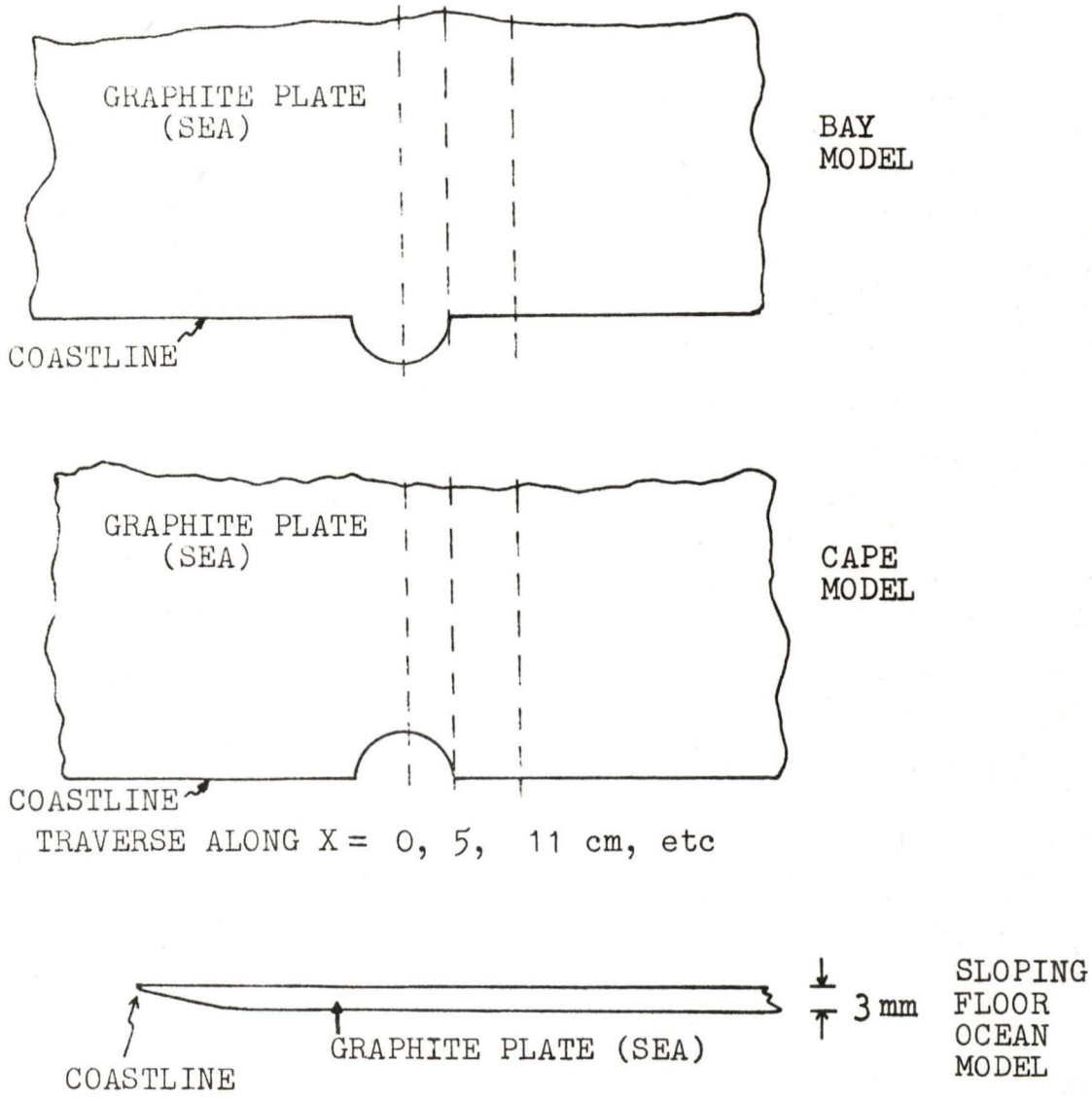


Fig. 5. The bay, cape, and sloping-floor ocean models.

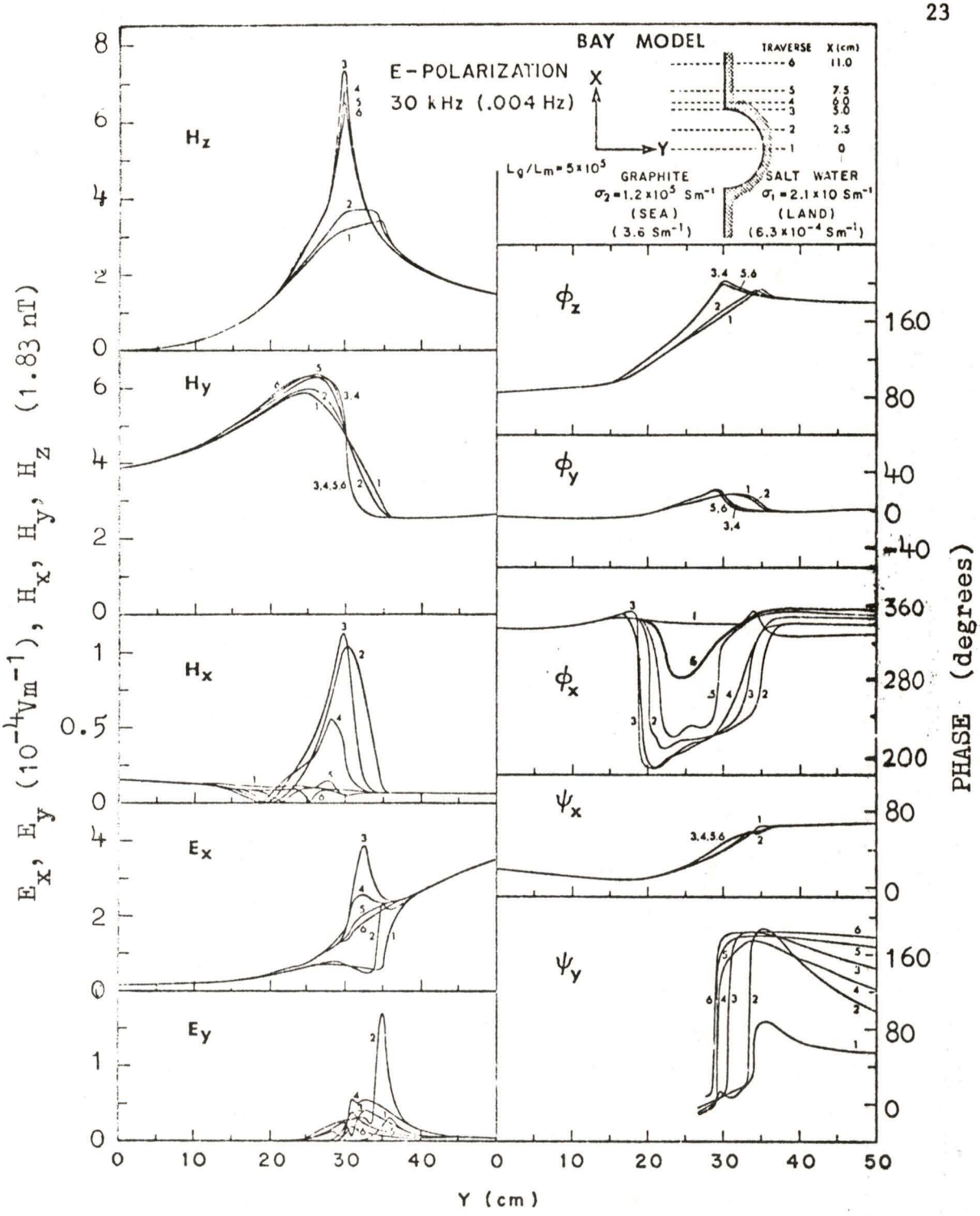


Fig. 6. Amplitudes and phase angles of the electric and magnetic field components along six traverses over the bay model (sloping-floor ocean) for the E polarization for a frequency of 30 kHz.

In Fig. 6, it is seen that except for $E_y$, all field components have maximum enhancements for traverse 3 in the vicinity of the corner of the bay. The coast effect is readily shown by the enhancement of $H_z$ for all traverses with maxima at the graphite-salt solution interface. Along the coastline, $H_z$ increases from traverse 1 (passing through the centre of the bay, x = 0 cm) to traverse 2 (x = 2.5 cm) and reaches a maximum rapidly for traverse 3 (passing by the corner of the bay, x = 5.0 cm). It then decreases gradually along the straight coastline and reaches a minimum at traverse 6 (x = 11.0 cm). For traverses crossing the bay, there is an absence of sharp peaks in the $H_z$ anomaly. Further, the maxima are roughly half as large as those along traverses crossing the straight coastline. This is closely related to the channelling of electric current along the bay coastline as discussed later. The enhancement of the horizontal magnetic field component, $H_y$, is over the conducting ocean side and falls off sharply at the sea-land interface. It is interesting to note that the $H_y$ curves all intersect at y = 30, indicating that over the coastline, $H_y$ has the same value as over the diameter which joins the two corners of the bay. $H_y$ for traverses 1 and 2, which pass through the bay, show smaller and more spread out enhancements than for traverses 3 to 6, which all cross the straight coastline. Also, the maxima for traverses 1 and 2 are shifted further towards the sea than for traverses 3 to 6. The phase angles $\phi_z$ and $\phi_y$ do not show much change from traverse to traverse except for the shifts of the peaks moving with the y-coordinate of the coastline. The third magnetic field component, $H_x$, shows very little enhancement for traverses 1, 5 and 6, while small enhancements are present for traverses 2, 3 and 4 (note there is a change in the scale for $H_x$). This indicates that

there is a y-component of the electric field at the corner of the bay as well as at the point where traverse 2 crosses the coastline. The phase $\phi_x$ goes through a dip of approximately 160° for traverses 2 to 5 on moving from the sea towards the land, but is relatively unaffected for traverse 1.

In Fig. 6, the maxima in the x component of the electric field, $E_x$, for traverses 2, 3 and 4 occur over the landward side. Depression in this component is present for all traverses at the coastline (not so pronounced for traverses 3 to 6). This considerable attenuation in $E_x$ for traverses 1 and 2 indicates that there is relatively less current at the interface through the central region of the bay than at the straight coastline boundary. In addition to the maximum for $E_y$ over land for all traverses, there is another local maximum for traverses 2, 3 and 4 over the sea, but with much smaller amplitudes. The larger $E_y$ maxima for traverses 2, 3 and 4 are associated with large $E_x$ enhancements which indicate that there is dispersion of current into the coastal region near the corner of the bay. $E_x$ and $E_y$ components have comparable amplitudes where traverse 2 crosses the coastline. The phase $\psi_y$ indicates that $E_y$ is pointing in the negative y direction at the instant when $E_x$ is positive. Hence, the resultant of the electric field is directed away from the bay. This indicates the deflection of induced current by the shallow bay. The phase $\psi_y$ changes by 160° rapidly at the respective minima in $E_y$ for traverses 2, 3 and 4, and upon crossing the coastline for traverses 5 and 6. In contrast, $\psi_y$ of traverse 1 shifts by not more than 90°.

Laboratory field measurements over the same model for a frequency of 3 kHz (simulating 0.0004 Hz) are presented in Fig. 7. In general, the

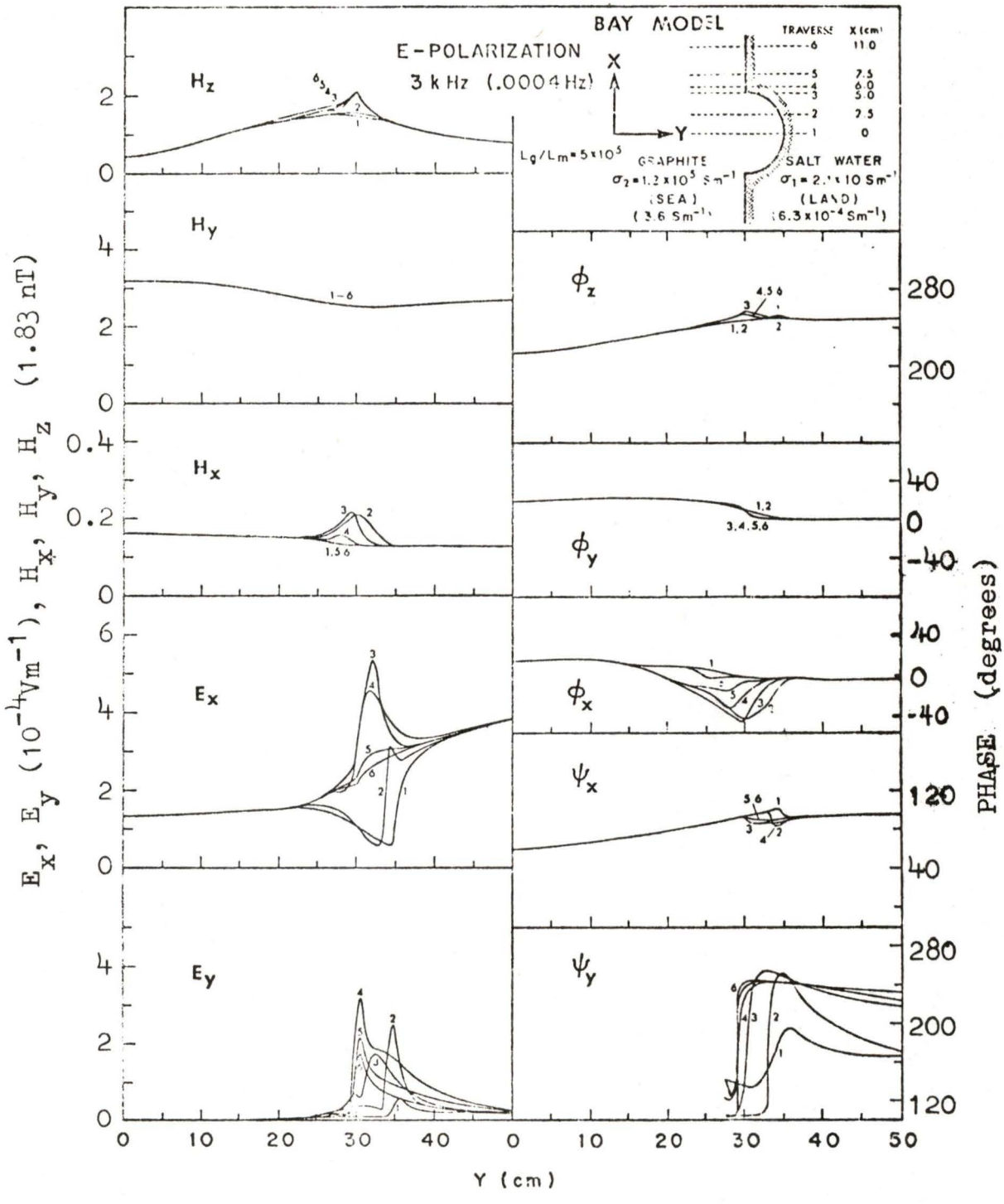


Fig. 7. Amplitudes and phase angles of the electric and magnetic field components along six traverses over the bay model (sloping-floor ocean) for the E polarization for a frequency of 3 kHz.

amplitudes and phase angles of the magnetic field components are much less affected by the bay than was the case for 30 kHz. In particular, $H_y$ shows no change from traverse to traverse. The electric field anomalies, especially for $E_y$, are larger for 3 kHz than for 30 kHz. The spaital variation patterns for $H_z$, $H_x$, $\phi_z$, $\phi_y$, and $\phi_x$ are very similar to the respective components for 30 kHz. This is also true for $E_x$, $E_y$, however, does show differences in that for traverses 2, 3, 4, 5 and 6, the enhancements become larger at the coastline for 3 kHz. Also, the $E_y$ maximum in traverse 3 exceeds that for traverse 2, while for 30 kHz, the opposite is the case. Again, traverse 2 has similar $E_x$ and $E_y$ amplitudes at the coastline, indicating that the deflection of current is also present at this frequency.

The amplitude ratios $H_z/H_y$ and $E_x/H_y$, and phase differences $\phi_z - \phi_y$ and $\psi_x - \phi_y$ over this simple bay model with sloping-floor ocean are shown in Fig. 8. For 30 kHz, all the $H_z/H_y$ curves show definite peaks at the coastline as against the broadened anomalies for traverses 1 and 2 in $H_z$. However, for 3 kHz, the variations of $H_z/H_y$ resemble that of the corresponding $H_z$. The coast effect of $H_z/H_y$ enhancements along the bay coastline is approximately 75% of that along the straight coastline for both frequenceis while the phase difference $\phi_z - \phi_y$ along the whole coastline does not seem to vary. The $E_x/H_y$ ratio at the centre of the bay is roughly ten times smaller than that at the corner of the bay for both frequencies, but again, the phase differences do not show appreciable changes.

Fig. 9 shows the apparent resistivity $\rho_a$ which is defined as $(\mu_o\omega)^{-1}(E_x/H_y)^2$, for both 30 and 3 kHz. In the 30 kHz case, $\rho_a$ over the

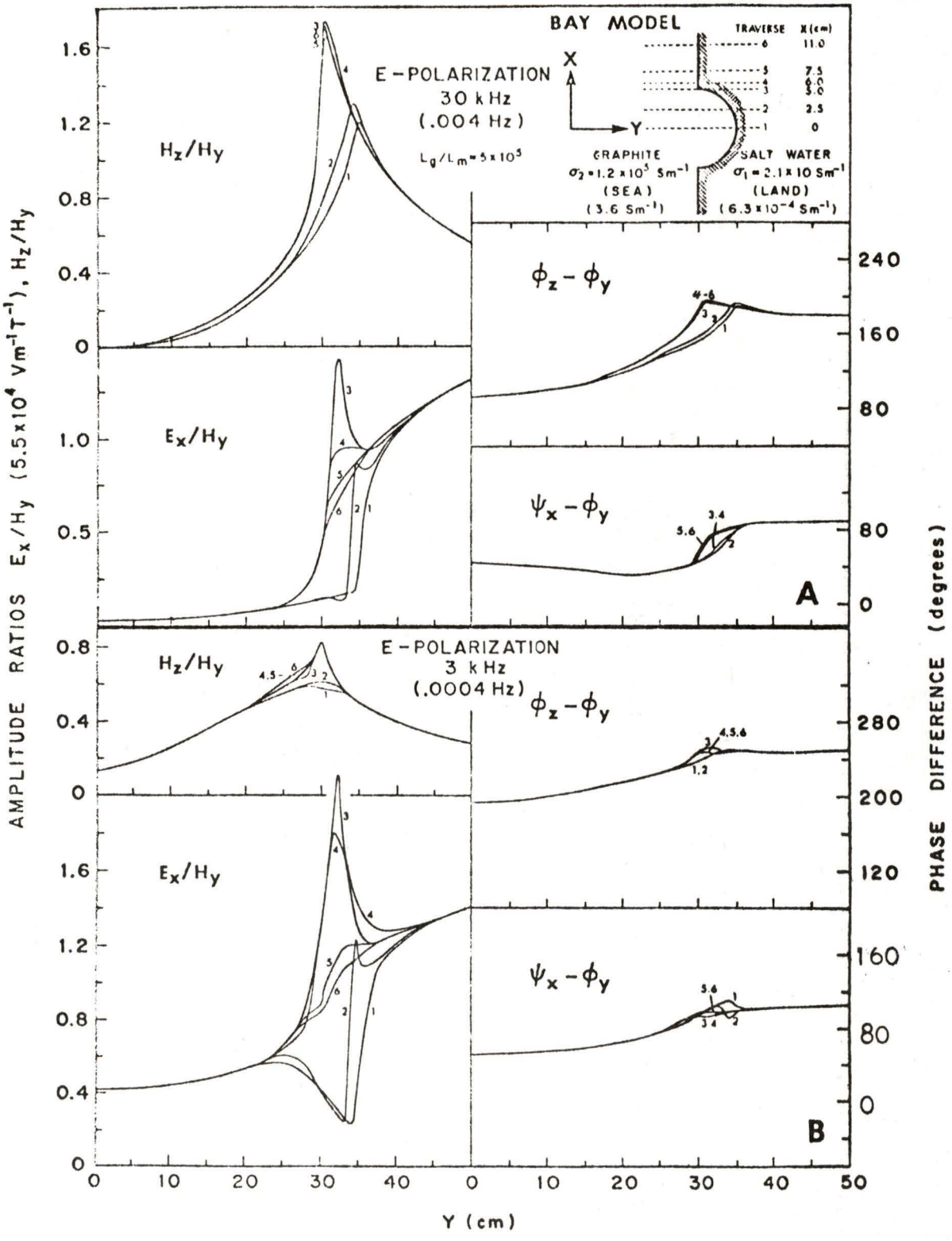


Fig. 8. Amplitude ratios $H_z/H_y$, $E_x/H_y$ and phase differences $\phi_z - \phi_y$ and $\psi_x - \phi_y$ along six traverses over the bay model (sloping-floor ocean) for the E polarization for frequencies of 30 and 3 kHz.

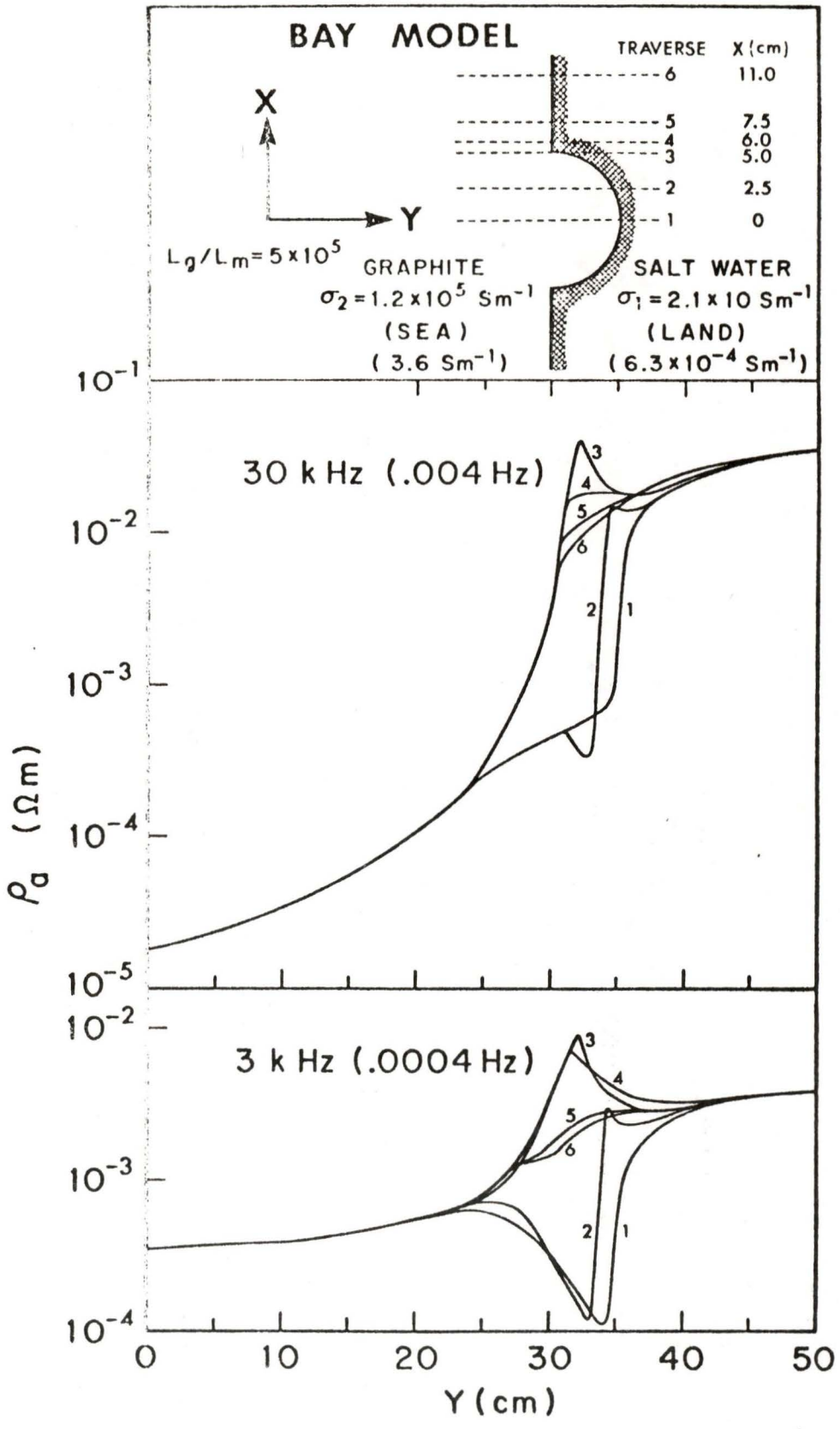


Fig. 9. Apparent resistivity along six traverses over the bay model (sloping-floor ocean) for the E polarization for frequencies of 30 and 3 kHz.

graphite approaches the resistivity of graphite ($1.2 \times 10^5$ $Sm^{-1}$) while over the salt solution, $\rho_a$ approached the resistivity of saturated salt solution ($2.1 \times 10$ $Sm^{-1}$). However, for 3 kHz, $\rho_a$ over the salt solution and well away from the bay is roughly one order of magnitude lower than the actual resistivity. This is due to the fact that at 3 kHz, the 3 mm thick graphite plate (the sea) is only 12% of the skin depth of graphite and the 63.4 cm saturated salt solution is only 1/3 of the skin depth of salt solution. Hence, the induced current, and therefore the apparent resistivity at the surface is somewhat affected by the highly conducting graphite layer at the bottom of the tank. A rapid increase in $\rho_a$ ($\sim$ 10 times) is seen for all traverses upon crossing the coastline from the sea side. At the coastline, $\rho_a$ for traverse 1 is approximately one order of magnitude lower than $\rho_a$ for traverses 3 for both frequencies. This indicates the perturbation in the current density along the coastal region by the contour of the coastline, in accordance with the electric current pattern near the bay.

Laboratory model results for the cape model (with sloping-floor ocean) for the E polarization case and a frequency of 30 kHz (simulating 0.004 Hz) are presented in Fig. 10. At the coastline, the enhancement in $H_z$ decreases from traverse 1 to traverses 2 and 3 and attains a minimum at traverse 4. The $H_z$ enhancement then increases moderately for traverses 5 and 6. It is interesting to note that the $H_z$ maximum at the tip of the cape is twice as large as $H_z$ along the straight coastline, while in the case of the bay model (Fig. 6), the anomaly at the straight coastline is seen to be twice as large as the $H_z$ maximum at the coastline for the traverse through the center of the bay. In both cases the large

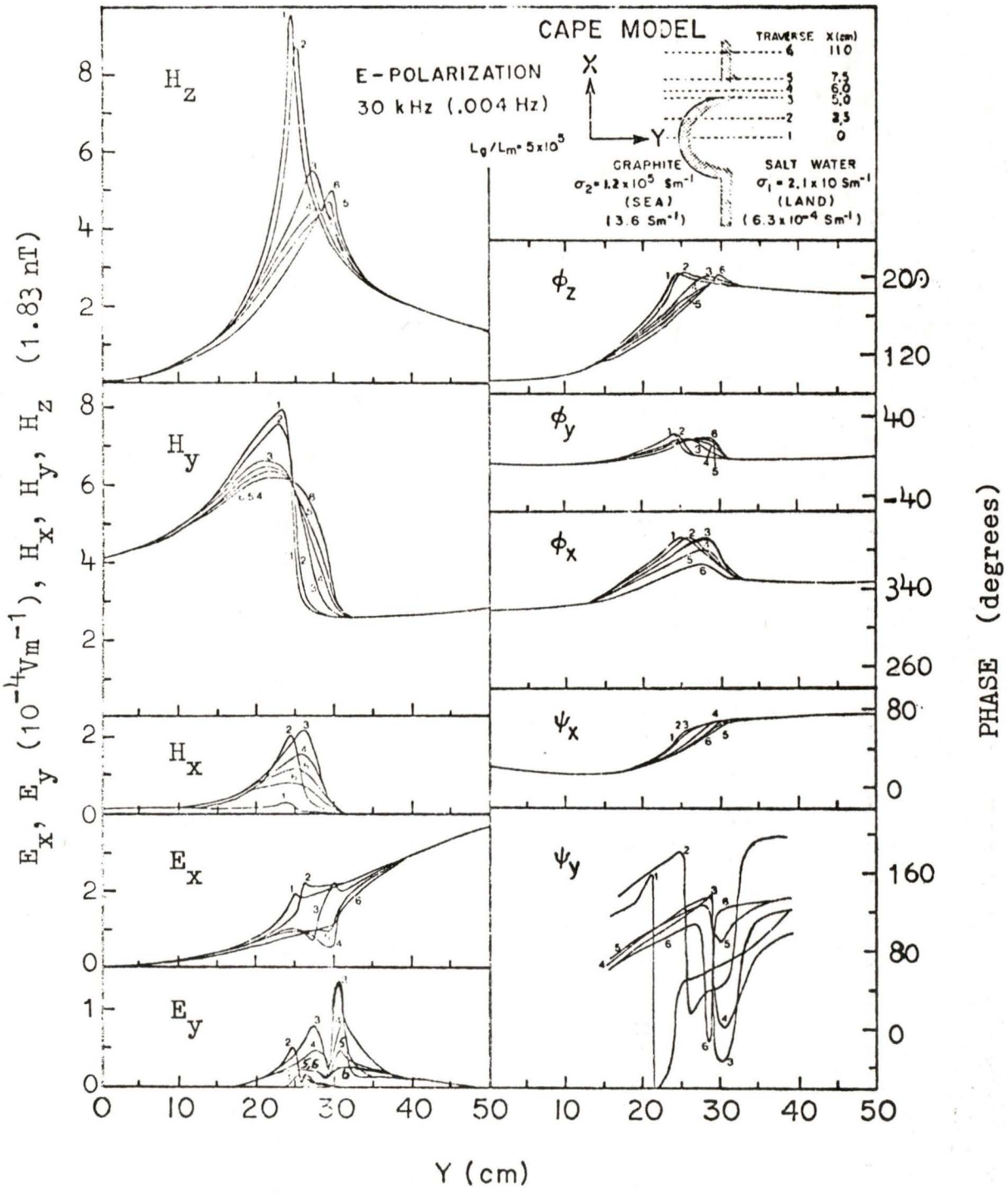


Fig. 10. Amplitudes and phase angles of the electric and magnetic field components along six traverses over the cape model (sloping-floor ocean) for the E polarization for a frequency of 30 kHz.

$H_z$ is characteristic of large current concentration in the good conductor. The presence of the cape leads to a shift of the $H_z$ maxima in traverses 3, 4, and 5 towards the sea side. For $H_y$, the maxima for these three traverses are shifted more towards the highly conducting ocean. Along a line tangential to the tip of the cape, the $H_y$ component is the same for all traverses (Cf. in Fig. 6, there is a line for the bay model over which $H_y$ does not vary between traverses). Deflection of electric current around the cape structure is evident by the presence of the $H_x$ and $E_y$ enhancements off the coast for traverses 2 to 5. The phase $\psi_y$ along the coastline, which is quite complicated, nevertheless indicates that the resultant of the horizontal electric field is roughly tangential to the cape.

Fig. 11 shows the model field measurements for the cape model (with sloping-floor ocean) for the E polarization case for a frequency of 3 kHz. The enhancements in the magnetic field components are in general smaller than for the 30 kHz case. $H_y$ again shows no change from traverse to traverse for this lower frequency. The other components $H_z$, $H_x$, and $E_y$ follow the same behaviour as for 30 kHz.

The amplitude ratios and the phase differences for traverses over the cape model are presented in Fig. 12. For both frequencies, the $H_z/H_y$ maxima for some of the traverses (3, 4 and 5) do not occur exactly at the coastline. This is in agreement with the behaviour of the corresponding $H_z$ amplitudes. The $H_z/H_y$ maxima for each traverse for 30 kHz are twice as large as for the 3 kHz results. This was also the case for the simple bay model results shown in Fig. 8. Hence, the coast effect $H_z/H_y$ is seen to decrease with decreasing frequency. Figs. 8 and 12 show

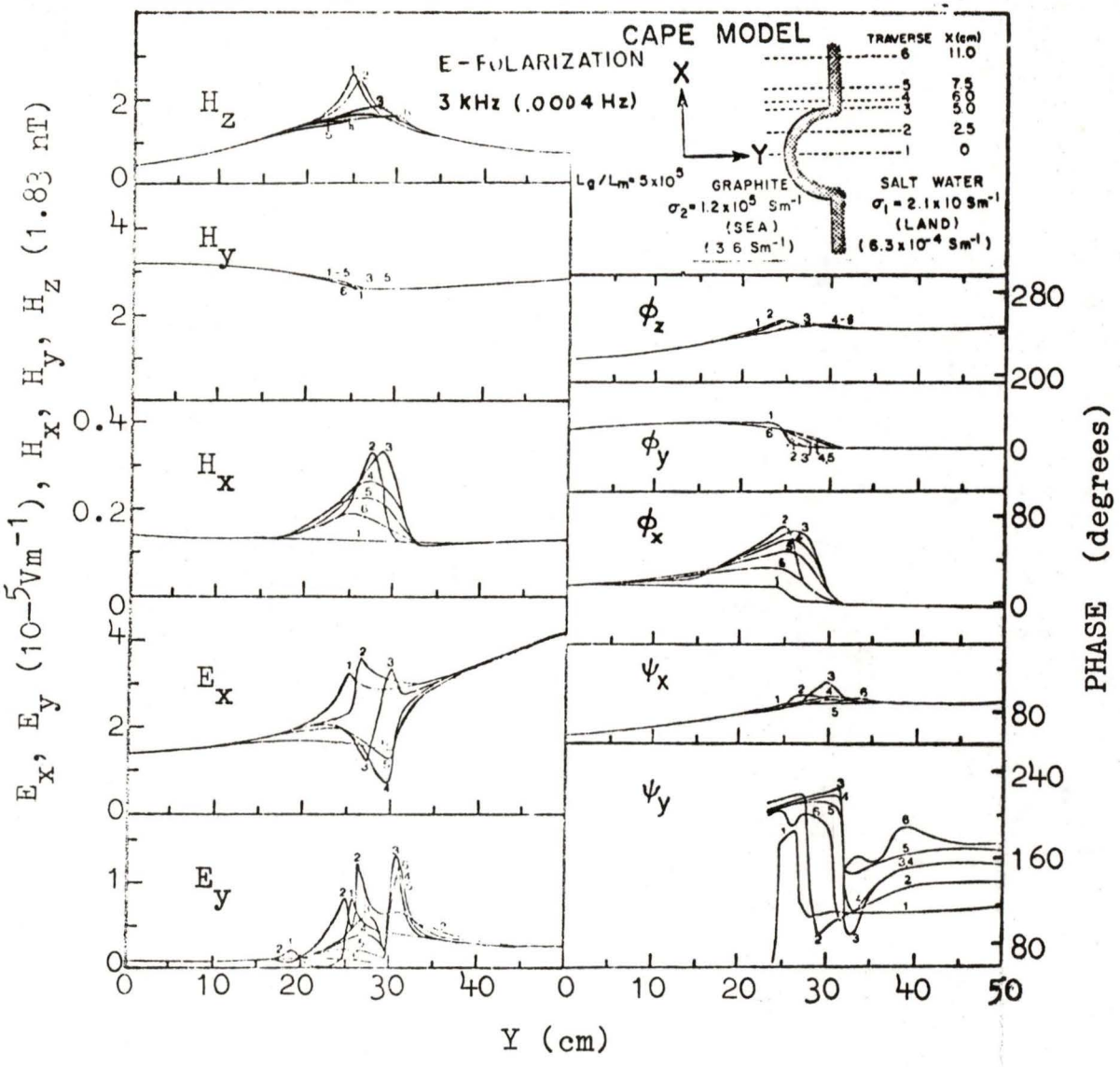


Fig. 11. Amplitudes and phase angles of the electric and magnetic field components along six traverses over the cape model (sloping-floor ocean) for the E polarization for a frequency of 3 kHz.

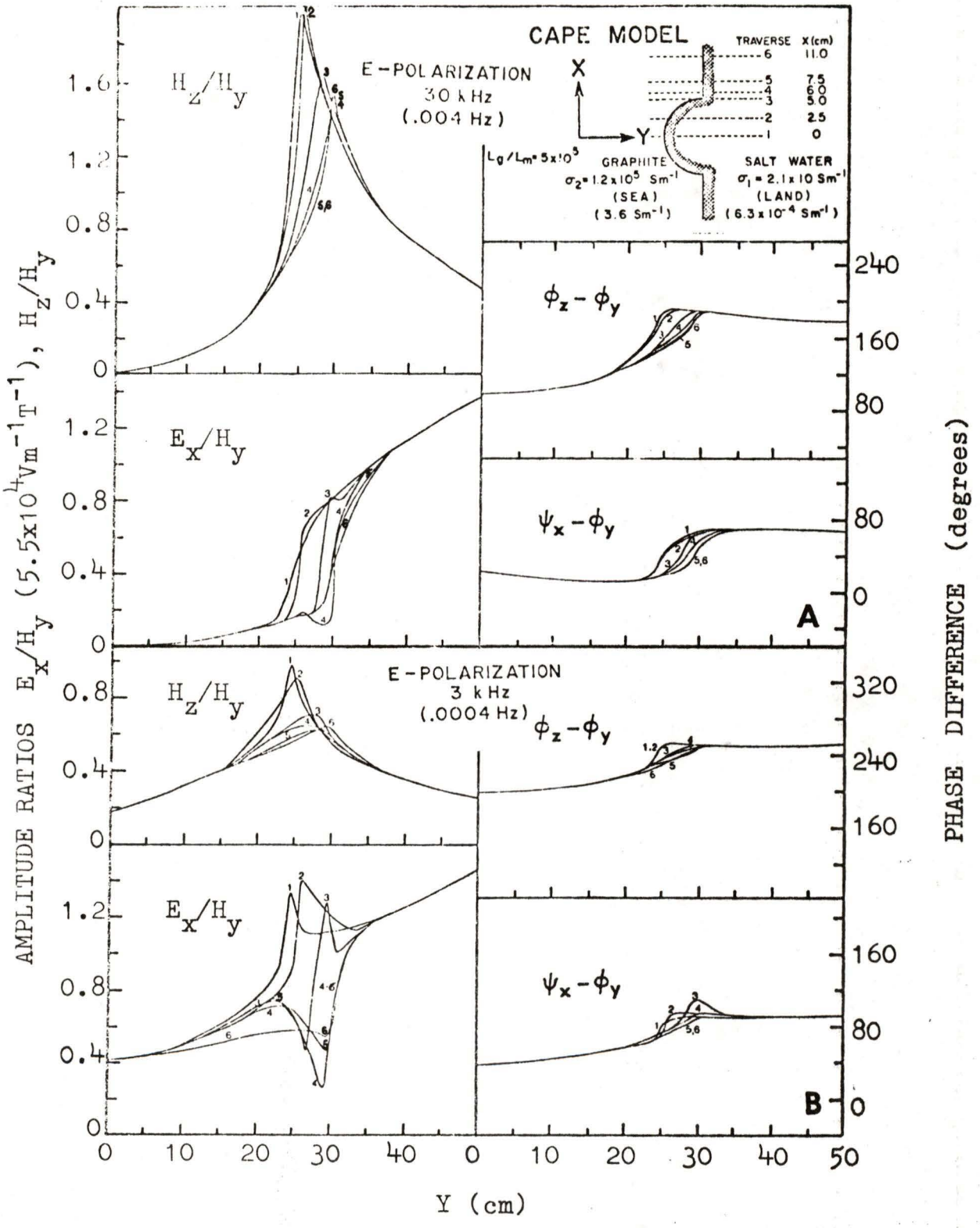


Fig. 12. Amplitude ratios $H_z/H_y$, $E_x/H_y$ and phase differences $\phi_z - \phi_y$, and $\psi_x - \phi_y$ along six traverses over the cape model (sloping-floor ocean) for the E polarization for frequencies of 30 and 3 kHz.

that at y = 45 cm (or at a distance of approximately one and a half diameters of the cape or the bay from the straight coastline), $E_x/H_y$ has approximately the same value (1.2 units. N.B. this is not the reference $E_x/H_y$ value which is 1.7 units) for both models and for each frequency.

The apparent resistivity profiles for traverses over the cape model for the E polairzation case are shown in Fig. 13. The frequency effect discussed for the bay model is still present. At both frequencies, $\rho_a$ along the coast of the cape is fairly constant (this extends to the point at which traverse 3 crosses the coastline). However, at approximately 1 cm from the cape along the coast, $\rho_a$ decreases by about one order of magnitude. Hence, the apparent resistivity profiles of the bay and cape models indicate that $\rho_a$ along the coastline is very sensitive to the coastline irregularities.

## 3.3 Analogue Model Study of the Cape and Bay Shaped Coastlines for a Constant Depth Ocean (E Polarization)

The constant depth ocean models (hereafter abbreviated as CDO models) employed a graphite plate 3 mm thick while the sloping-floor ocean models (hereafter abbreviated as SFO models) employed a wedged shaped plate changing in thickness from 0 mm to 3 mm in a distance of 20 cm. Analogue model measurements, for the E polairzation and 30 kHz, for the constant depth ocean bay and cape models are presented in Figs. 14 and 15, respectively. Field components are shown for the same six traverses as described in section 3.2. It is apparent that the various enhancements of the magnetic field components in the CDO models are larger than for the SFO models. Further, the anomalies are seen to have much more acute

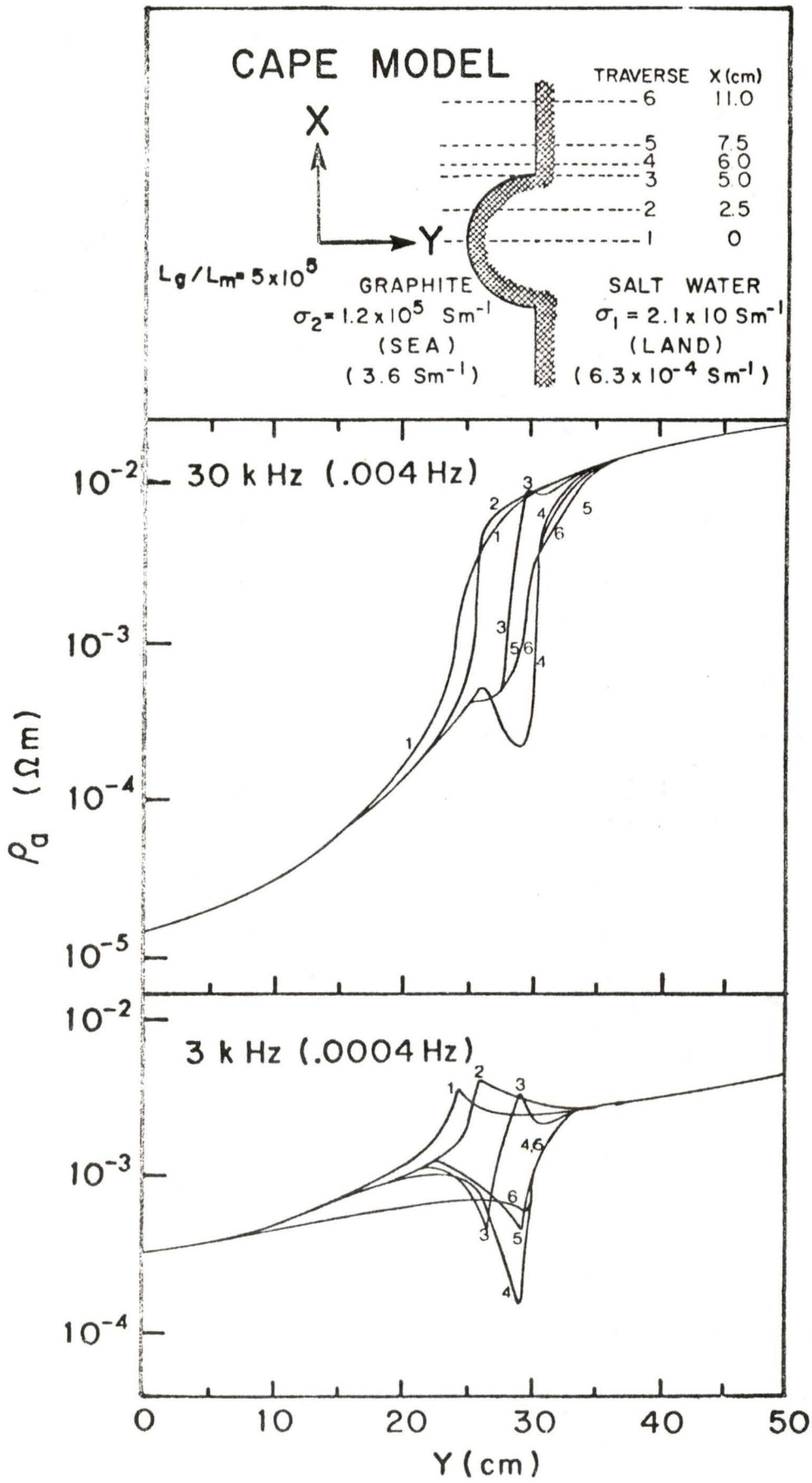


Fig. 13. Apparent resistivity along six traverses over the cape model (sloping-floor ocean) for the E polarization for frequencies of 30 and 3 kHz.

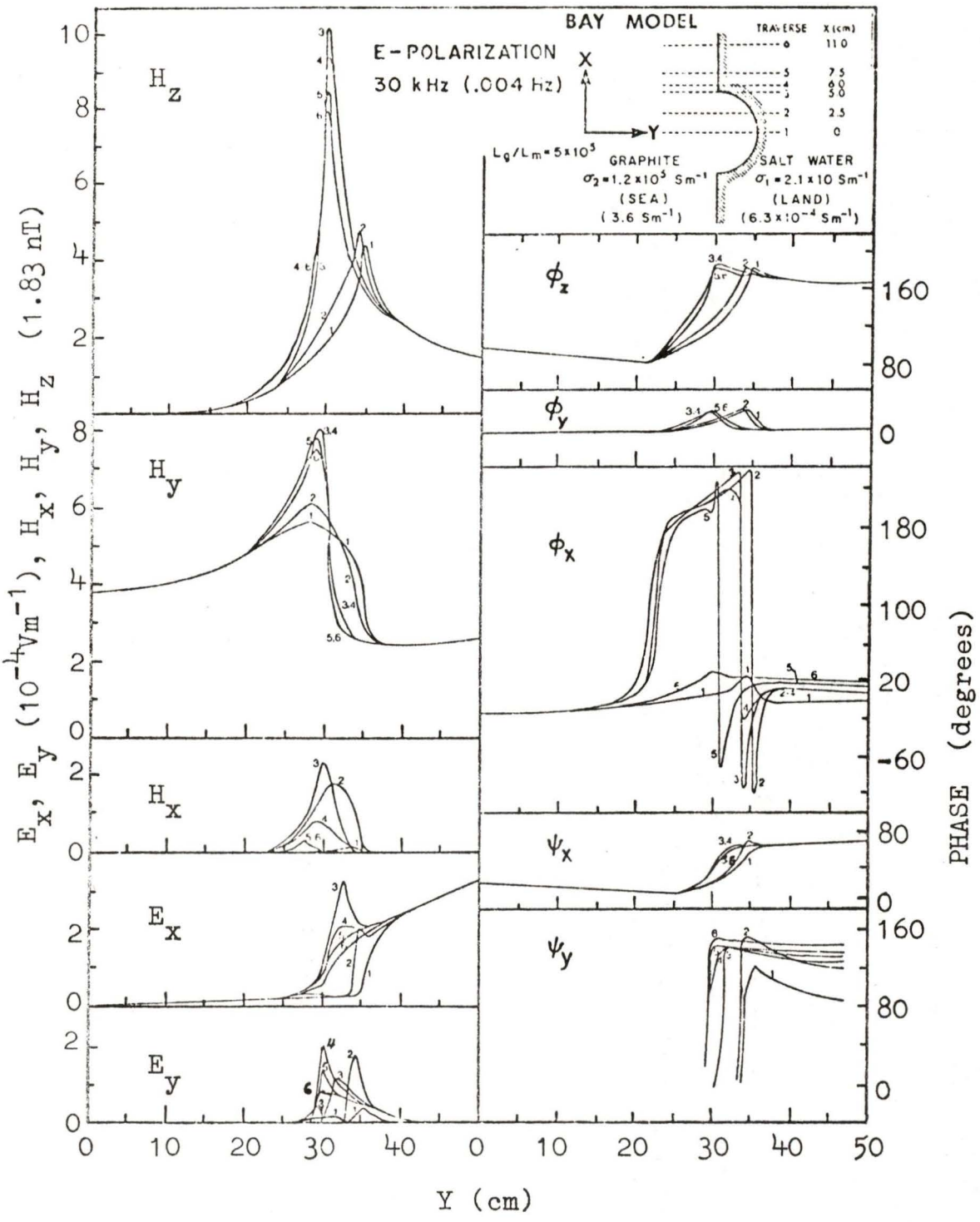


Fig. 14. Amplitudes and phase angles of the electric and magnetic field components along six traverses over the bay model (constant depth ocean) for the E polarization for a frequency of 30 kHz.

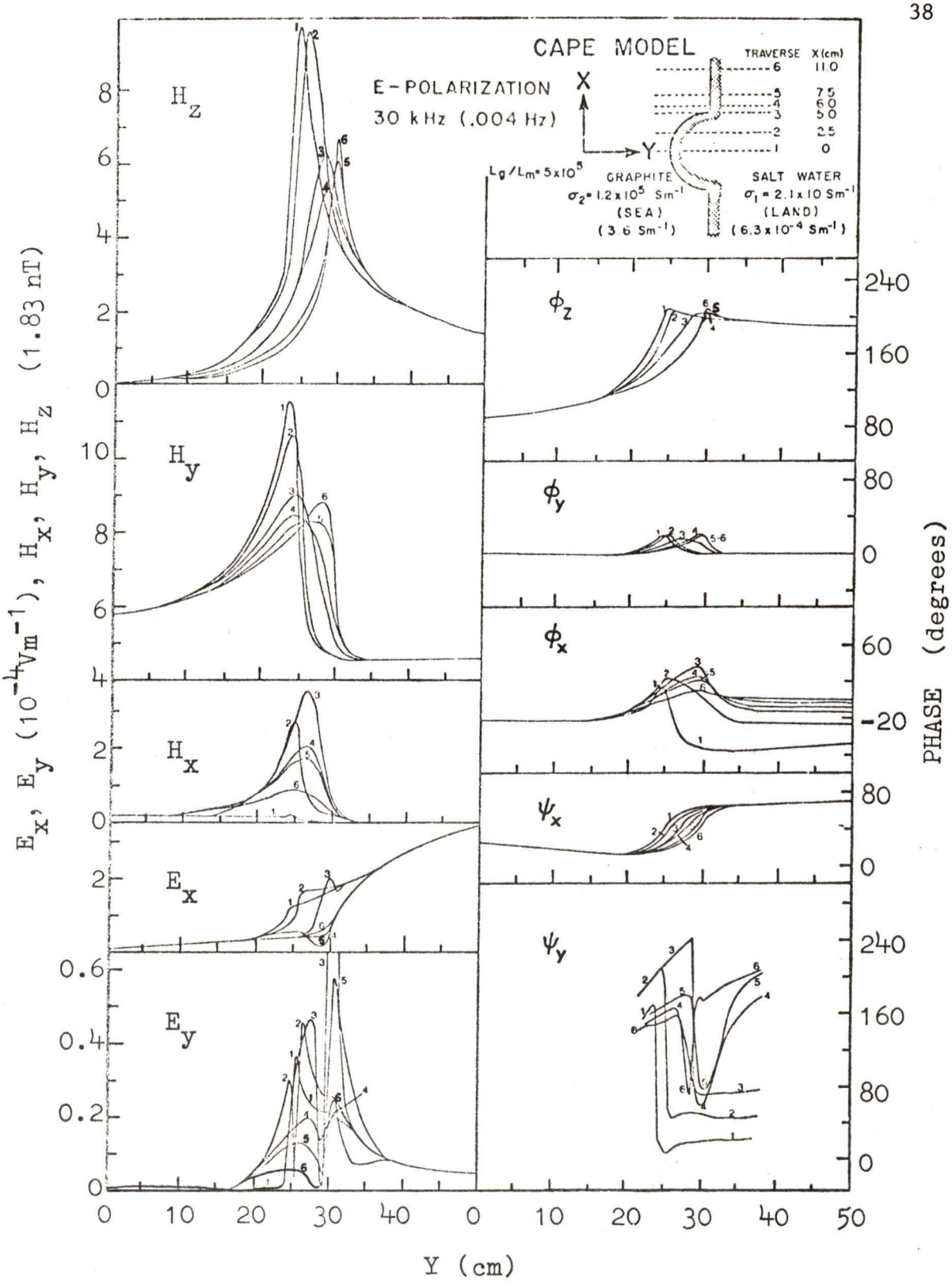


Fig. 15. Amplitudes and phase angles of the electric and magnetic field components along six traverses over the cape model (constant depth ocean) for the E polarization for a frequency of 30 kHz.

changes at or around the coast in the CDO cases. In particular, the $H_z$ enhancements for traverses 1 and 2 in the CDO bay model show definite sharp peaks at the coastline. The spatial variations in the phases $\phi_z$, $\phi_y$ and to some extent $\psi_y$, are very similar for the CDO and the SFO models of the same coastline contour. However, $\phi_x$ goes through a much larger shift in the SFO case for the bay model than for the cape model. The $E_x$ component and the corresponding phase $\psi_x$ are apparently not sensitive to the two types of ocean models. The $E_y$ anomaly over the straight coast is seen much more enhanced for the CDO bay model than for the cape model (compared to the respective SFO models). But, for traverses intersecting the bay coastline, the $E_y$ maxima remain the same as in the SFO case.

## 3.4 Analogue Model Study of the Cape and Bay Shaped Coastlines (H Polarization)

For the H polarization case, the electric field of the inducing source is perpendicular to the straight portion of the coastline. This condition is achieved in the laboratory by simply repositioning the bay or cape model so that the straight coastline is parallel to the y-direction, at x = 30 cm). For this polarization, measurements of the amplitudes and phase angles of the electric field components over the bay and cape models are shown in Figs. 16-21. Results along traverses 1 to 6 with y-coordinates equal to 0, -2.5, -5.0, -6.0, -7.5, and -11.0 cm are presented.

The analogue model results for traverses over the bay model for the case of sloping-floor ocean for frequencies of 30 and 3 kHz are presented in Figs. 16 and 17 respectively. $H_y$ and $H_x$ show only small enhancements for all traverses at 30 kHz. $H_z$ too has much smaller enhancements for this H polarization than for the E polarization case. For the

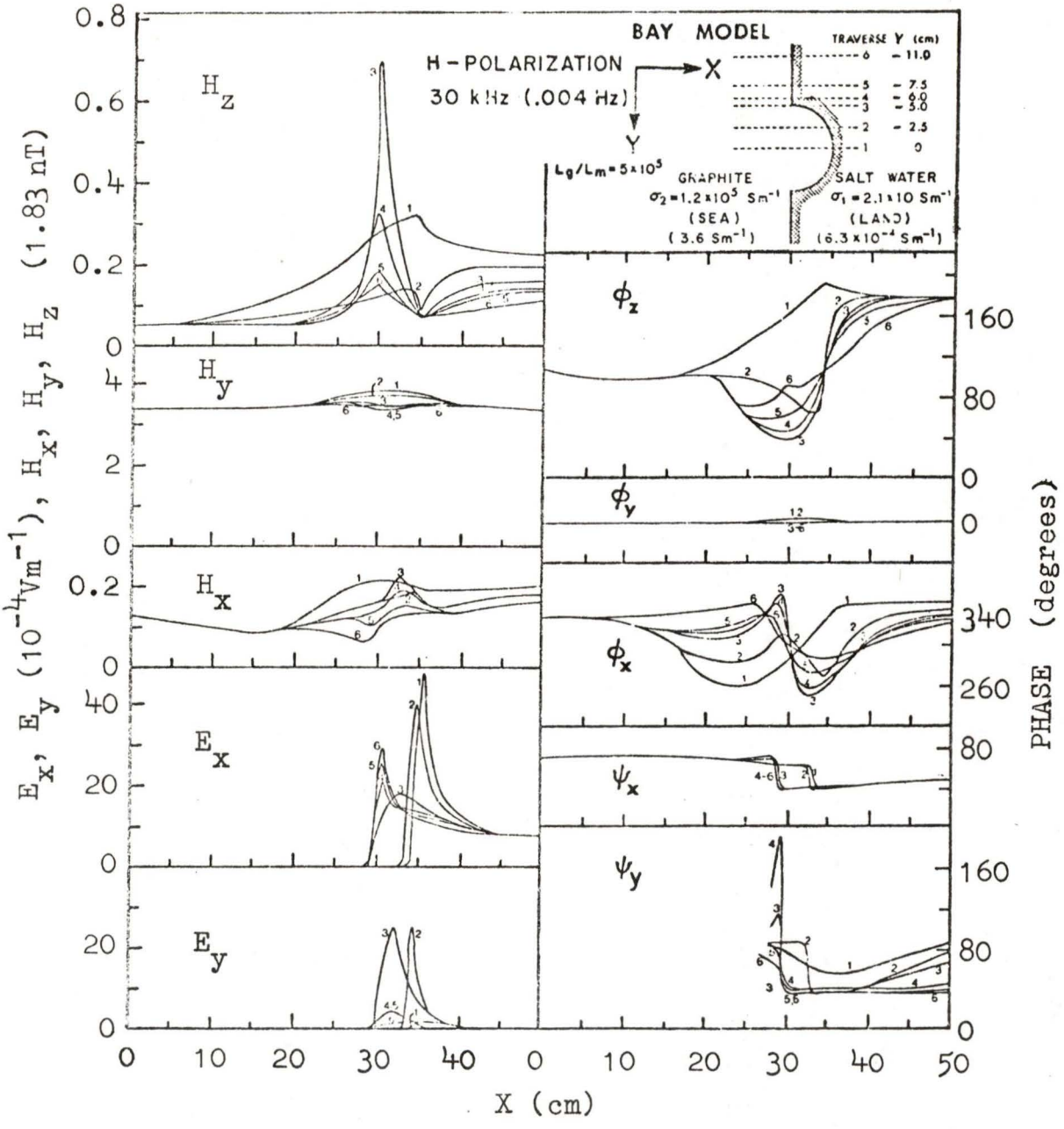


Fig. 16. Amplitudes and phase angles of the electric and magnetic field components along six traverses over the bay model (sloping-floor ocean) for the H polarization for a frequency of 30 kHz.

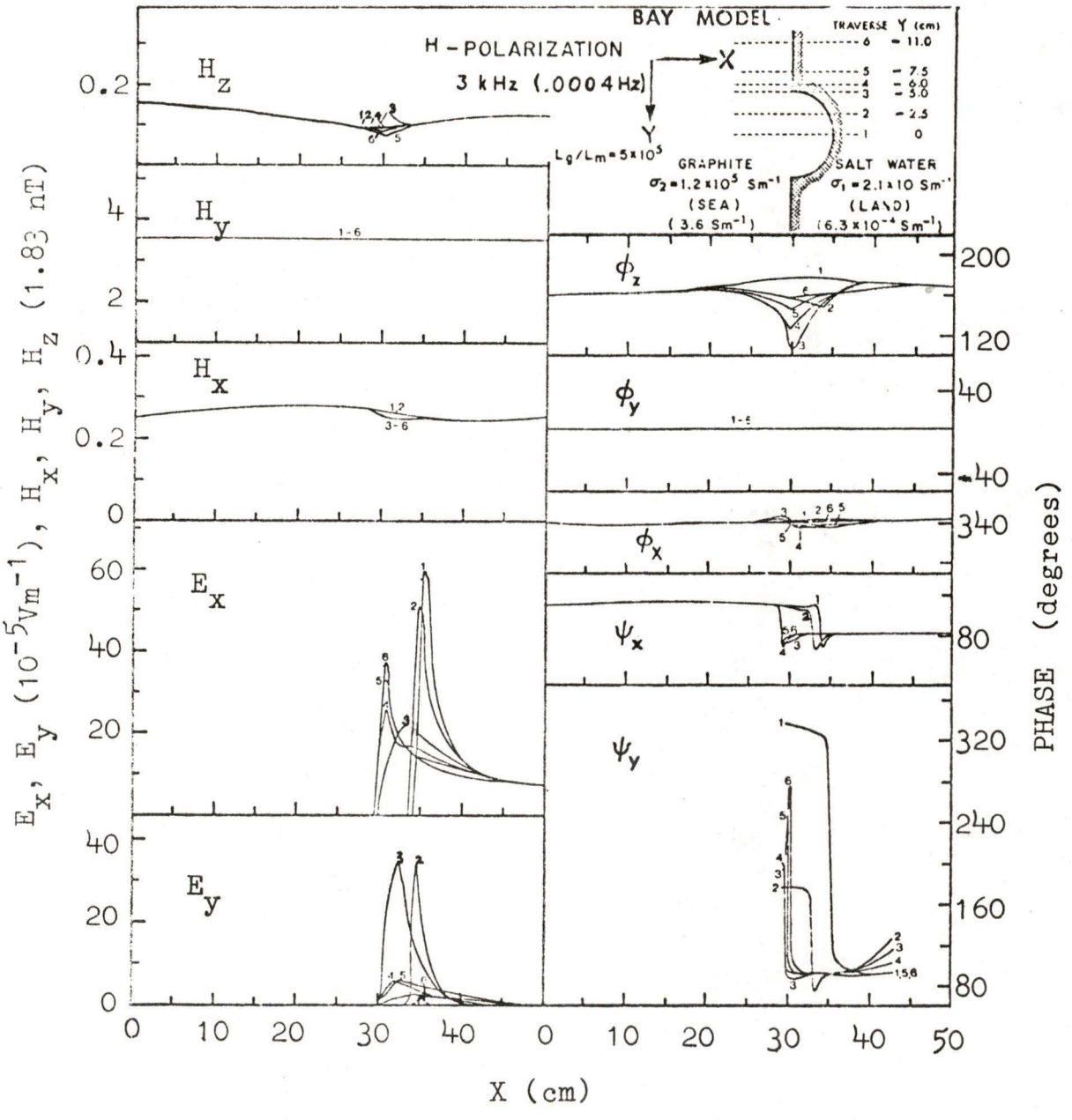


Fig. 17. Amplitudes and phase angles of the electric and magnetic field components along six traverses over the bay model (sloping-floor ocean) for the H polarization for a frequency of 3 kHz.

$H_z$ component for 3 kHz, there are depressions instead of enhancements at the coastline for traverses 5 and 6. Depressions also appear in the $H_z$ component for 30 kHz along a line tangential to the bay and parallel to the y-axis. It is seen that for both frequenceis, the largest enhancement in $H_z$ occurs for traverse 3 (similar to the E polarization case). Maximum enhancement in $E_x$ occurs for traverse 3 at the coastline of the bay for 30 kHz, indicating that induced currents tend to follow the contour of the coastline. This is also indicated by the $H_x$ and $H_y$ enhancements at the coastline for traverses 1 and 3.

The electric field components have the same pattern of spatial variations for frequencies of 30 and 3 kHz. $E_x$ shows maximum enhancements at the coastline except for traverse 3 where the $E_x$ maximum is shifted towards the landward side. $E_y$ has large anomalies at the coastline for traverses 2 and 3, and much reduced anomalies for traverses 1, 4, 5, and 6. This indicates the deflection of induced current along the bay coastline and in the vicinity of the corner of the bay. For both frequencies studied, the electric field enhancements for the H polarization case are an order of magnitude larger than for the E polarization case.

The analogue model results for traverses over the cape model for the case of sloping-floor ocean for frequencies of 30 and 3 kHz are presented in Figs. 18 and 19 respectively. The magnetic field components show much smaller coastline anomalies for 3 kHz than for 30 kHz, while both the amplitudes and phases for the two electric field components are very similar for the two frequencies. $H_z$ and $H_x$ show larger anomalies for the H polarization than for the E polarization. However, $H_y$ is not at all affected by the cape for 3 kHz and only slightly affected for 30 kHz.

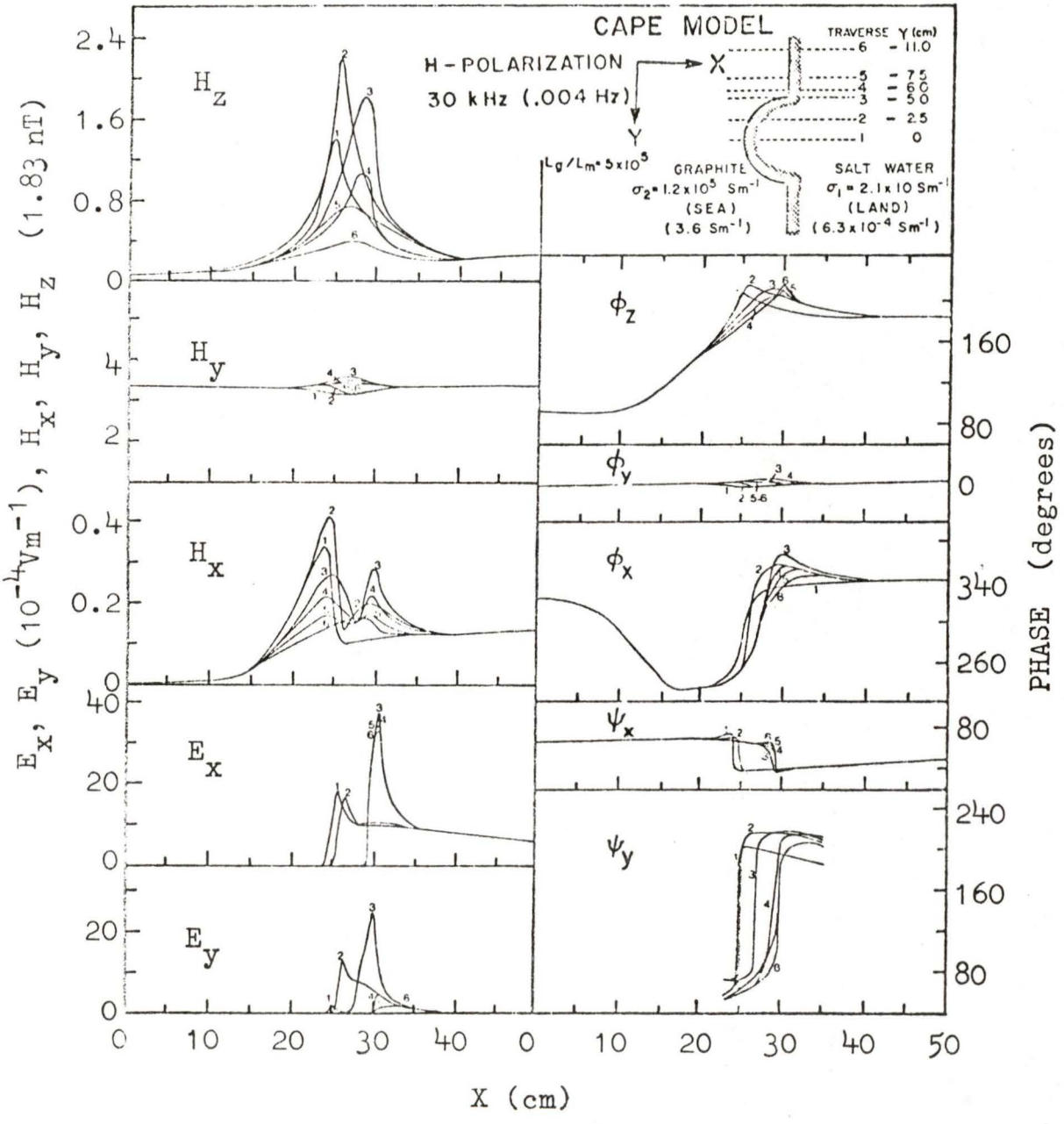


Fig. 18. Amplitudes and phase angles of the electric and magnetic field components along six traverses over the cape model (sloping-floor ocean) for the H polarization for a frequency of 30 kHz.

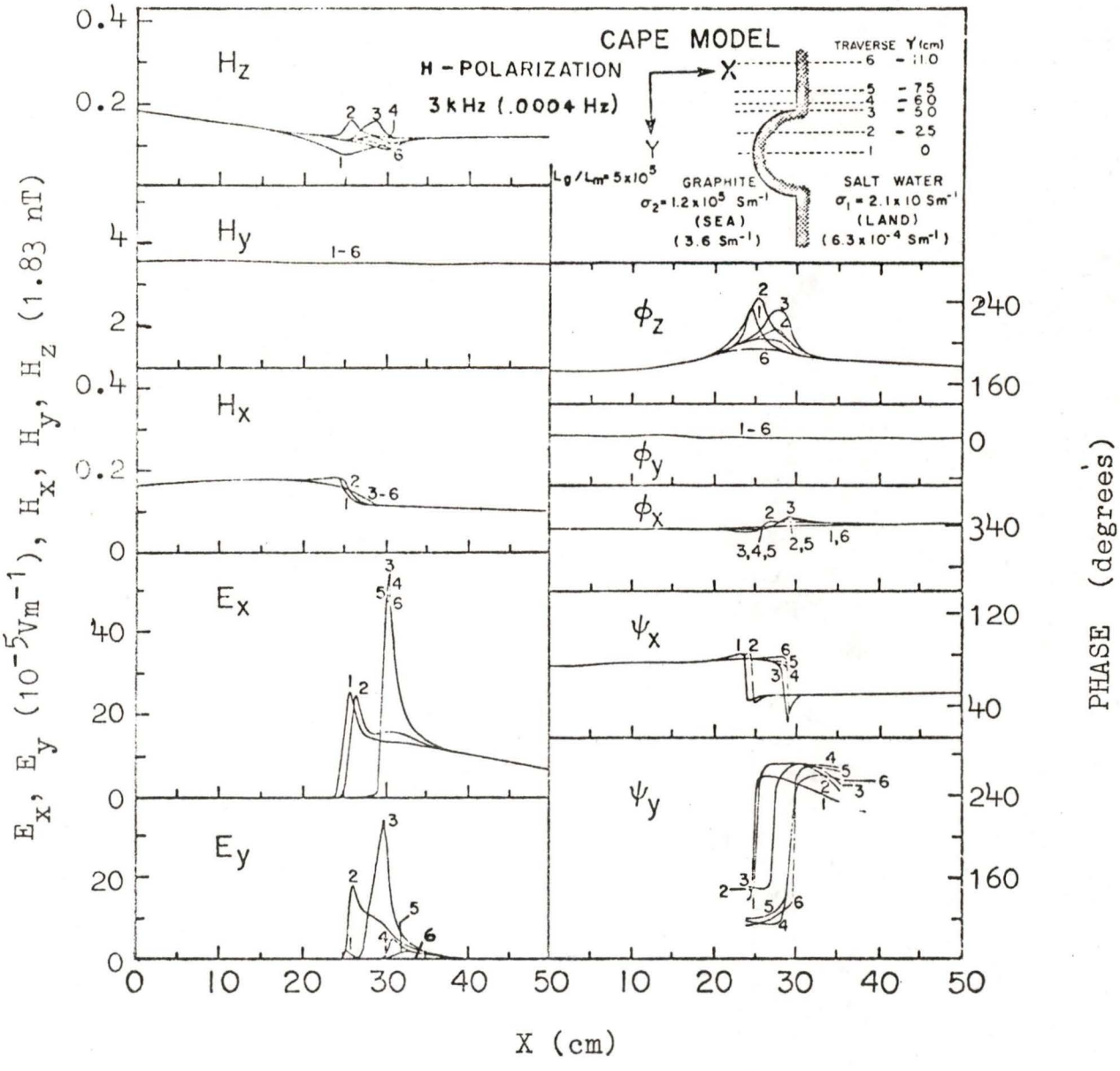


Fig. 19. Amplitudes and phase angles of the electric and magnetic field components along six traverses over the cape model (sloping-floor ocean) for the H polarization for a frequency of 3 kHz.

The $H_z$ maxima in 4, 5, and 6 for the H polarization are shifted seaward (note that for the E polarization case, the $H_z$ maxima for traverses 3, 4, and 5 were also shifted seaward). $H_x$ in Fig. 18 has a rather interesting feature. In addition to the maxima at the coastline, traverses 3, 4, and 5 have second maxima at a distance of approximately one cape radius from the coastline. For traverse 6, the two maxima merge to form a single maximum at roughly a quarter of the cape radius from the coastline.

Large $E_y$ anomalies are seen at the coastline for traverses 2 and 3 indicating that induced electric current is perturbed by the presence of the cape. For this polarization, the $E_x$ maxima are approximately a factor of 2 larger for traverses over the straight coastline (traverses 4, 5, 6) than for traverses over the central region of the cape (traverses 1 and 2); while for the bay model, the $E_x$ maxima at the straight coastline are half as large as those for traverses through the central region of the bay. A rapid shift of approximately 40° in the phase $\psi_x$ upon crossing the coastline is common for both models for the two frequencies considered.

The H polarization analogue model results for traverses over the bay and the cape models with CDO's (constant depth oceans), for a frequency of 30 kHz, are shown in Figs. 20 and 21 respectively. For this polarization, it appears that for both the bay and the cape models, the spatial variation patterns in the amplitude and phase angles of the magnetic and electric field components are similar for both types of ocean models. Similar to the SFO model results, the magnetic field enhancements for both the cape and bay models are larger for the E polarization case

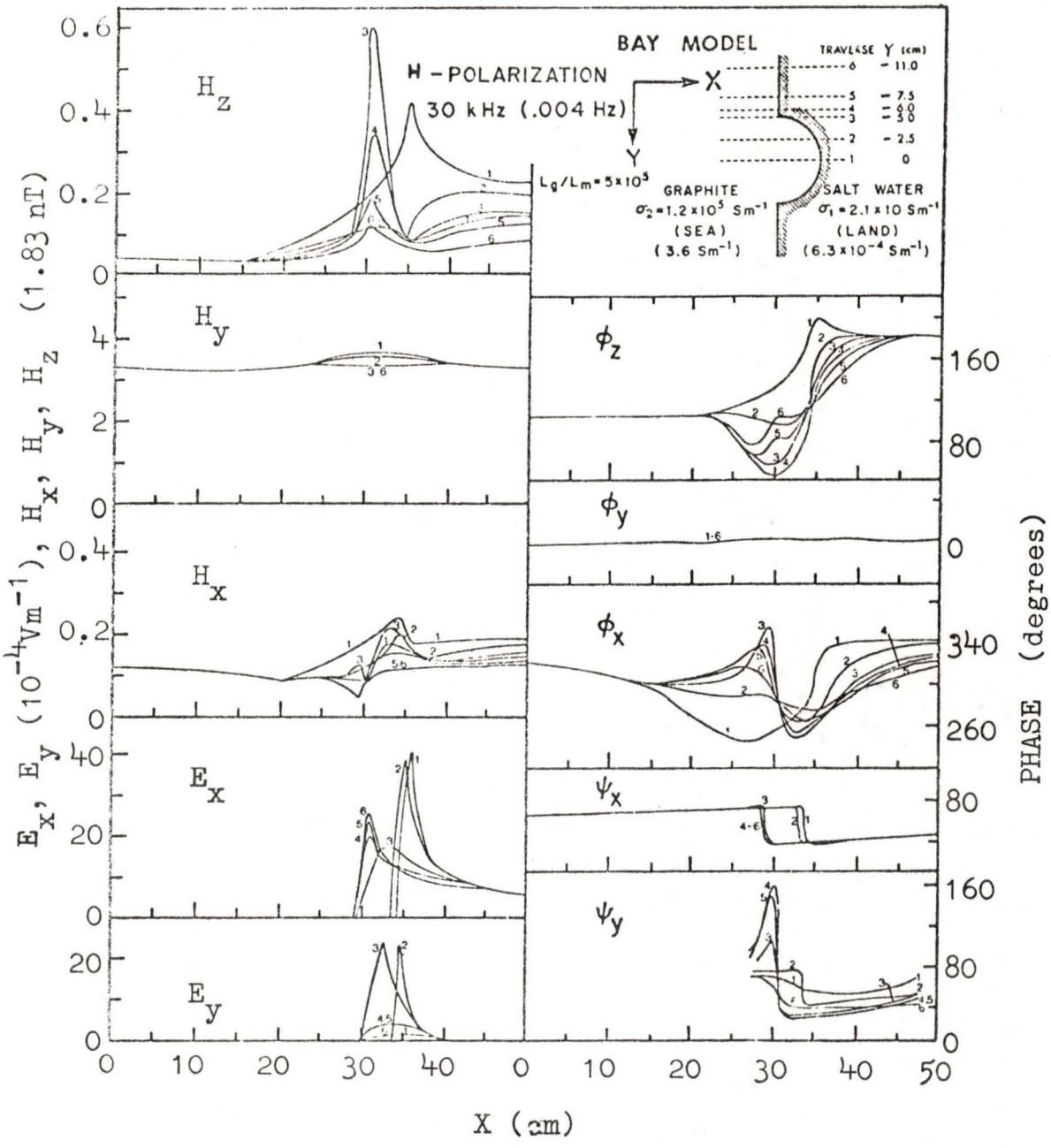


Fig. 20. Amplitudes and phase angles of the electric and magnetic field components along six traverses over the bay model (constant depth ocean) for the H polarization for a frequency of 30 kHz.

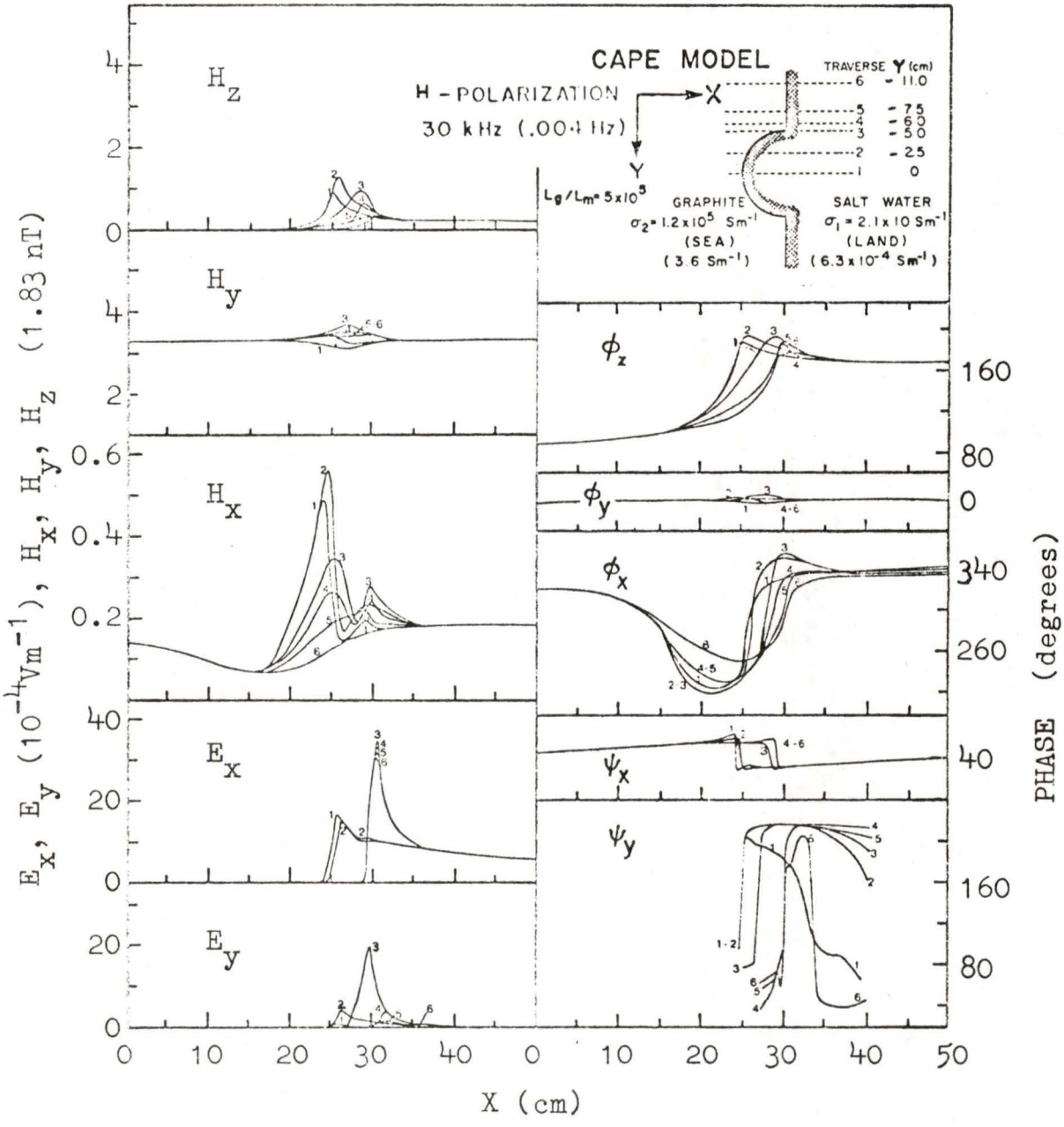


Fig. 21. Amplitudes and phase angles of the electric and magnetic field components along six traverses over the cape model (constant depth ocean) for the H polarization for a frequency of 30 kHz.

than for the H polarization case, while the electric field enhancements are larger for the H polarization case than for the E polarization case.

## 3.5 Analogue Model Study of a Bay Adjacent to a Cape for a Sloping-Floor Ocean

To simulate a coastline with a bay immediately adjacent to a cape, a model was constructed by cutting one side of a graphite plate to have the contour shown in the insert of Fig. 22. The cape radius and bay radius are each 5 cm (simulating a bay and a cape each with a diameter of 50 km). The scaling factors used in the earlier models apply here as well. Analogue model measurements of the field components $H_z$, $H_y$ and $E_x$ and their phase angles are presented in Fig. 22 along eleven traverses over the bay-cape model with sloping floor ocean.

Comparing the results in Fig. 22 with the measurements for the simple bay and cape models in Fig. 8 and 10, it is seen that the $H_z$ enhancements in the bay-cape model along traverses 1, 2, 3, and 4 are similar to those along traverses 4, 3, 2, and 1 in the cape model, while results along traverses 8, 9, 10 and 11 are similar to those along traverses 1, 2, 3, and 4 in the bay model. This similarity applies to the other two field components $H_y$ and $E_x$ and the phases $\phi_z$, $\phi_y$ and $\psi_x$ as well. The $H_z$ enhancement for traverse 6 for the cape-bay model appears to be the average of the enhancements for traverses 3 for the bay (Fig. 8) and the cape (Fig. 10) models separately.

The $H_z/H_y$ ratios along traverses 4 and 9 for the bay-cape model are found to be very similar to those along traverse 1 for the cape and the bay models, respectively (in the 30 kHz SFO case). Fig. 23 shows these two profiles (in solid lines) together with the $H_z/H_y$ curves along a

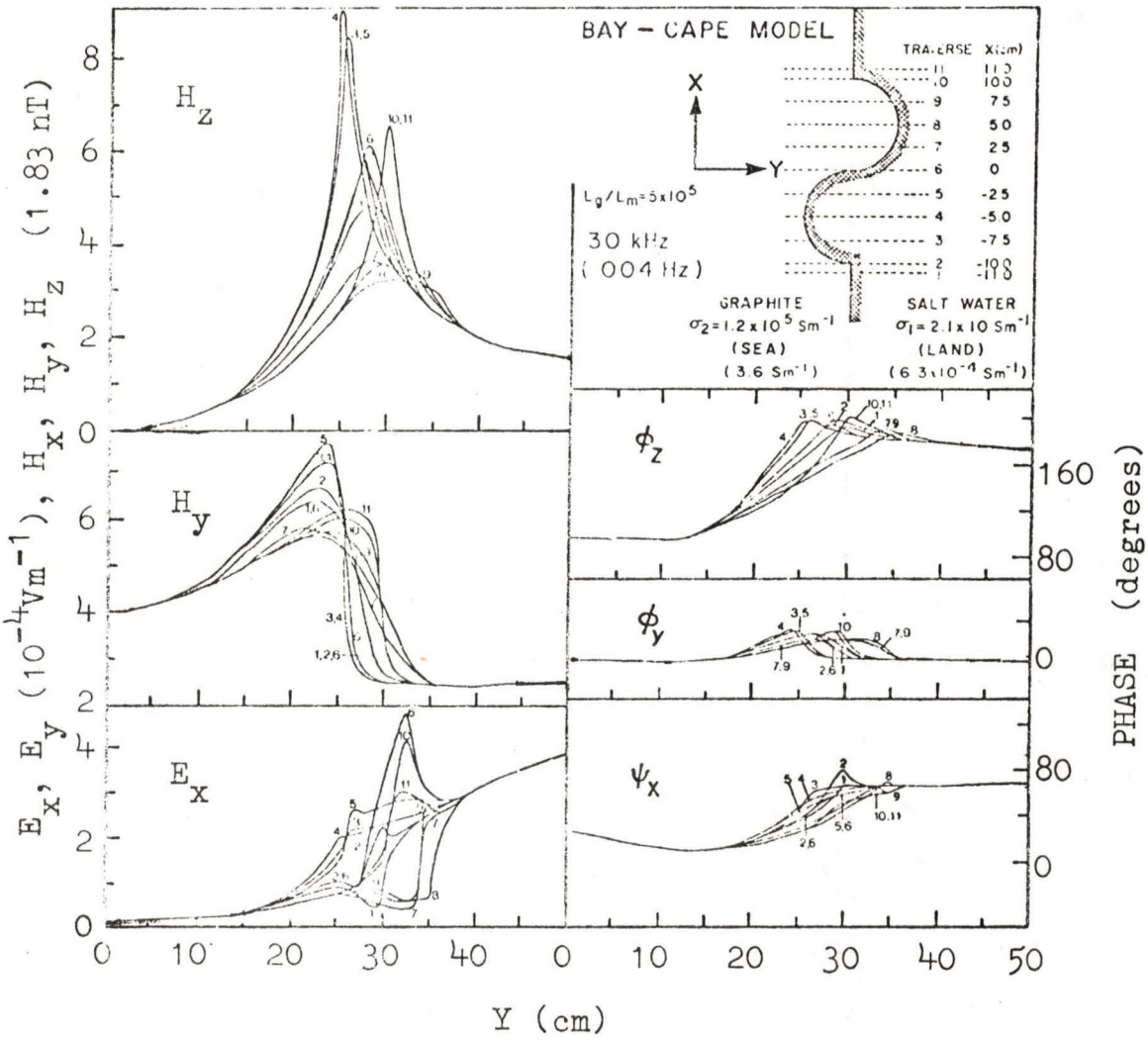


Fig. 22. Amplitudes of $H_z$, $H_y$ and $E_x$ and the corresponding phases along eleven traverses over the bay-cape model for the E polarization for a frequency of 30 kHz.

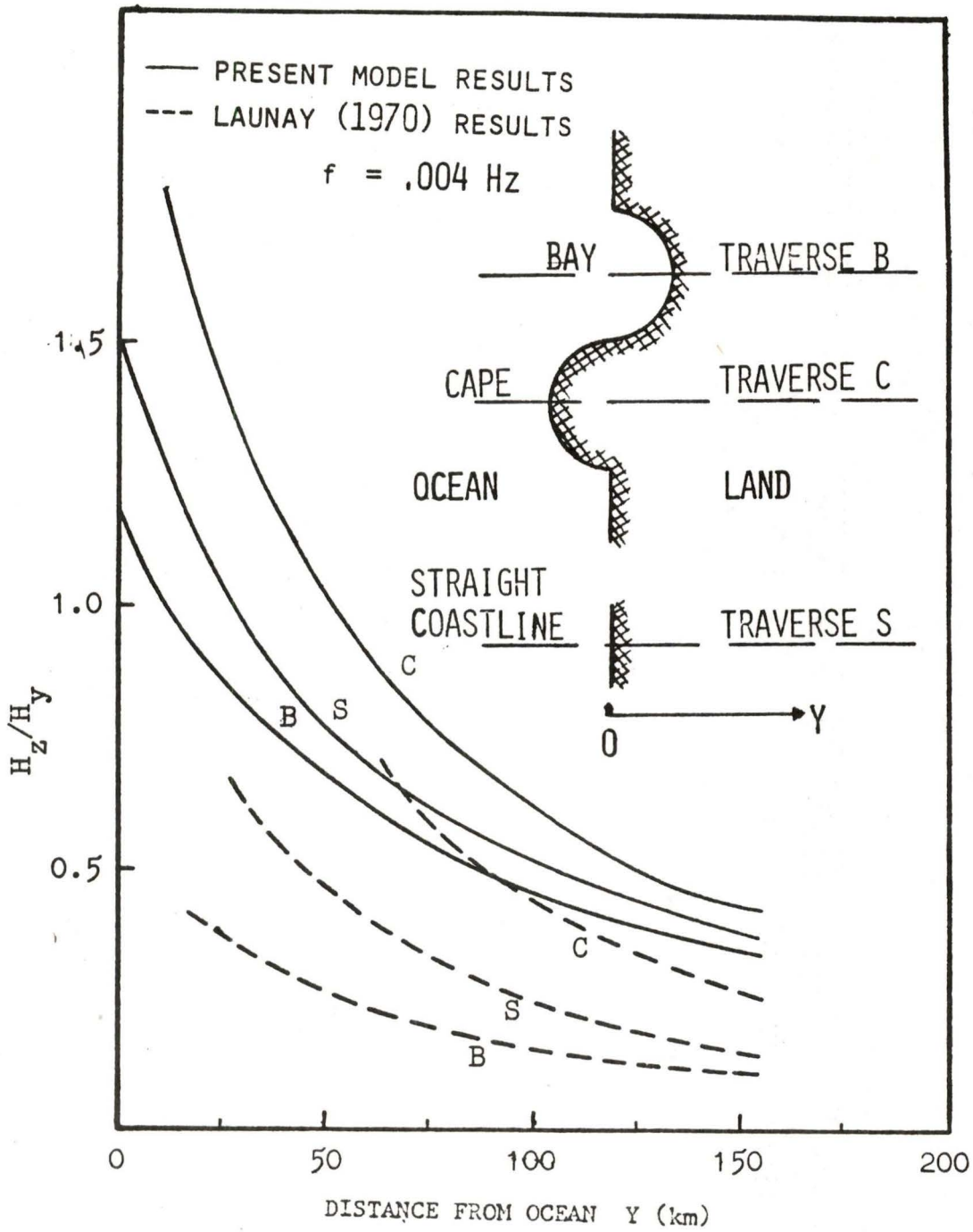


Fig. 23 A comparison of the coast effect $H_z/H_y$ for the present models and the Launay (1970) models.

traverse crossing a straight coastline (a model with a straight coastline and sloping-floor ocean was constructed for this). Both present models simulate oceans changing in depth from 0 km to 1.5 km in a distance of 100 km from the shore. Here y = 0 is chosen at the sea-land interface and the positive y-axis lies over land. The curves for each traverse are shifted so that y measures the distance from the interface. The laboratory model frequency is 30 kHz. Launay (1970) used a laboratory scaled model to study the coast effect over a coastline having a sinusoidal bay adjacent to a sinusoidal cape. The results of the coast effect along three chosen traverses are shown in Fig. 23 (in dashed lines) after modifications according to the procedure described by Dosso (1973) for comparing results obtained from two different analogue modelling systems each employing a different set of scaling factors. The frequency scaling factor in Launay's system is changed by a factor of 14.4 so that results in both models correspond to the same geophysical frequency of 0.004 Hz. Accordingly, Launay's length scaling factor is adjusted by a factor of 1/ 14.4. The Launay ocean depth becomes 1 km while the width of the bay or the cape is 150 km (a factor of 3 larger than for the present models). The conducitivity scaling factor remains unchanged. In each set of results, the coast effect is seen to be the largest in the case of a cape, medium for the straight coastline and least in the case of a bay. Comparing the present analogue model results with those of Launay (1970), it is seen that along each of the three traverses, C, S, or B, $H_z/H_y$ is smaller, as much as a factor of 3 at some locations for Launay's models. This could be attributed to one or more of the following differences between the Launay (1970) models and the present

models. First, Launay's cape-bay model has a constant ocean depth of 1 km and a conducting mantle at 130 km; a sloping-floor ocean case (0 to 1.5 km) is considered in the present model and the graphite layer at the bottom of the tank simulates a conducting layer 300 km beneath the surface. The nearby conducting mantle in Launay's (1970) models would considerably attenuate the magnitude of the $H_z/H_y$ curves over the landward side. Another major difference is that in Launay's model, the conductivity contrast between copper (a good conductor simulating the ocean) and air (essentially a perfect insulator simulating land) is virtually infinite while a realisitic finite difference between $\sigma_{ocean}$ and $\sigma_{land}$ is used in the present models. Other features differing for the two sets of models are the size of the bay and cape (3 times larger for Launay's models) and the basic contours (sinusoidal in Launay's and semi-circular in the present models). The total effect of the physical differences in the models would account for the differences in the results.

### 3.6 Analogue Model Study of an Elliptical Island Situated Near Various Continental Coastlines

The graphite plate used to simulate a sloping-floor ocean with a straight coastline treated in section 3.5 is considered further here. An elliptical hole with a semi-major axis of 10 cm and semi-minor axis of 5 cm was cut as depicted in the upper right portion of Fig. 24. The separation between the centroid of the ellipse and the straight coastline was 7 cm. When placed at the surface of concentrated salt solution, the graphite plate simulated a sloping-floor ocean with an elliptical island situated off a continental coastline. The bay and cape models were treated similarly. These three new models are shown in the insert of

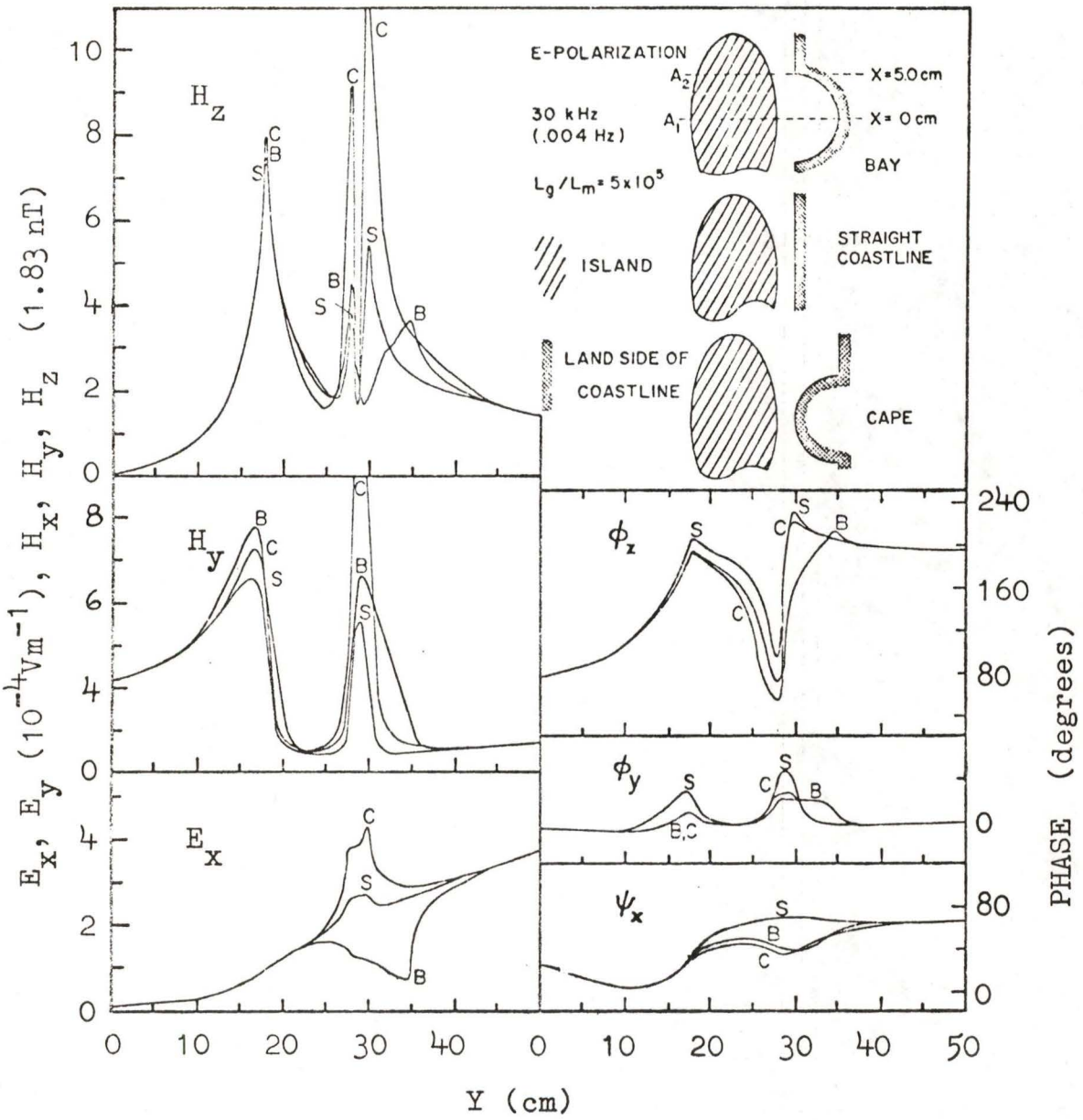


Fig. 24. Amplitudes of $H_z$, $H_y$ and $E_x$ and the phase angles $\phi_z$, $\phi_y$ and $\psi_x$ along traverse A1 (x = 0 cm) for an elliptical island situated off i) bay-shaped (B), ii) straight (S), and iii) cape-shaped (C) coastlines for the E polarization for a frequency of 30 kHz.

Fig. 24. Laboratory model measurements along 2 traverses (along x = 0 cm and 5.0 cm) are presented in Figs. 24 and 25 for the E polarization for a model frequency of 30 kHz.

Fig. 24 shows $H_z$, $H_y$, and $E_x$ and the corresponding phases along traverse A1 (x = 0 cm) which bisects the elliptical island along the minor axis. In the discussion that follows, the island coastline on the side facing the continental coastline is designated as island coastline 1, and the other on the seward side, island coastline 2. The presence of the bay or cape slightly increases the $H_z$ enhancement at the coastline 2. $H_z$ at coastline 1 is very much enhanced by the proximity of the tip of the cape. Together with the large $H_z$ anomaly at the continental coastline, this indicates that there is very large current density in the cape-island channel. The $H_z$ enhancement at the coastline of the bay is relatively unaffected by the presence of the island. The $H_y$ anomaly near coastline 2 is also enhanced in the presence of either the bay or the cape. The 180° change in $\phi_z$ about the centre of the island is related to the induced current deflected around the island (Nienaber et al., 1978). The phase $\phi_y$ shows very small changes even though $H_y$ has large enhancements near coastline 2 and over the channels.

Fig. 25 shows the result for traverse A2. The proximity of the corner of the bay becomes important in affecting the $H_z$, $H_y$ and $E_x$ anomalies near coastlines 1 and 2. The $H_z$ and $H_y$ enhancements at all the coastlines for the case of the straight coastline show little change from traverse A1 to A2, however, $E_x$ has a small depression for A2 instead of the slight enhancement for A1 over the channel as shown in Fig. 24. $E_x$ undergoes a large change from traverse A1 to A2 for both the bay and cape coastlines.

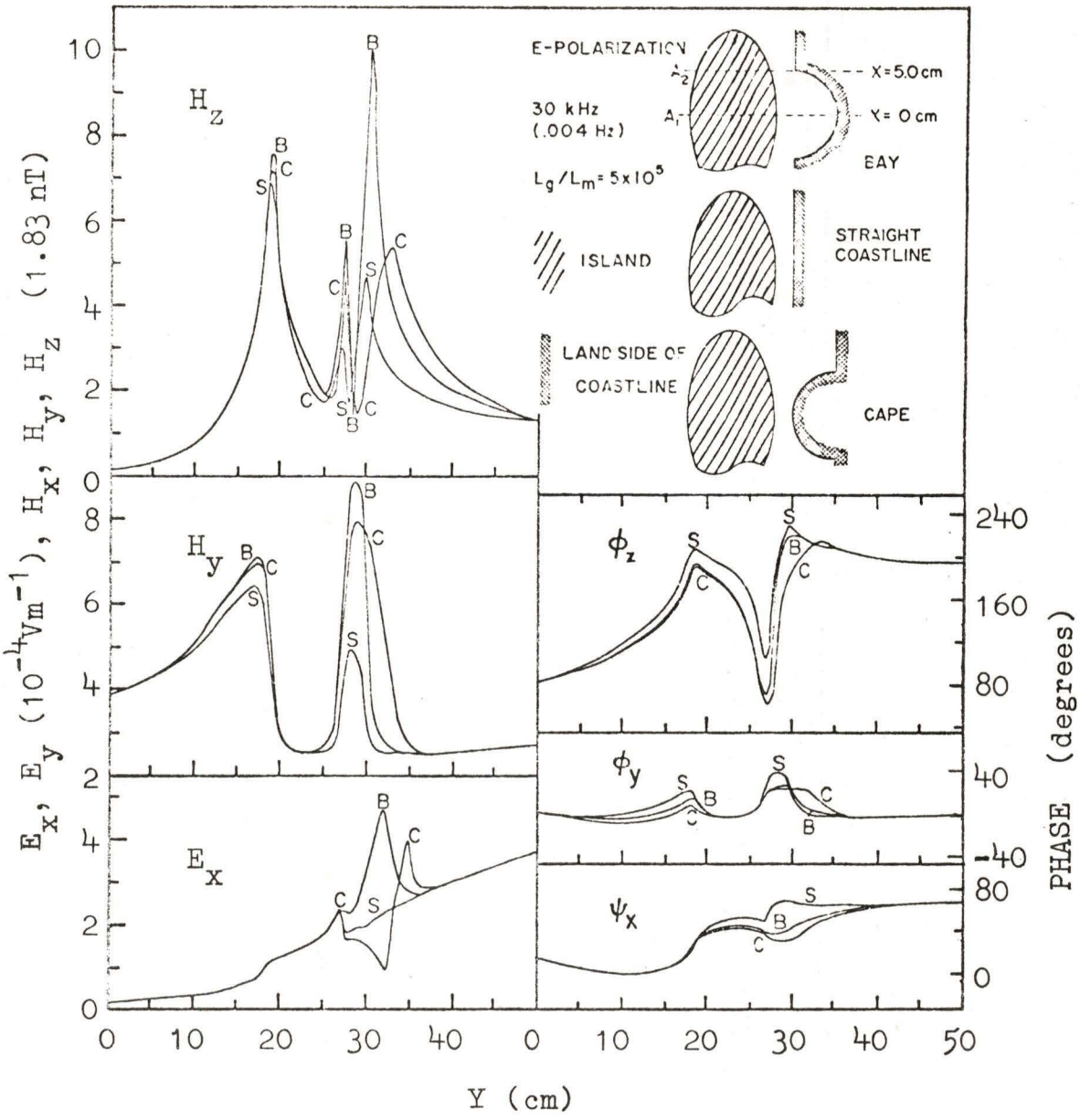


Fig. 25. Amplitudes of $H_z$, $H_y$ and $E_x$ and the phase angles $\phi_z$, $\phi_y$ and $\psi_x$ along traverse A2 (x = 5.0 cm) for an elliptical island situated off i) bay-shaped (B), ii) straight (S), and iii) cape-shaped (C) coastlines for the E polarization for a frequency of 30 kHz.

In the case of the bay, a large enhancement along A2 replaces the depression along A1; while in the case of the cape, there is a second maximum along A2 near the vicinity of the continental coastline and the enhancement near the coastline 1 decreases by about one half.

All models presented in this chapter are of idealized simple shapes. But, the various results obtained from the laboratory measurements would serve as a useful tool in examining more complicated coastline contours.

# CHAPTER 4

## ANALOGUE MODEL AND FIELD STATION RESULTS FOR THE SAN JUAN BAY REGION

Figure 26 shows the location of San Juan Bay along the Juan de Fuca Strait which separates southeastern Vancouver Island from Washington State, U.S.A. Analogue model measurements for a laboratory model of the San Juan Bay region were carried out for frequencies of 30 and 3 kHz for E and H polarizations. The E polarization in this model is defined to be that of the electric field of the inducing source parallel to a straight line which approximates the moderately winding west coast of Vancouver Island in the San Juan Bay region. This line is almost parallel to the local magnetic east-west direction. The H polarization is simply the case in which the electric field of the source is perpendicular to this line.

Simultaneous geomagnetic observations were recorded at two of the three field stations operated in the San Juan Bay area in October, 1977. The data obtained was analysed and the results compared with the model measurements.

### 4.1 Analogue Model Study of the San Juan Bay Region

A model of the Juan de Fuca Strait and the nearby shallow ocean was constructed using a graphite plate. The conductivity scaling factor was the same as for the previous models. However, a different length scaling factor of $L/L' = 10^{-5}$ was chosen to permit a detailed study of

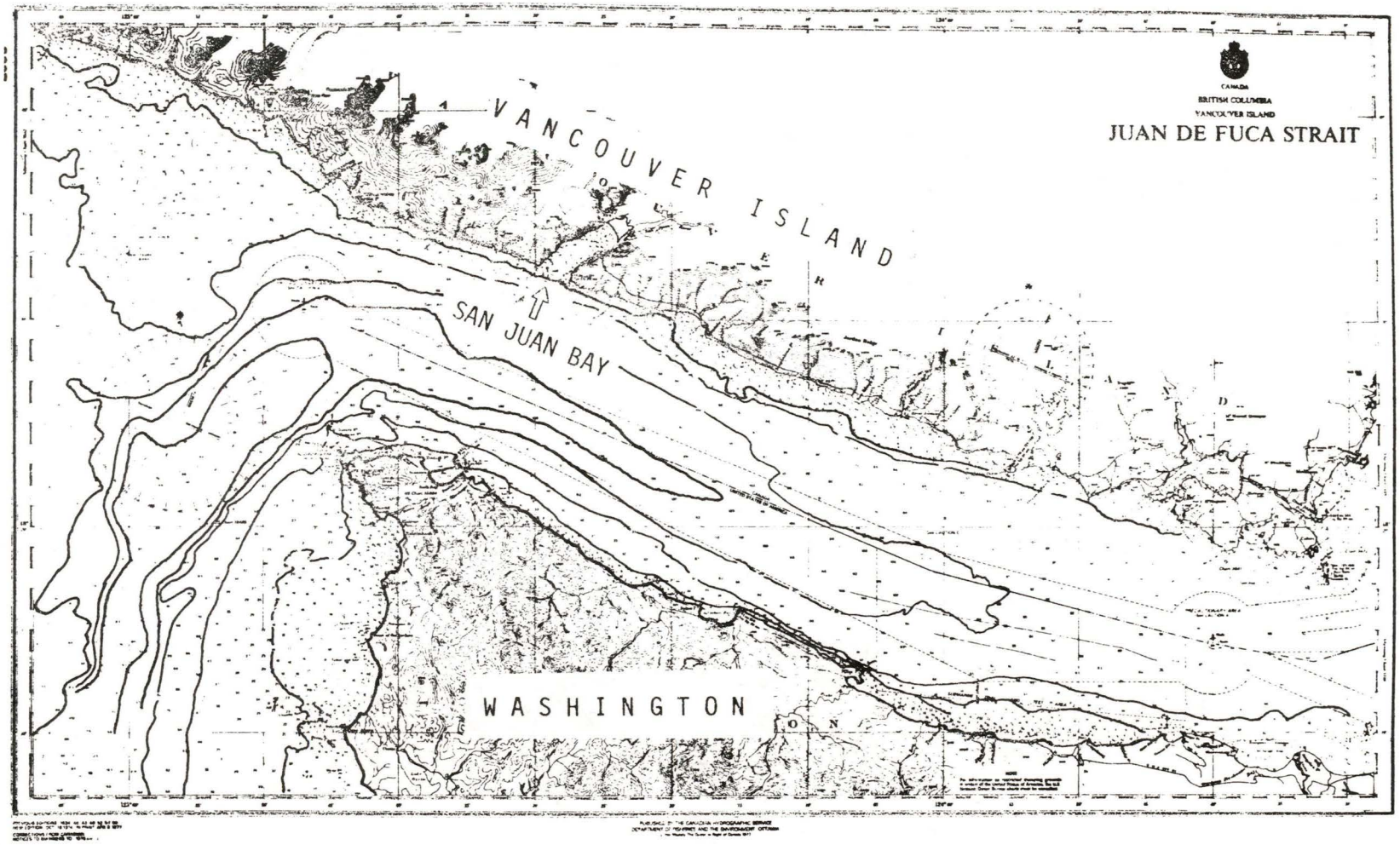


Fig. 26. Map of Juan de Fuca Strait showing the location of San Juan Bay.

a rather small bay and a shallow ocean. For this length scaling factor, 1 cm in the model represents 1 km in the geophysical scale. San Juan Bay has dimensions roughly 7.5 cm long and 2 cm wide in the model. A graphite plate, 1 m long, 0.5 m wide and 3 mm thick, was used to model the Strait with the bay structure at the middle. The graphite model was machined to have the appropriate thickness to simulate the bathymetric contours as indicated in Fig. 27. For the frequency scaling factor $f/f' = 3 \times 10^5$ used for the San Juan Bay model, frequencies of 30 and 3 kHz simulate frequenceis of 0.1 and 0.01 Hz in the geophysical system. For the E polarization case, the two ends of the graphite model were electrically connected to the stainless steel sheets at the tank walls so as to minimize the end effect due to the limited size of the model.

Fig. 27 shows a simplified map of the Juan de Fuca Strait and indicates the position of the model traverses and the locations of the three field stations (SJ-San Juan Point, AH-Adze Head and GR-Gordon River). Analogue model measurements of the electric and magnetic field components along 14 traverses were made, but only the 7 indicated in Fig. 27 are selected for discussion. The coordinates of the traverses shown are for the E polarization case. Traverses T1 to T6 cover most of the bay area while T7 is approximately a distance of one "bay diameter" from T5.

Analogue model results of the amplitudes and phases of the electric and magnetic field components for a frequency of 30 kHz for the E polarization case are shown in Fig. 28 for the odd-numbered traverses and in Fig. 29 for the even-numbered traverses for the purpose of clearer presentation.

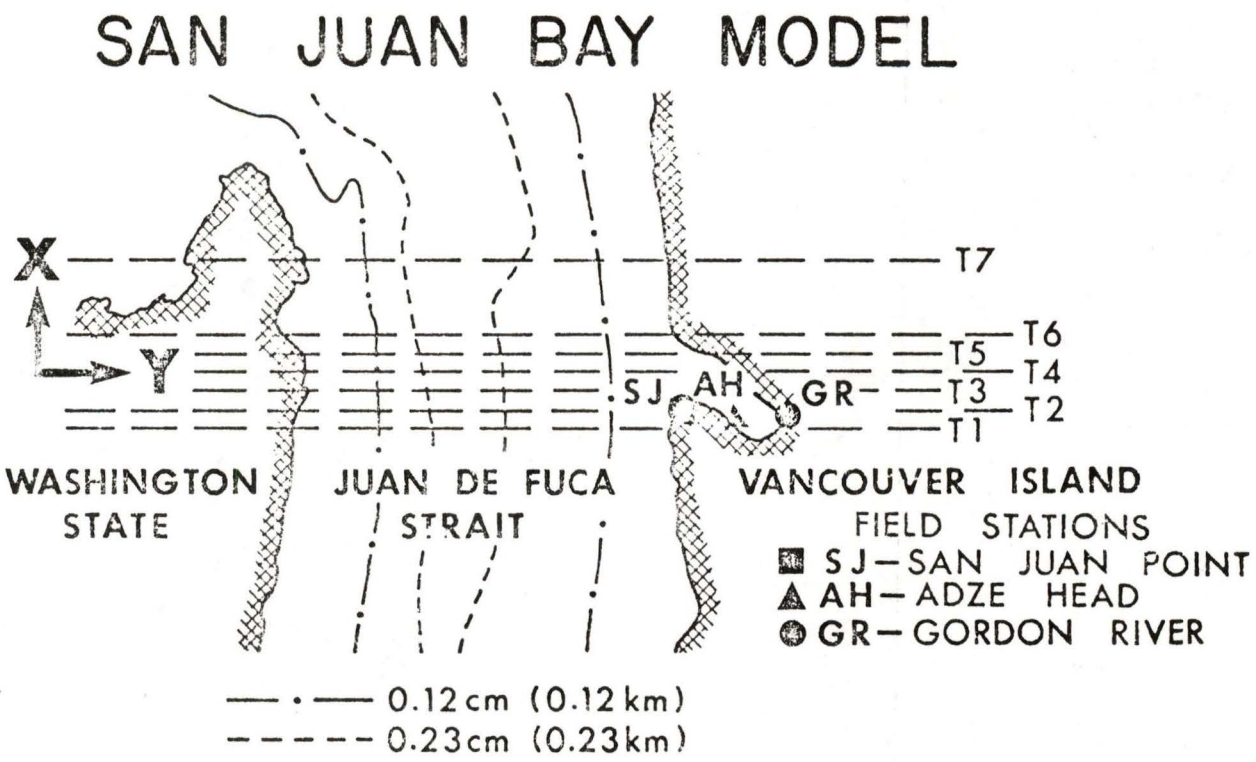


| | MODEL | GEOPHYSICAL |
|---|---|---|
| LENGTH | 1 cm | 1 km |
| FREQUENCY | 30 kHz | .1 Hz |
| $\sigma_1$ $Sm^{-1}$ (LAND) | 21 | $6.3 \times 10^{-4}$ |
| $\sigma_2$ $Sm^{-1}$ (SEA) | $1.2 \times 10^{5}$ | 3.6 |

| TRAVERSES | | |
|---|---|---|
| T1 ALONG | X = -3 cm | -3 km |
| T2 | -2 | -2 |
| T3 | -1 | -1 |
| T4 | 0 | 0 |
| T5 | 1 | 1 |
| T6 | 2 | 2 |
| T7 | 6 | 6 |

Fig. 27. Simplified map of the San Juan Bay region with model traverses and field station locations.

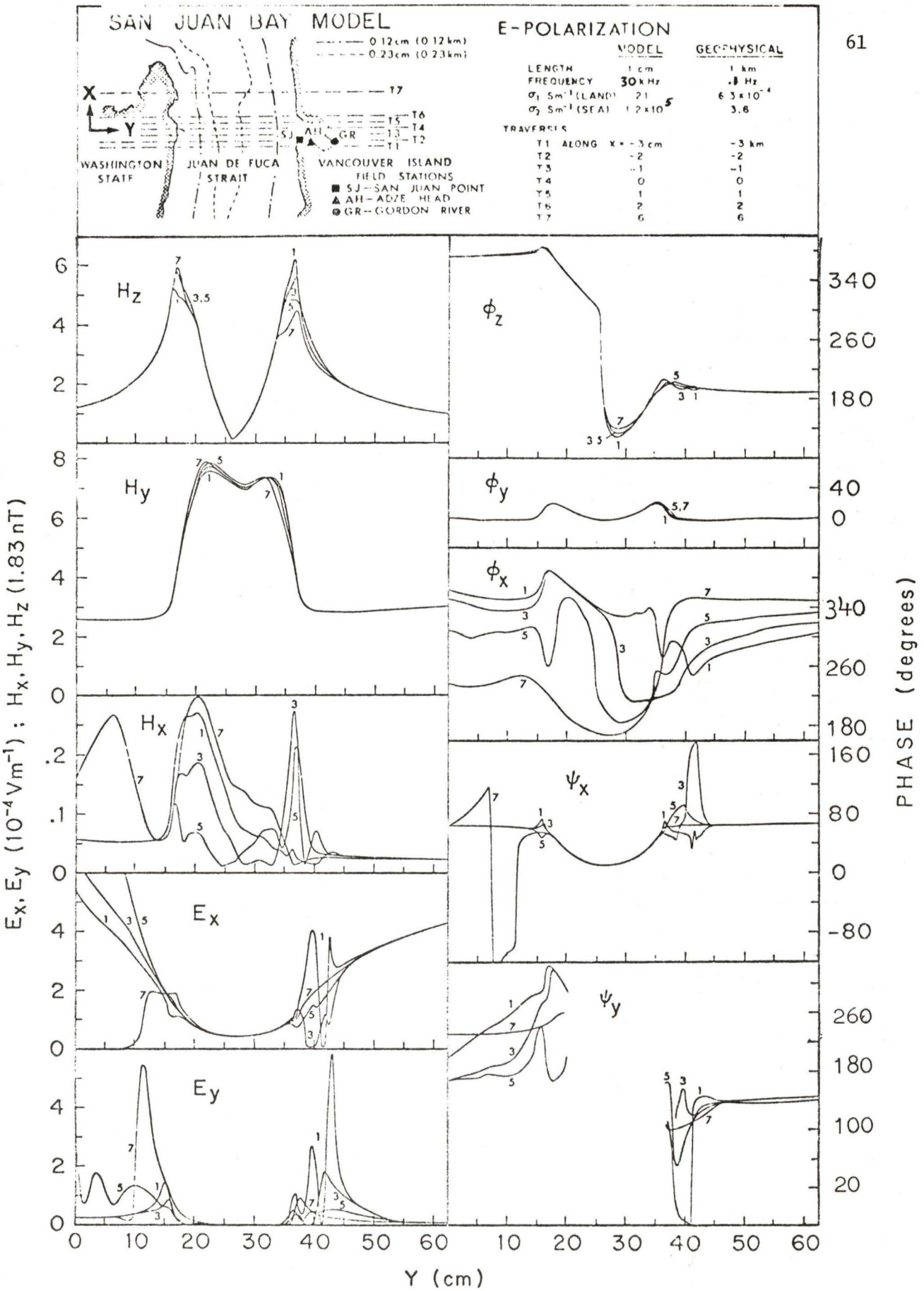


Fig. 28. Amplitudes and phase angles of model field components along the odd-numbered traverses over the San Juan Bay model for the E polarization for a frequency of 30 kHz.

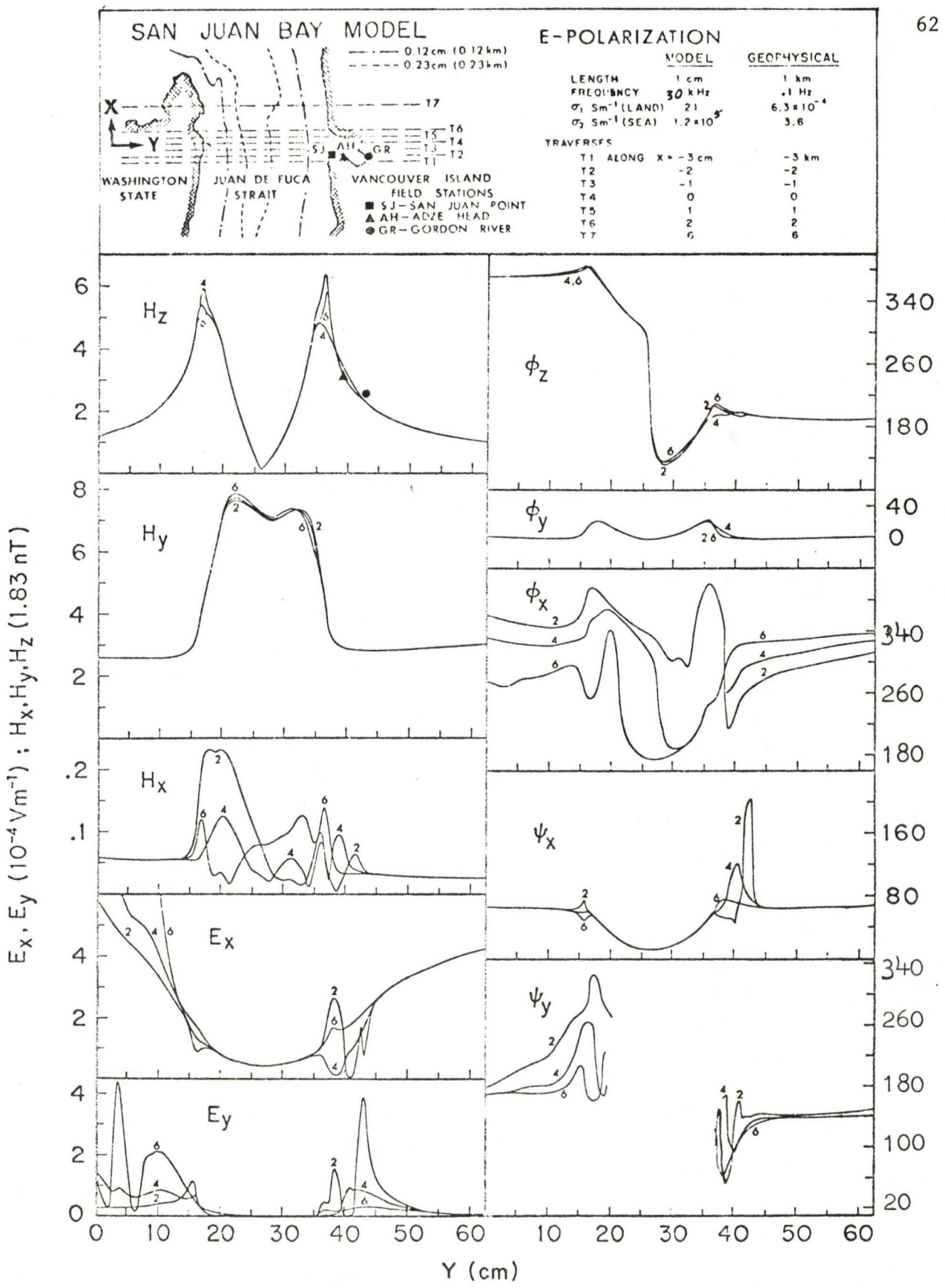


Fig. 29. Amplitudes and phase angles of model field components along the even-numbered traverses over the San Juan Bay model for the E polarization for a frequency of 30 kHz.

The vertical magnetic field component is much enhanced at each sea-land interface with the maxima directly over the coastline. The spatial variations in $H_z$ along traverses T4, T5, T6 and T7 are similar to those along traverses 1, 2, 3 and 4 for the bay model (Fig. 6) for the case of a sloping-floor ocean. The $H_z$ maxima for T4 and T5 at the mouth of the bay, are smaller than for other traverses through the bay and slightly shifted towards the Strait (similar behaviour in $H_z$ is noted for T6 crossing the Washington coastline which appears to be roughly bay-shaped). The largest maximum for $H_z$ over the Vancouver Island coastline occurs for T6 at the corner of the bay (also for T1 and T2 which passes by the other corner of the bay). Results for traverses beyond T7 (not shown) show little change from that for T7 and therefore it can be concluded that the effect of the San Juan Bay is confined to within a distance of approximately one "bay diameter" from the centre of the bay, along the coastline. $H_y$ is enhanced over the conducting Strait. $H_x$ is enhanced over the Strait, with relatively smaller and more complicated enhancements over the bay region. This indicates the presence of some induced current in the y-direction. The variation in the phases of the magnetic components along the Vancouver Island coastline behave as expected, on the basis of the results for the case of a simple bay model discussed earlier (Fig. 6).

Sharp increases in the electric field are seen in the vicinity of the bay. The deflection of electric current along the contour of the bay is indicated by the amplitudes and phases of the electric field at the two locations (field stations) indicated by the symbols AH and GR in the upper diagrams in Figs. 28 and 29. First, the amplitudes of the

$E_x$ anomalies at the two locations are very similar, but the phases $\psi_x$ differ by more than 160°, indicating that the x components of current at these two locations are in opposite directions. Second, the coastline at AH makes an angle of approximately 45° with the direction of the electric field of the inducing source. $E_x$ and $E_y$ at the AH location are comparable in amplitude and the corresponding phases indicate that the resultant of the horizontal electric field is pointing approximately parallel to the shoreline of the Bay. From these results, it is evident that electric currents are channelled in such a fashion as to follow the coastline contour of the bay.

Analogue model results for the San Juan Bay model for a model frequency of 3 kHz are shown in Figs. 30 and 31. As expected, the magnetic field components are less enhanced for this frequency. The spatial variation in the $H_z$ component for 3 kHz is very similar to that for 30 kHz. However, the $H_y$ depression between the two maxima over the Strait for 30 kHz vanishes for the 3 kHz measurements. In general, the electric field anomaly pattern is very similar for the two frequencies and the main difference is the expected larger enhancements in both $E_x$ and $E_y$ for the lower frequency case. The flow of induced electric current along the bay contour is also apparent.

For the H polarization case, the model was repositioned with the general coastline in the y-direction and perpendicular to the electric field of the inducing source as shown in Fig. 32. The model field results for 30 kHz are shown in Figs. 32 and 33. The amplitudes and phases of the two horizontal magnetic field components are moderately perturbed by the presence of the bay. $H_z$ is much less enhanced along the two coastlines

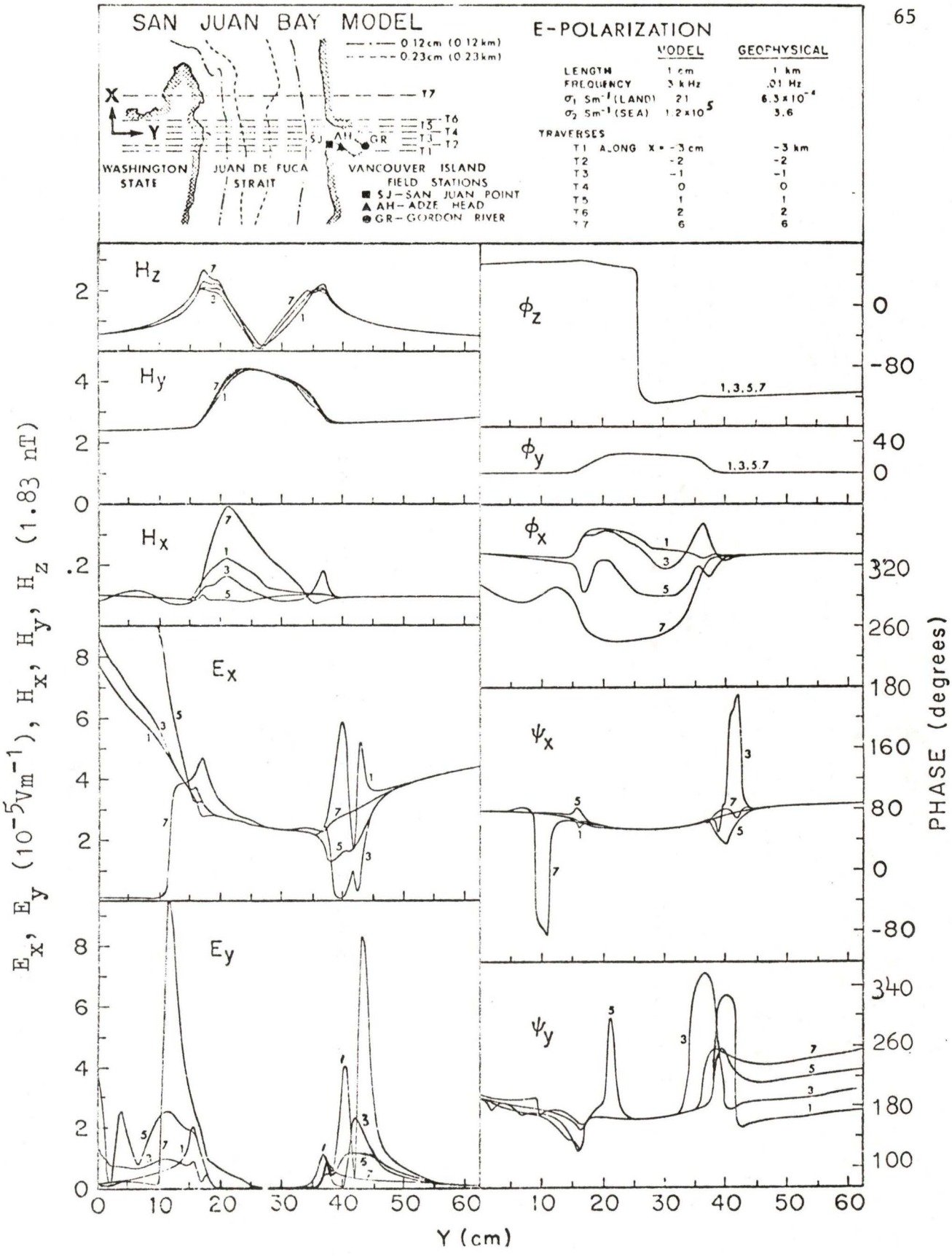


Fig. 30. Amplitudes and phase angles of model field components along the odd-numbered traverses over the San Juan Bay model for the E polarization for a frequency of 3 kHz.

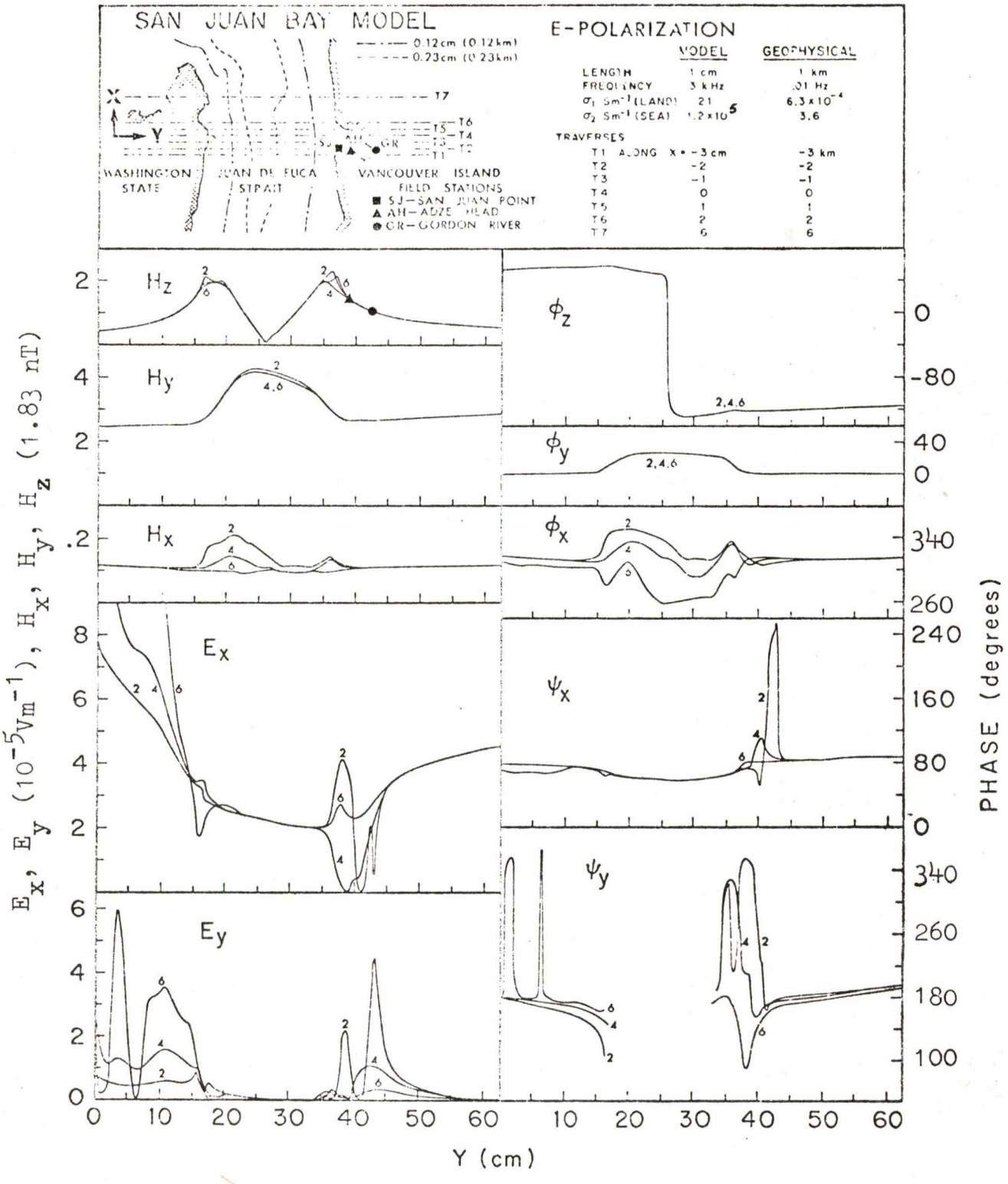


Fig. 31. Amplitudes and phase angles of model field components along the even-numbered traverses over the San Juan Bay model for the E polarization for a frequency of 3 kHz.

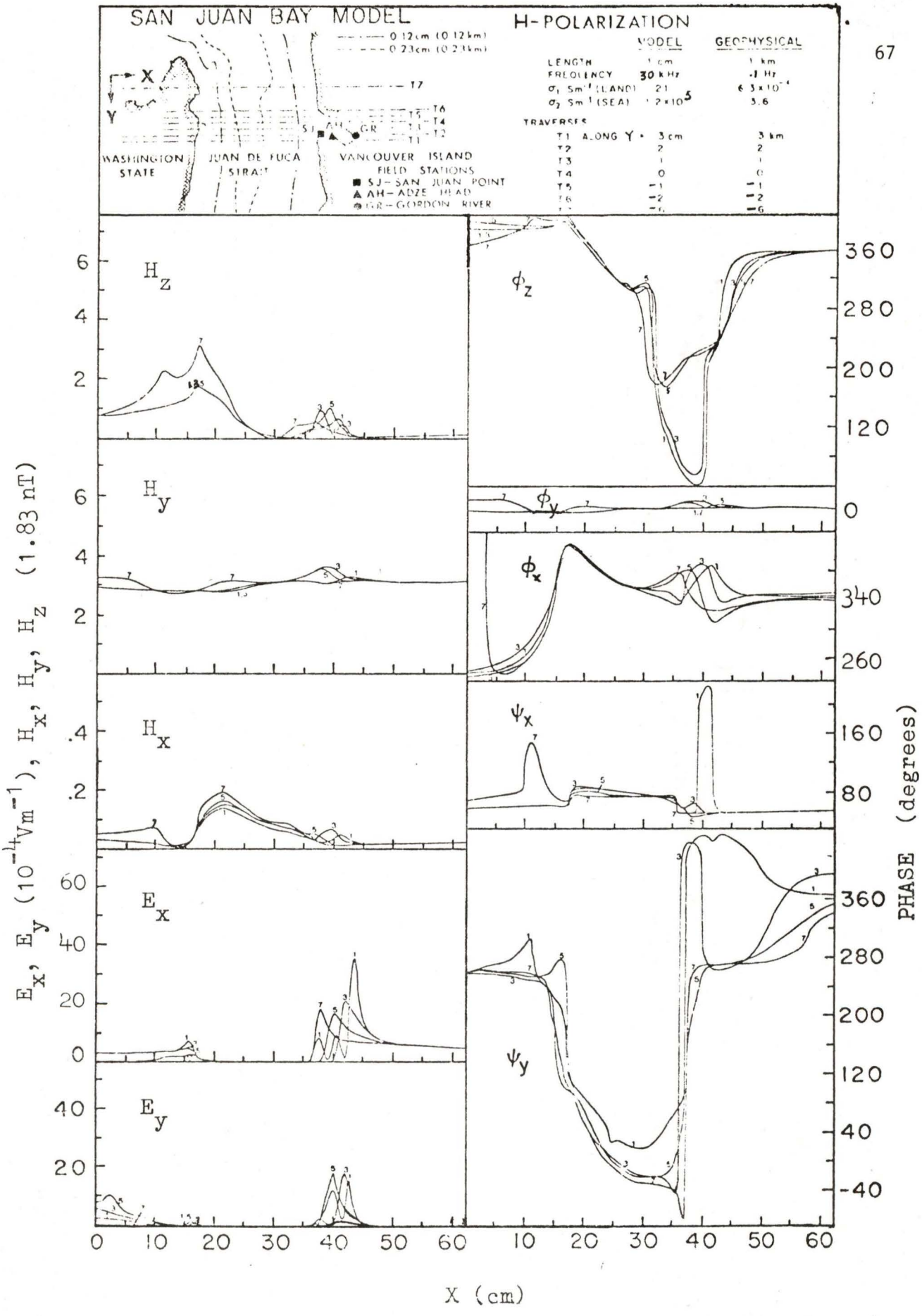


Fig. 32. Amplitudes and phase angles of model field components along the odd-numbered traverses over the San Juan Bay model for the E polarization for a frequency of 30 kHz.

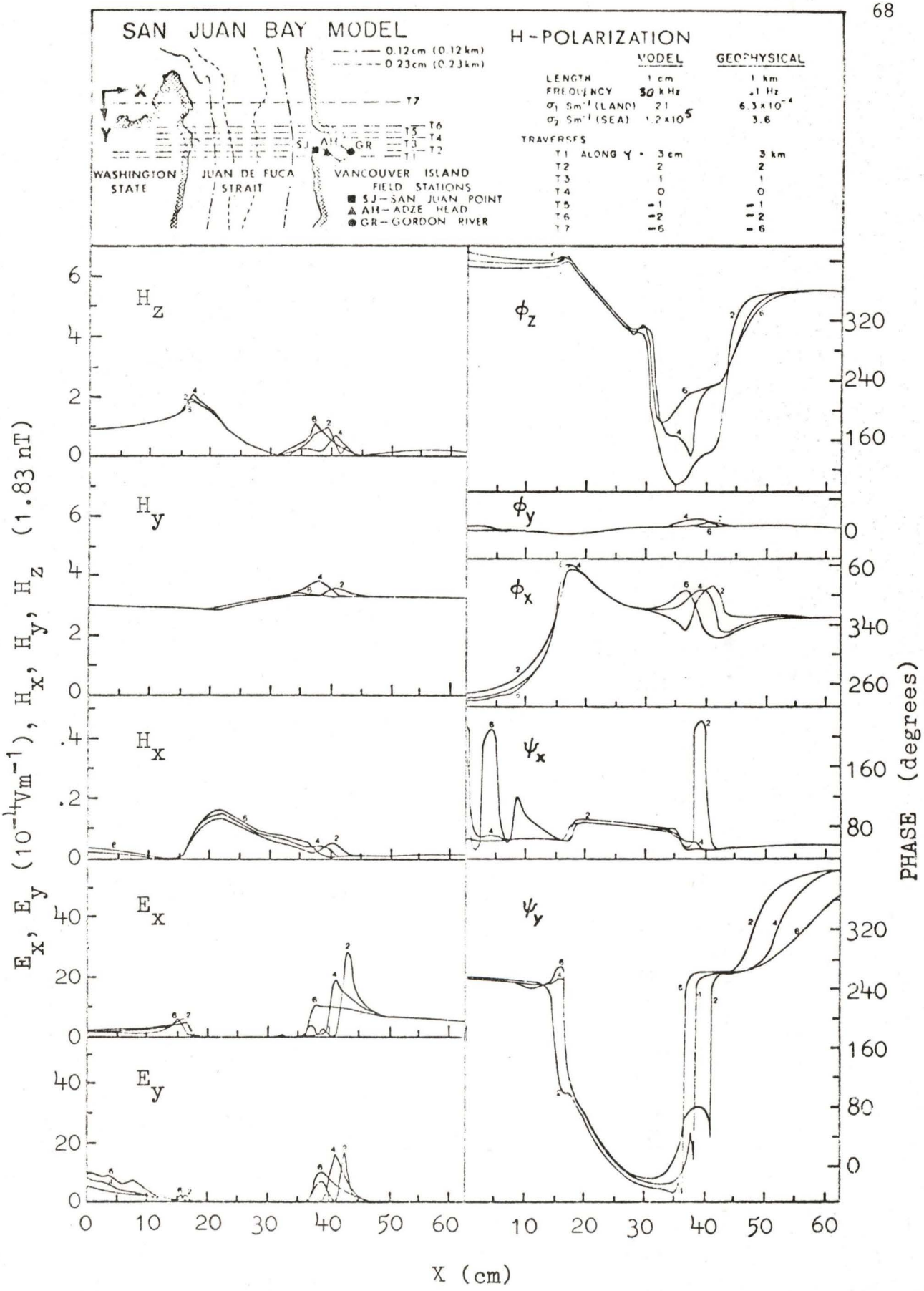


Fig. 33. Amplitudes and phase angles of model field components along the even-numbered traverses over the San Juan Bay model for the H polarization for a frequency of 30 kHz.

for this H polarization than for the E polarization. Along the Washington State coastline, which outlines more or less a peninsula, the $H_z$ enhancements are much larger than those over the bay area along the Vancouver Island coastline. This is similar to that noted earlier for the simple bay and cape models (SFO, H polarization). The net change in $\phi_z$ upon crossing the Strait is approximately 180°. It is noted that there is a local shift of 180° in $\phi_z$ near the mouth of the bay.

The electric field components at the Vancouver Island coastline are enhanced by roughly a factor of 5 more for the H polarization case than for the E polarization case. However, the $E_y$ anomalies along the Washington coastline are approximately equal for the two polarizations. The large $E_y$ anomalies in the San Juan Bay area indicate that deflection of current by the coastline contour is also important in H polarization case.

The model results for 3 kHz for the H polarization are shown in Figs. 34 and 35. In agreement with the previous models, the enhancements in the magnetic field components are much smaller than for the 30 kHz case while the electric field components remain unchanged. The general behaviour of the various components are similar for the two frequencies.

## 4.2 Field Station Measurements in the San Juan Bay Area and Comparison with Analogue Model Results

As part of this work, in October, 1977, three field stations were set up along the coastline of the San Juan Bay. The station locations are designated as SJ (San Juan Point), AH (Adze Head) and GR (Gordon River) and are shown in Fig. 27. Each site employed a fluxgate magnetometer (Trigg, et al., 1970), an amplifier and the corresponding filter

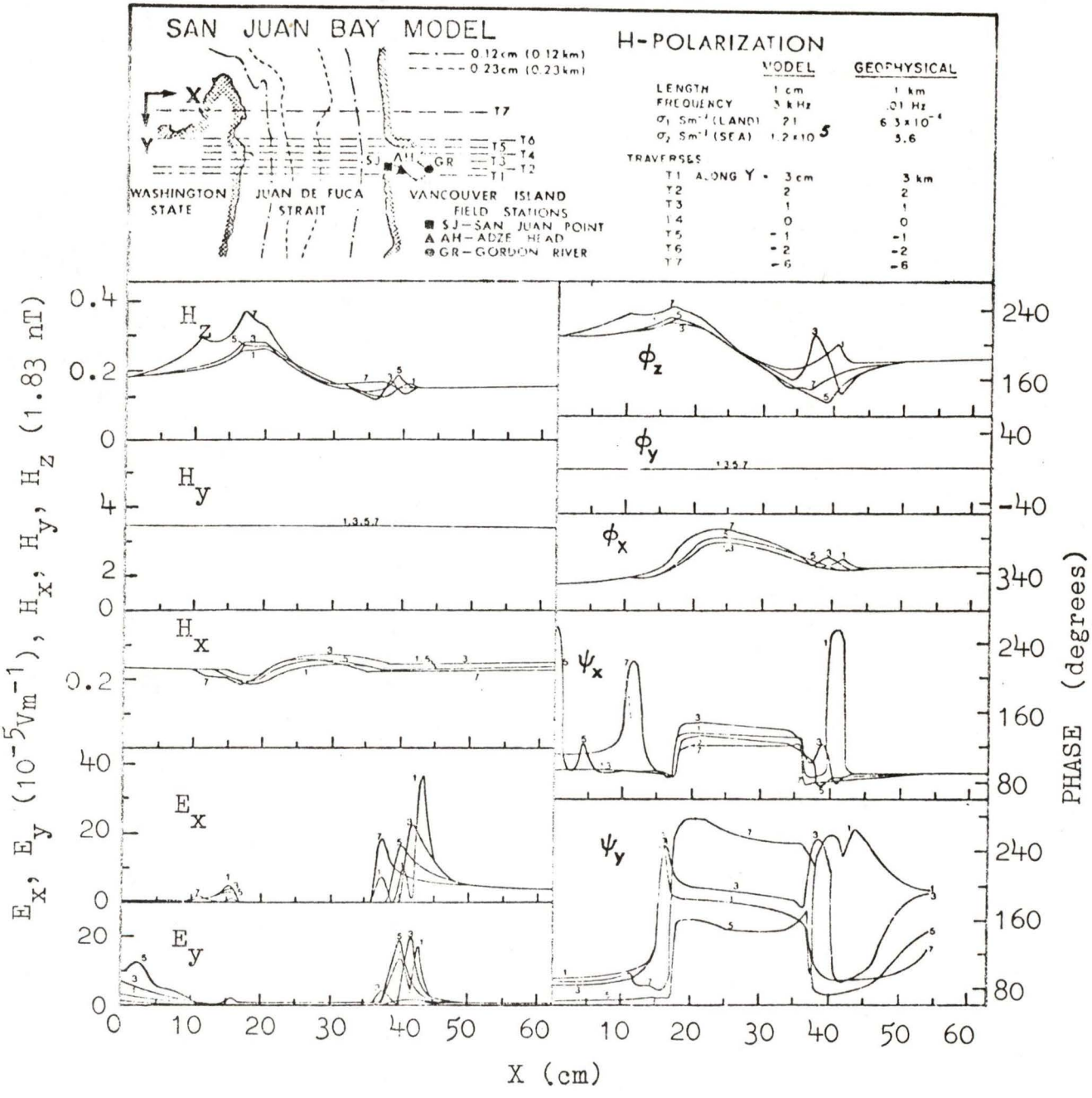


Fig. 34. Amplitudes and phase angles of model field components along the odd-numbered traverses over the San Juan Bay model for the H polarization for a frequency of 3 kHz.

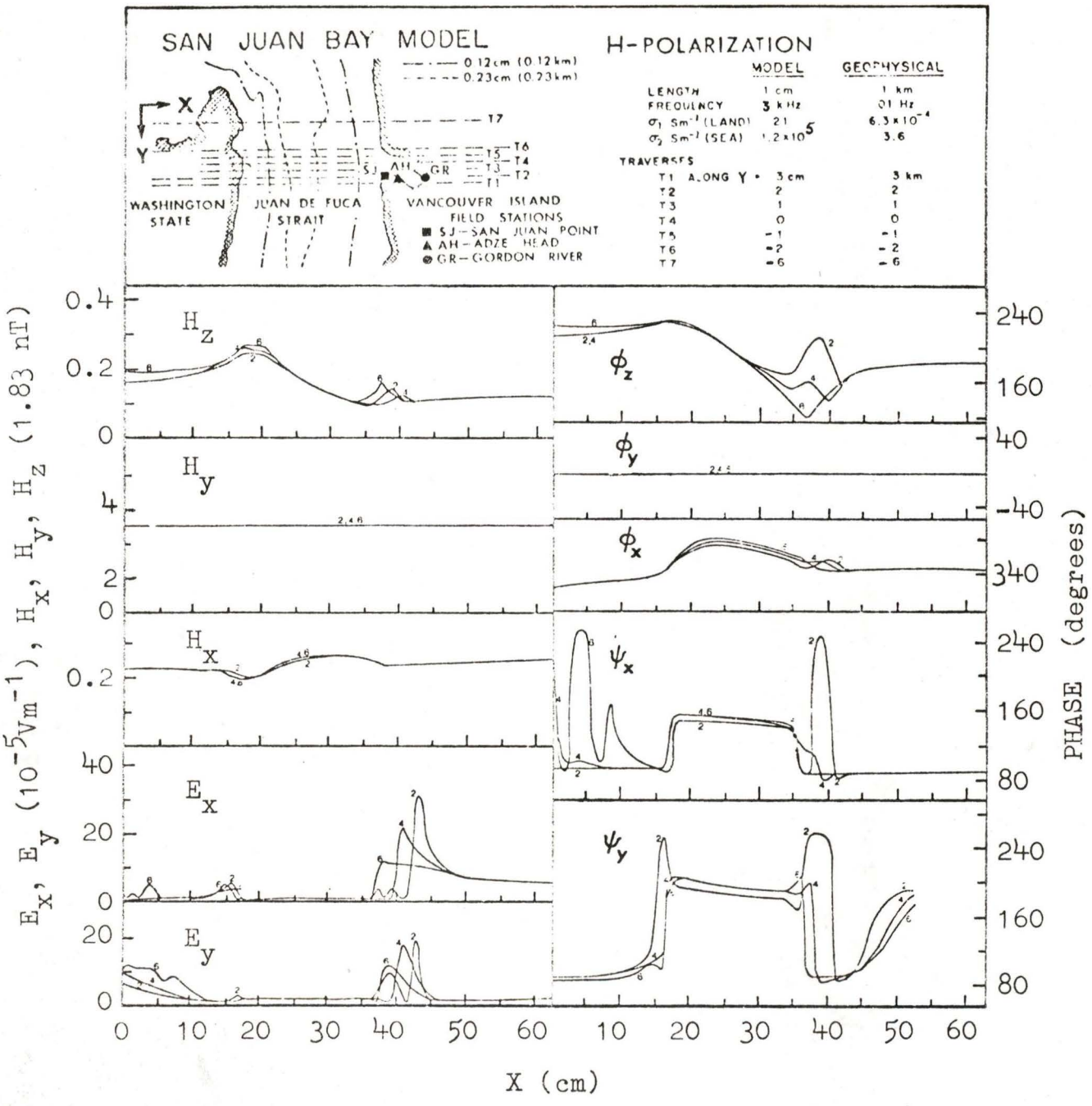


Fig. 35. Amplitudes and phase angles of model field components along the even-numbered traverses over the San Juan Bay model for the H polarization for a frequency of 3 kHz.

system (Trigg, 1972) with a frequency response of $10^{-4}$ - 1 Hz and sensitivity of approximately 1 nT. The three orthogonal time varying magnetic components Z (vertical), D (magnetic east-west) and H (magnetic north-south) were measured. After amplification, the signals were multiplexed and recorded on a Datel Systems Inc. digital cassette recorder, triggered by a digital clock with a sampling interval of 1 second. Due to equipment breakdown, no useable data were obtained from the San Juan Point station.

Three 12 hour records were obtained at both the AH and GR stations. A two hour section, during which there was high magnetic activity, was selected for single station transfer function analysis, similar to that used by Everett and Hyndman (1967). For each of the three magnetic components, the trend of the data was removed by subtracting a least squares sloped straight line and end effects were reduced by applying a cosine bell to the first and last 10% of the record (see Kanasewich, 1975 for standard processing techniques). Fourier transforms were computed for each 24 minute section of record. Stable average spectra were obtained by averaging symmetrically about selected centre frequencies (Parsen windows). For each centre frequency, the Fourier amplitudes z, h and d of the respective magnetic components were calculated. These values were then used to obtain the vertical transfer function (A,B) from the equation $z = Ah + Bd$. The two components A and B in the transfer function give the North-South and East-West components of the induction arrow which indicates the direction of best correlation between the vertical and horizontal fields. In this work, the in-phase induction arrows (using the in-phase part of the complex A and B components) are reversed to follow the Parkinson convention (i.e. the horizontal projection

of the arrows will point towards the current concentration).

The directions and relative magnitudes of the inphase Parkinson (or induction) arrows at frequenceis of 0.1 and 0.01 Hz are shown in Fig. 36. At the lower frequency (period = 100 sec), the arrows at both the AH and GR stations point approximately perpendicular to the Vancouver Island coastline while at the higher frequency (period = 10 sec), the arrows are parallel to the coastline of the bay at the respective locations.

Induction arrows can also be obtained from the model measurements of $H_z$, $H_y$, $\phi_z$, and $\phi_y$ for the E and H polarizations at the respective locations. The arrows for 3 and 30 kHz at the AH location are found to point to 207.6° and 217.7°, respectively, in true bearing (recall that the Vancouver Island coastline is approximately parallel to the magnetic east-west and that the magnetic south has a true bearing of 202.5°). Therefore, for the lower frequency, the induction arrow is pointing almost parallel to the magnetic south or perpendicular to the Vancouver Island coastline, much similar to the result obtained from the field station data. This lower frequency is nevertheless a relatively high frequency in magnetotelluric studies; and that the induction arrow points towards the conducting strait as as expected (Nienaber et al., 1978). The direction of the arrow for the higher frequency of 30 kHz indicates that it does tend to point towards a direction parallel to the coastline of the bay, though not as conspicious as demonstrated by the arrow obtained from the field station result. This could in part be due to the induced current (absent at the lower frequency) in the shallow coastal waters to the west of the bay. Results for the GR

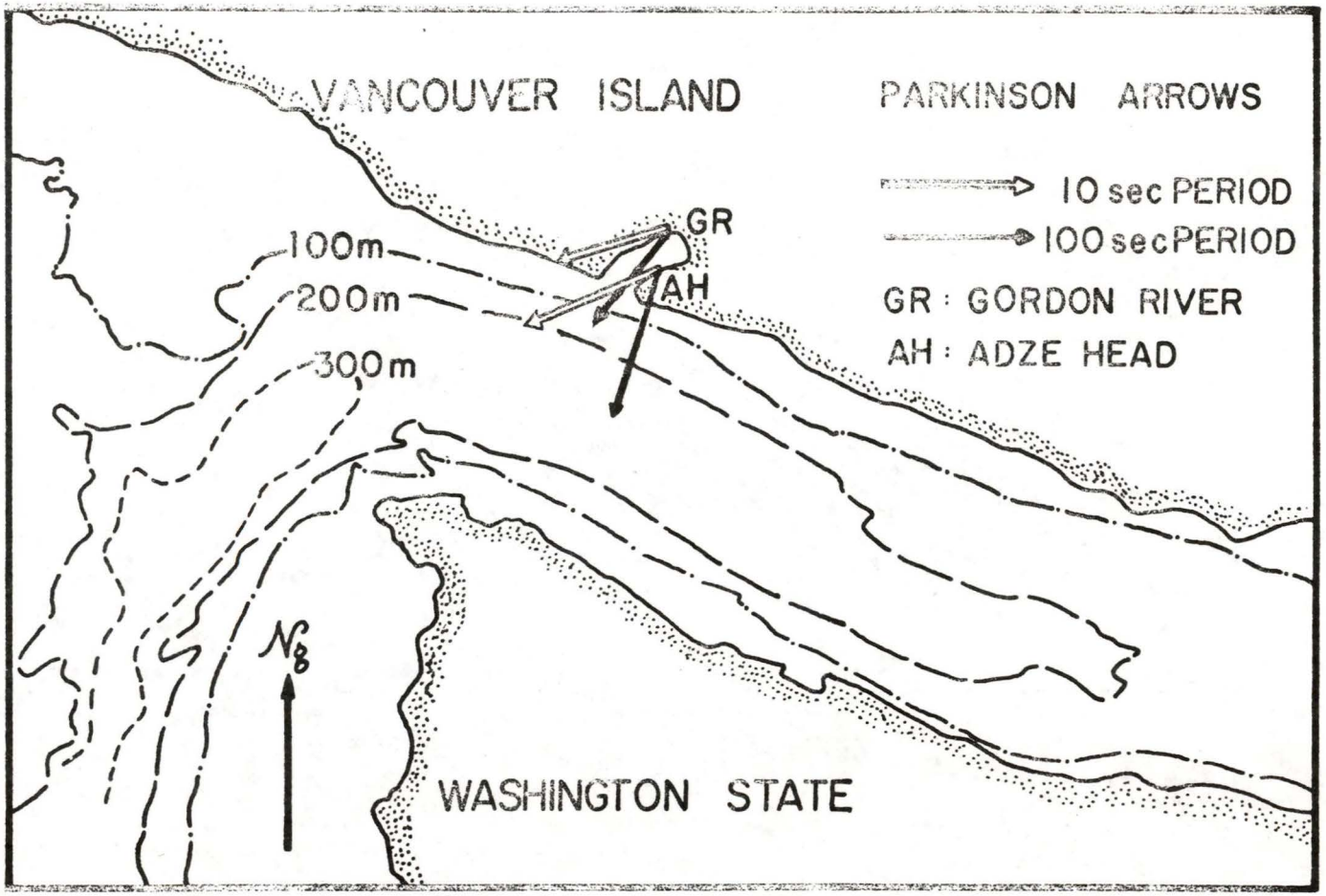


Fig. 36. In-phase Parkinson Arrows (or Induction Arrows) at the Adze Head (AH) and Gordon River (GR) field stations.

location show similar degree of agreement between analogue model measurements and field station values.

The vertical magnetic field $H_z$ at the AH and GR locations were obtained from the transfer functions (using the field station data) for the E polarization. The magnitudes for each frequency were nomalized against the model $H_z$ measurement at the AH location (i.e. the field station $H_z$ value at the model measurement. The scaling factor is then used to adjust the $H_z$ value at GR obtained from field station data). The field station results at the GR stie, as shown in Figs. 29 and 31, are seen to agree very well with the analogue model measurements for both frequencies.

# CHAPTER 5

## SUMMARY AND CONCLUSIONS

A study of the effect of coastline contours on electromagnetic induction has been presented in this work. Analogue models of non-rectilinear coastlines for simple semi-circular bays, capes, and a combination of a bay and a cape were studied for E and H polarizations of a uniform horizontal inducing field. The case of elliptical islands near these bays and capes were also studied. The case of an actual bay, San Juan Bay on Vancouver Island, was studied using analogue model results and field station data.

The spatial variations of the electric and magnetic field components over the simple bay or cape model indicate that the effect of an irregular coastal feature along an otherwise straight coastline is confined to within a distance approximately equal to the dimension (e.g. diameter of a bay) of the irregularity. It is interesting to note that within the regions near both the bay and the cape models where $H_y$ varies rapidly along a traverse, there is a line, parallel to the straight coastline, over which $H_y$ has the same value for each traverse.

$H_z$ at the middle of the bay coastline is found to be half as large as it is along the nearby straight coastline. This together with the $H_x$ and the electric field enhancement near the bay coastline suggest that the current induced in the ocean tends to follow the contour of the coastline. This agrees with Jones' (1974) results of channelling of induced current by shallow bays. The same is true for the cape-shaped

coastline (in this case, $H_z$ at the top of the cape is twice as large as it is along the nearby straight coastline and the $H_x$ and the electric field components profiles are different from those of the bay coastline model). Diffusion of telluric current into the coastal region of the bay or cape in the vicinity of the nearby straight coastlines is indicated by the spatial variations in $E_x$ and $E_y$.

Over the bay coastline, the coast effect $H_z/H_y$ is smaller than over the nearby straight coastline for both frequencies studied, whereas the coast effect is larger over the cape coastline than it is over the straight coastline. The apparent resistivity profiles indicate that there is an order of magnitude difference in $\rho_a$ between the mid-point of a bay and a point where the bay coastline meets the straight coastline. The same is true in the case of a cape.

For the bay and cape type coastlines, the magnetic and electric field anomalies are very sensitive to a change in model frequency (from 30 kHz to 3 kHz, say). It was seen that the magnetic field anomalies decrease with decreasing frequency while the electric field anomalies increase with decreasing frequency. The spatial variation in each of the field components for changing frequency is nevertheless preserved.

For the H polarization measurements, it is seen that the perturbation in $H_z$ due to a cape is much greater than that due to a bay. Comparing the results for the two polarization cases, it is noted that the magnetic field anomalies are larger for the E polarization than for the H polarization while the electric field anomalies are larger for the H polarization than for the E polarization. Another feature for the H polarization case is that the $E_x$ anomalies are larger at the cape

coastline and smaller at the bay coastline than at the respective nearby straight coastlines. The reverse is true for the E polarization case. Hence, although it was evident that channelling of currents by the bay or cape was also present for the H polarization, the current system is quite different from that of the E polarization case, as indicated by the respective electric field spatial variation patterns.

The results obtained above apply to coastlines near a sloping-floor ocean. Measurements for models with uniform depth oceans show that the magnetic anomalies become slightly larger and sharper at the interface. The $E_y$ component shows much difference for the two cases, especially over the straight coastline for the bay models, where the $E_y$ enhancement becomes 2 to 3 times larger for the CDO model than for the SFO model.

For the bay-cape combination model, $H_z$ and $H_y$ are similar to the superposition of the results from the individual simple bay and cape models. Further, the $H_z$ anomaly at the junction of the bay and the cape is approximately the average value of the $H_z$ anomalies at the corner of the bay and at the corner of the cape model.

The caost effects at three types of coastlines (bay, cape, and rectilinear) were compared with Launay's (1970) model results. The $H_z/H_y$ ratio for both the present model results and Launay's (1970) results is largest for the cape, smallest for the bay and intermediate for the straight coastline. The coast effect, however, for Launay's model is smaller than that for the present model). This difference is explained in terms of the phsycical differences of the two models, such as the conductivity contrast between the ocean and land, the position of the

mantle and the size of the cape and the bay simulated.

Models of an elliptical island situated near bay-shaped, cape-shaped, and straight coastlines were constructed and studied. Both the bay and cape type coastlines were found to enhance the vertical magnetic field at the island coastline on the sea-ward side. The proximity of the tip of the cape or the corner of the bay govern the changes in the $H_z$ anomaly at the island coastline facing the continental coastline and the $H_y$ anomaly on the sea-ward island coastline.

Model field measurements for the San Juan Bay analogue model indicate that the effect of the rather complicated coastline is very similar to that of a simple bay model, especially in the trends of spatial variation of the magnetic and electric field components. Also, it is seen that the effect of the San Juan Bay extends to approximately one "bay diameter" from the centre of the bay. The deflection of current along the coastline of the bay is observed for both E and H polarization.

Induction arrows were obtained by transfer function analysis of field station data obtained at the AH and GR locations. At the frequency of 0.01 Hz, the induction arrows at both sites were found to point towards the Juan de Fuca Strait as expected, while at 0.1 Hz, the arrows had a direction parallel to the coastline of the bay at the two field station sites. This effect of the bay on the induction arrow is supported to some extent by the direction of the arrows obtained from the analogue model measurements. The normalized vertical magnetic field obtained from the transfer functions show reasonable agreement with analogue model measurement.

This study indicates the importance of the coastline contour in affecting the time varying electromagnetic fields at coastal regions. The agreements between the laboratory measurements and the field station observations demonstrates the usefulness of analogue modelling in studying complex induction problem. The result is useful for determining the location of a coastal magnetotelluric station. To extend the present work, a field station study for the case of a suitable cape-shaped coast would be of considerable interest.

# REFERENCES

Bailey, R.C. and Edwards, R. N. 1976. The effect of source field polarization on geomagnetic variation anomalies in the British Isles. Geophys. J.R. Astro. Soc., 45, 97-104.

Brewitt-Taylor, C.R. 1975. A model for the coast effect. Phys. Earth Planet. Inter., 10, 151-158.

Cagniard, L. 1953. Basic theory of the mangetotelluric method of geophysical prospecting. Geophysics, 8, 605.

Campbell, W. H. 1967. Geomagnetic storms. in Physics of Geomagnetic Phenomena. ed. by S. Matsushita and W.H. Campbell. A.P. New York and London.

Caner, B., Camfield, P.A., Andersen, F. and Niblett, E.R. 1969. A large-scale magnetotelluric survey in western Canada. Can. J. Earth Sci., 6, 1245-1261.

Chapman, S. 1967. Perceptive. in Physics of Geomagnetic Phenomena, ed. by S. Matsushita and W.H. Campbell, A.P., New York and London.

Chapman, S. and Whitehead, T.T. 1922. The influence of electrically conducting material within the earth on various phenomena of terrestrial magnetism. Trans. Cambr. Phil. Soc., 22, 463.

Cox, C.S., Filloux, J.H., and Larsen, J.C. 1970. Electromagnetic studies of ocean currents and electrical conductivity below the ocean floor. in The Sea, ed. by A.E. Mazwell, Interscience, New York, 637-693.

d'Erceville, I. and Kunetz, G. 1962. The effect of a fault on the earth's natural electromagnetic field. Geophysics, 27, 651-665.

Dosso, H.W. 1966a. A plane-wave analogue model for studying electromagnetic variations. Can. J. Phys., 44, 67-80.

Dosso, H.W. 1966b. Analogue model measurements for electromagnetic variations near vertical faults and dykes. Can. J. Earth Sci., 3, 287-303.

Dosso, H.W. 1967. Analytical and Analogue Methods of Studying Electromagnetic Variation at the Earth's Surface. Ph.D. Thesis, University of British Columbia.

Dosso, H.W. 1969. Analogue model study of electromagnetic variations over an anisotropic conductor. J. Geomag. Geoelectr., 21, 647-753.

Dosso, H. W. 1973. A review of analogue model studies of the coast effect. Phys. Earth Planet. Inter., 7, 294-302.

Dosso, H. W. and Jacobs, J.A. 1968. Analogue model measurements of electromagnetic variations in the near field of an oscillating line current. Can. J. Earth Sci., 5, 23-29.

Dosso, H.W., Ramaswamy, V., Jones, F.W., Thomson, D.J. 1974. On the comparison of laboratory electromagnetic analogue model measurements and finite-difference numerical calculations. Phys. Earth Planet. Inter., 9, 108-110.

Dulany, E. N., and Madden, T.R., 1962. Analogue relaxation net calculation of two-dimensional magnetotelluric response curves. S.E.G. Yearbook, 265 (Abstract).

Edwards, R.N., Law, L.K., and White, A. 1971. Geomagnetic variations in the British Isles and their relationship to electrical currents in the ocean and shallow seas. Phil. Trans. Roy. Soc., 270, 289.

Everett, J.E., and Hyndman, R.D. 1967. Geomagnetic variations and electrical conductivity structure in south-western Australia. Phys. Earth Planet. Inter., 1, 24-34.

Frischknecht, F.C. 1971. Electromagnetic scale modelling. in Electromagnetic Probing in Geophysics, ed. by J.R. Wait, the Golem Press, Boulder, Colorado.

Geyer, R.G. 1972. The effect of a dipping contact on the electromagnetic field. Geophysics, 37, 337.

Green, V.R. 1978. The Two-Dimensional Theory of Electromagnetic Induction in Thin Sheets with Applications to the Earth. M.Sc. Thesis, University of Victoria.

Hermance, J.F. 1968. Model studies of the coast effect on geomagnetic variations. Can. J. Earth Sci., 5, 515-522.

Hibbs, R.D., Jones, F.W., Ramaswamy, V., and Dosso, H.W. 1978. Electromagnetic analogue model measurements and finite-difference numerical calculations of the response of a conducting slab to three different source fields. Phys. Earth Planet. Inter., 16, In Press.

Honkura, Y. 1971. Geomagnetic variation anomaly on Miyakejima Island. J. Geomag. Geoelectr., 23, 307-333.

Hyndman, R.D. and Cochrane, N.A. 1971. Electrical conductivity structure by goemagnetic induction at the continental margin of Atlantic Canada. Geophys. J.R. Astr. Soc., 25, 425-446.

Jones, F. W. 1974a. The perturbation of slowly varying electromagnetic fields by three-dimensional conducting bodies. Can. J. Phys., 52, 1195-1202.

Jones, F.W. 1974b. The effect of an island and bay structure on alternating fields at three periods. Geophys. J., 36, 627-639.

Jones, F.W. and Lokken, J.E. 1975. Irregular coastline and channelling effects in three-dimensional geomagnetic perturbation models. Phys. Earth Planet. Inter., 10, 140-150.

Jones, F.W. and Pascoe, L.J. 1971. A general computer program to determine the perturbation of alternating electric currents in a two-dimensional model of a region of uniform conductivity with an embedded inhomogeneity. Geophys. J., 24, 3-30.

Jones, R.W. and Price, A.T. 1970. The perturbations of alternating geomagnetic fields by conductivity anomalies. Geophys. J.R. Astr. Soc., 20, 317-334.

Jones, F.W. and Price, A.T. 1971. Geomagnetic effects of sloping and shelving discontinuities of earth conductivity. Geophysics, 36, 58-66.

Kertz, W. 1964. The conductivity anomaly in the upper mantle found in Europe. J. Geomag. and Geoelectr., 15, 185-192.

Klein, D.P. 1976. Magnetic Variations (2-30 cpd) on Hawaii Island and Mantle Electrical Conductivity. Ph.D Dissertation, University of Hawaii, Honolulu, Hawaii.

Kulik, S.N., Rokityanskii, I.I., Fornarev, G.A., Shneer, V.S. 1973. Simulation of coast effect in variation of the geomagnetic vertical field component. Academy of Science of the Ukrainian S.S.R., Publication 54, 82-84.

Lamb, H. 1883. On electrical motions in a spherical conductor. Phil. Trans. Roy. Soc., 174, 526.

Latka, R. 1966. Modellrechnungen zur Induktion im elektrisch leitfahigen untergrund, Zeitschrift für Geophysik, 32, 512-517.

Launay, L. 1970. Studies on edge effect through scale models. Ann. Geophys., 26, 805-810.

Lines, L.R. and Jones, F.W. 1973a. The perturbation of alternating geomagnetic fields by three-dimensional island structures. Geophys. J., 32, 133-154.

Lines, L.R. and Jones, F.W. 1973b. The perturbation of alternating geomagnetic fields by an island near a coastline. Can. J. Earth Sci., 10, 510-518.

Lipskaya, N.V. 1953. On certain relationships between harmonics of the periodic variations of the terrestrial electric and magnetic fields. Izv. Akad. Nauk, USSR, Geophysics Series 1, 41.

Mann, J.E. 1970. A perturbation technique for solving boundary value problems arising in the electrodynamics of conducting bodies. Appl. Sci. Res., 22, 113.

Mason, R.G. 1963. Spatial dependence of the time variations of the geomagnetic field on Oahu, Hawaii. Trans. A.G.U., 44, 40-41.

Matsushita, S. 1967. Solar quiet and lunar daily variation fields. in Physics of Geomagnetic Phenomena. Ed. by S. Matsushita and W.H. Campbell. A.P. New York and London.

Neves, A. 1957. The generalized magneto-telluric method, Ph.D. Thesis, Dept. of Geol. and Geophys., M.I.T.

Nienaber, W., Dosso, H.W., Law, L.K., Jones, F.W., Ramaswamy, V. 1976. An analogue model study of electromagnetic induction for island-continent ocean channels. Phys. Earth Planet. Inter., 13, 169-183.

Nienaber, W., Dosso, H.W., Law, L.K., Jones, F.W., Ramaswamy, V. 1977. An analogue model study of electromagnetic induction for island-continent ocean channels for the H polarization. Phys. Earth Planet. Inter., 15, 69-76.

Nienaber, W., Dosso, H.W., Law, L.K., Jones, F.W., Ramaswamy, V. 1979. Analogue model study of the electromagnetic induction in the Vancouver Island region. J. Geomag. Geoelectr., (in press).

Ogunade, S.O. 1973. Electromagnetic Response of a Sphere Embedded in a Layered Conducting Earth. Ph.D. Thesis, University of Victoria.

Ogunade, S.O., Ramaswamy, V., and Dosso, H.W. 1974. Electromagnetic response of a conduction sphere buried in a conducting earth. J. Geomag. Geoelectr., 26, 417-427.

Ogunade, S.O., and Dosso, H.W. 1977. Subsurface electromagnetic response of a conducting sphere embedded in the lower layer of a two-layer earth. Acta Geodaet., Geophys. et Montanist. Acad. Sci. Hung., 12 (1-3), 311-314.

Parker, R.L. 1968. Electromagnetic induction in a thin strip. Geophys. J.R. Astr. Soc., 14, 487-495.

Parkinson, W.D. 1959. Directions of rapid geomagnetic fluctuations. Geophys. J.R. Astr. Soc., 2, 1-14.

Parkinson, W.D. 1962. The influence of continents and oceans on geomagnetic variations. Geophys. J.R. Ast. Soc., 6, 441-449.

Patrick, F.W., and Bostick, F.X. 1969. Magnetotelluric modelling techniques. Tech. Rept. 59, Electronics Research Center, Univ. of Texas, Austin.

Price, A.T. 1950. Electromagnetic induction in a semi infinite conductor with a plane boundary. Quart. J. Mech. Appl. Math., 3, 385-410.

Price, A.T. 1962. The theory of magneto-telluric methods when the source field is considered. J. Geophys. Res., 67, 1907.

Ramaswamy, V. 1973. Electromagnetic Fields of a Horizontal Magnetic Dipole Situated Above and Within a Two-layer Earth. Ph.D. Thesis, University of Victoria.

Ramaswamy, V. and Dosso, H.W. 1977. The response of a conducting cylinder to the inducing fields of various sources. J. Geomag. Geoelectr., 29, 181-189.

Ramaswamy, V. and Dosso, H.W. 1978. Analogue model measurements for a horizontal magnetic dipole embedded within a conducting medium. Phys. Earth Planet. Inter., 17, 295-299.

Rankin, D. 1962. The magneto-telluric effect on a dike, Geophysics, 27, 666-676.

Reddy, I.K., and Rankin, D. 1975. Magnetotelluric response of laterally inhomogeneous and anisoptropic media, Geophysics, 40, 1035-1045.

Rikitake, T. 1973. Global electrical conductivity of the earth. Phys. Earth Planet. Inter., 7, 145-250.

Roden, R.B. 1964. The effect of an ocean on magnetic diurnal variations. Geophysics Journal, 8, 375-388.

Rokityanskii, I.I. 1963. The shore effect in variations of the earth's electromagnetic field. Izv. Geophys. Ser. No. 12, 1814-1822 (Engl. trans. by Irving Emin).

Schmucker, U. 1959. Erdmagnetische Tiefensondierung in Deutschland 1957/59: Magnetogramme und Erste Auswertung. Abh. Akad. Wiss. Gott., Math. Phys. Kl., Beitr. z I.G.J. Heft 5.

Schmucker, U. 1964. Anomalies of geomagnetic variations in the south-western United States. J. Geomag. Geoelectr., 15, 193.

Schmucker, U. 1970. Anaomalies of geomagnetic variations in the southwestern United States. Bull. Scripps Inst. Oceanography., 13.

Schmucker, U. 1971. Interpretation of induction anomalies above nonuniform surface layers. Geophysics, 36, 156-165.

Schuster, A. 1889. The diurnal variation of terrestrial magnetism. Phil. Trans. Roy. Soc., London, A, 180, 467.

Sinclair, G. 1948. Theory of models of electromagnetic systems. Proc. I.R.E., 36, 1264-1370.

Strangway, D.W. 1966. Electromagnetic scale modelling. in Methods and Techniques in Geophysics, ed. by S.K. Runcorn, Interscience, New York, 1-31.

Swift, C.M. 1967. A Magentotelluric Investigation of an Electrical Conductivity Anomaly in the Southwestern United States, Ph.D. Dissertation, Massachusetts Institute of Technology, Cambridge, Massachusetts.

Thomson, D.J., Ramaswamy, V., and Dosso, H.W. 1972. Model measurements of electromagnetic variations near a coastline for localized source fields. J. Geomag. Geoelectr., 24, 317-336.

Tikhonov, A.N. 1950. Determination of the electric characteristics of the deep strata of the earth's crust. Dok. Akad. Nauk USSR, 73, 295.

Trigg, D. 1972. An amplifier and filter system for telluric signals. Publs. Earth Phys. Br., 44, no. 1, Ottawa.

Trigg, D.G., Serson, P.H., and Camfield, P.A. 1970. A solid state electrical recording magnetometer. Publs. Earth Phys. Br., 41, Ottawa.

Troitshaya, V.A. 1964. Rapid Variations of the Electromagnetic Field of the Earth. in Research in Geophysics, ed. by H. Odishaw, M.I.T.

Vozoff, K. and Swift, C.M. 1968. Magnetotelluric measurements in the north German basin. Geophys. Prospect., 16, 545-473.

Wait, J.R. 1954. On the relation between telluric currents and the earth's magnetic field. Geophysics, 19, 281.

Ward, S.H. 1967. The electromagnetic method. in Mining Geophysics, II, Soc. Expl. Geophysics, Tulsa, Okla., 224-372.

Weaver, J.T. 1963. The electromagnetic field within a discontinuous conductor with reference to geomagnetic micropulsations near a coastline. Can. J. Phys., 41, 484-495.

Weaver, J.T. and Thomson, D.J. 1972. Induction in a non-uniform conducting half-space by an external line current. Geophys. J., 28, 163-185.

Weidelt, P. 1971. The electromagnetic induction in two thin half-sheets. Zeitschrift fur Geophysik, 37, 649-665.

Yukutake, T. 1967. Publ. Dom. Obs., Ottawa, Ontario, 35(8).

Zienkiewicz, D.C. 1971. The Finite Element Method in Engineering Science. McGraw-Hill, New York.

# VITA

Surname: CHAN Given Names: Gee Hung

Place of Birth: HONG KONG Date of Birth: MARCH 3, 1954

Educational Institutions Attended, with Dates of Entering and leaving:

UNIVERSITY OF VICTORIA, B.C. 1972 to 1976

UNIVERSITY OF VICTORIA, B.C. 1976 to 1979

Degrees, Diplomas, Etc., Awarded, with Dates and Names of Institutions:

B.Sc. 1976 University of Victoria

Honours and Awards:

University of Victoria Graduate Scholarship, 1976/77

University of Victoria Fellowship, 1977/78

Papers Presented at Scientific Meetings:

Chan, G.H., Dosso, H.W. and Law, L.K. 1978. The effect of a coastline contour on electromagnetic induction for the case of a bay. Program and Abstracts, 4th Workshop on Electromagnetic Induction in the Earth and Moon. IAGA, West Germany, 4.12, Abstract.

PARTIAL COPYRIGHT LICENSE

I hereby grant the right to lend my thesis or dissertation (the title of which is shown below) to users of the University of Victoria Library, and to make single copies only for such users or in response to a request from the library of any other university, or similar institution, on its behalf or for one of its users. I further agree that permission for extensive copying of this thesis for scholarly purposes may be granted by me or a member of the University designated by me. It is understood that copying or publication of this thesis for financial gain shall not be allowed without my written permission.

Title of Thesis

A Study of the Effect of Coastline Contours on Electromagnetic Induction

Author [redacted]

signature

Gee H. Chan

name

3 April, 1979

date